2006-01-01

Wideband Dual Polarized Directional Base Station Antenna

Francisco L. Lerma
Technological University Dublin

DUBLIN INSTITUTE of TECHNOLOGY
Institiúid Teicneolaíochta Bhaile Átha Cliath

Wideband Dual Polarized Directional Base Station Antenna

Francisco León Lerma

Bachelor of Engineering Electrical and Electronic

MPhil

Dublin Institute of Technology

Max Ammann

September 2006

ABSTRACT

The thesis presents a study of different microwave radiators for wireless applications in the frequency range of 2.2 - 2.5GHz. The performance of microstrip patch antennas and dual polarized dipole antennas were evaluated numerically and experimentally verified. A single microstrip patch and a four-element microstrip array were simulated, fabricated and tested. Simulation was carried out by the finite integration time domain (FITD) method. Polarization diversity is realised using crossed dipoles printed elements. For the crossed dipole elements, two different feed arrangements were studied. Parameters such as return loss, isolation, radiation pattern, gain and bandwidth were measured and found to be in good agreement with simulation. Several techniques were used to obtain broadband performance. Balanced and unbalanced feeder systems, substrates effects and the use of planar elements were investigated. Significant improvements were achieved in bandwidth and port-to-port isolation by optimizing the feed system and antenna geometry.

DECLARATION

I certify that this thesis which I now submit for examination for the award of MPHIL, is entirely my own work and has not been taken from the work of others save and to the extent that such work has been cited and acknowledged within the text of my work.

This thesis was prepared according to the regulations for postgraduate study by research of the Dublin Institute of Technology and has not been submitted in whole or in part for an award in any other Institute or University.

The work reported on in this thesis conforms to the principles and requirements of the Institute's guidelines for ethics in research.

The Institute has permission to keep, to lend or to copy this thesis in whole or in part, on condition that any such use of the material of the thesis be duly acknowledged.

Signature _____

Date 26/09/06

Candidate

FRANCISCO LEON LERMA

ACKNOWLEDGEMENTS

I wish to acknowledge Dr. Max Ammann for his entire support, without which it would never have been possible. I also would like to thank Max for giving me the opportunity to work with him on this project.

I wish to express my sincere gratitude to Giuseppe Ruvio for his suggestions and his help. I also would like to thank Sergio Curto and Mathias his help in the last days of the project.

I greatly appreciate the useful suggestions given by Niallo Carroll and Fergal Lawlor, from Sigma Wireless Technologies.

I would like to thank Ruben Sanchez, Moises Ruiz and Rymsa R&D dept. for their support on the final prototype manufacturing and pattern measurements.

I wish to acknowledge my parents and my brothers, Pedro and David for their encouragement and love.

To my love Inma for her support and help over the last two years and for her patience during the busy periods

TABLE OF CONTENTS

ABSTRACT **2**
DECLARATION **3**
ACKNOWLEDGEMENTS **4**
LIST OF FIGURES **8**
ACRONYMS **12**
CHAPTER 1 ..... **13**
INTRODUCTION **13**
CHAPTER 2 ..... **16**
BACKGROUND THEORY **16**
2.1 Principles of antennas 16
2.2 Dipole theory 21
2.2.1 Introduction 21
2.2.2 Half-wave cylindrical dipole 22
2.2.4 Printed dipoles 25
2.2.5 Reflector theory 26
2.3 Balanced and unbalanced feeder systems 27
2.3.1 Introduction 27
2.3.2 Microstrip balun 31
- 2.3.2.1 Marchand Balun 31
- 2.3.2.2 Log Periodic Balun 32
- 2.3.2.3 Tapered balun 33
- 2.3.2.4 Double Y balun 34
- 2.3.2.5 Radial stub balun 35
2.3.3 Quarter wavelength balun 36
2.4 Microstrip theory 38
2.4.1 Microstrip radiators 40
2.5 Electromagnetic Modelling Technique 41
2.6 Scattering Parameters 42
CHAPTER 3: **45**
STUDY OF MICROSTRIP PATCH ANTENNAS **45**
3.1 Introduction 45
3.2 Single patch design 45

3.3 Simulation of microstrip patch 47
3.4 Fabrication and Measurements 49
3.5 Optimisation 50
3.6 Array Design 51
3.7 Array Spacing 51
3.8 Calculation of the feed lines 52
3.9 Simulation and fabrication 53
3.10 Gain Measurement 54
3.11 Conclusion 56
CHAPTER 4: 57
CROSSED DIPOLE ANTENNA 57
4.1 Introduction 57
4.2 Initial theory and design 57
4.3 Modelling of printed dipoles 58
4.3.1 Simulation: Printed strip dipole 58
4.3.2 Dual polarized dipoles 60
4.3.3 Addition of a reflector 61
4.3.4 Addition microstrip feeders 62
4.4 Simulation and manufacturing 64
4.4.1 Radiation patterns and gain measurements 65
4.4.2 Optimisation 67
4.5 Conclusion 69
CHAPTER 5: 71
CROSSED DIPOLE ANTENNA WITH IMPROVED FEED SYSTEM 71
5.1 Introduction 71
5.2 Modelling 71
5.2.1 Substrate effects 71
5.2.2 Single printed dipole 73
5.2.3 Crossed printed dipoles 75
5.3 Final design 80
5.4 Fabrication and measurements 84
5.5 Dual polarization and circular polarization capabilities 86
5.6 Conclusion 87
CHAPTER 6: 89

CONCLUSION 89
REFERENCES 92
PUBLICATIONS 97
APPENDIX A1 98
Equipment 98
APPENDIX A2 102
Antenna fabricated 102
APPENDIX A3 105
3D Simulated Radiation Patterns 105
APPENDIX A4 107
Measured Radiation Patterns 107
APPENDIX A5 110
Gain and radiation patterns measurements 110
APPENDIX A6 112
Impedance and wavelength calculations 112
APPENDIX A7 113
Meshing and coordinate systems in CST Microwave Studio 113
APPENDIX A8 115
Substrate effects 115
APPENDIX A9 117
Regulations 117

LIST OF FIGURES

Fig.2.1: Antenna as a circuit element 16
Fig.2.2: Isolation between two antennas 17
Fig. 2.3: Spherical coordinate system (ϕ, θ, r) 18
Fig. 2.4: Polarization ellipses 20
Fig.2.5: Sinusoidal current and charge distribution on halfwave dipole 22
Fig. 2.6: Cylindrical dipole 24
Fig.2.7: Electrical equivalent radius 25
Fig.2.8: Planar reflector 27
Fig.2.9: Coaxial balun 29
Fig.2.10: Microstrip balun 29
Fig.2.11: Unbalanced coaxial cable 30
Fig.2.12: Dipole fed by a coaxial cable 30
Fig.2.13: Marchand balun 31
Fig.2.14: Log Periodic balun 32
Fig.2.15: Tapered balun 33
Fig.2.16: Marchand Tapered balun 33
Fig.2.17: Tapered balun use in a broad-band antenna 34
Fig.2.18: Double Y balun CPWFGP – CPS 34
Fig.2.19: Radial stub balun 35
Fig.2.20: LC balun using a radial stub balun 36
Fig.2.21: Quarter wavelength balun 37
Fig.2.22: Printed dipole antenna with a quarterwave microstrip balun 38
Fig.2.23: Microstrip transmission line 39
Fig.2.24: Electric and magnetic field lines of a Microstrip line 39
Fig.2.25 Time domain solver operation 42
Fig. 2.26: Transmission line with a two port network 43
Fig.3.1: Single patch antenna and coordinate system 46
Fig.3.2: Smith Chart showing the impedance at the edge of the patch 48
Fig.3.3: Simulated Return loss versus frequency for the patch with matching section 48
Fig.3.4: Measured Return loss over wide band (1-6 GHz) 49
Fig.3.5: Measured Return loss versus frequency for the single Patch 49

Fig. 3.6: Radiation pattern for single patch, E-plane (ZX-plane) 50
Fig.3.7: Radiation pattern for single patch, H-plane (ZY-plane) 51
Fig.3.8: Dimensions and array spacing 52
Fig.3.9: Modelled microstrip array and different feed lines 52
Fig.3.10: Return Loss for the microstrip array 53
Fig. 3.11: Radiation pattern for 2x2 array, E-Plane (ZY-plane) 54
Fig.3.12: Radiation pattern for 2x2 array, H-plane (ZY-plane) 54
Fig. 3.13: Two antenna system for the measurement of antenna gain 55
Fig. 4.1: Length of a dipole 58
Fig. 4.2: Single printed dipole 59
Fig.4.3: Simulated return loss vs frequency for single printed dipole 59
Fig.4.4: Orthogonal dipoles 60
Fig.4.5: Simulated return loss and isolation vs frequency for orthogonal dipoles 60
Fig. 4.6: Orthogonal dipoles & reflector 61
Fig. 4.7: Simulated return loss and isolation for orthogonal dipoles & reflector.. 62
Fig. 4.8: Dual polarized antenna, microstrip feeders 63
Fig. 4.9: Stripline , Plane XY 64
Fig.4.10: Return Loss for the dual polarized antenna 65
Fig. 4.11: Isolation for the dual polarized antenna 65
Fig.4.12: Radiation pattern for dual polarized antenna. H plane (ZX) 66
Fig.4.13: 3D Radiation pattern for dual polarized antenna. Illustrating the squint66
Fig. 4.14: New design of the dual polarized antenna 67
Fig.4.15: Simulated return loss for the new dual polarized antenna 68
Fig.4.16: Simulated isolation for the new dual polarized antenna 68
Fig. 4.17: 3D Radiation pattern for dual polarization antenna. No squint 69
Fig. 5.5: Quarter wavelength balun structure 74
Fig. 5.6: Quarter wavelength balun structure 74
Fig. 5.7: Return loss for a single dipole using a quarter wavelength balun 74
Fig. 5.8: Return loss for a single dipole using an optimized quarter wavelength balun 75
Fig. 5.9: Feeding structure for crossed dipoles 75
Fig. 5.10: Return loss for crossed dipoles using a quarter wavelength balun 76
Fig. 5.11: Isolation for crossed dipoles using a quarter wavelength balun 76
Fig. 5.12: Parasitic reflector centrally mounted 77

Fig. 5.13: Return loss for crossed dipoles and a parasitic reflector using a quarter wavelength balun 77
Fig. 5.15: Transformer lines 79
Fig. 5.16: Triangular shape 79
Fig. 5.17: Combined shape 79
Fig. 5.18: Geometry for the printed crossed-dipole antenna 80
Fig. 5.19: Final model and coordinate system 81
Fig. 5.20: Simulated return loss for the final design 81
Fig.5.21: Simulated isolation for the final design 82
Fig. 5.22: Normalised simulated radiation pattern for -45 degrees plane at 2.5GHz 83
Fig. 5.23: Normalised simulated radiation pattern for +45 degrees plane at 2.5GHz 83
Fig. 5.24: Photograph of the fabricated antenna 84
Fig. 5.25: Measured impedance bandwidth and isolation between ports for the crossed dipole antenna 85
Fig. 5.26: Normalised measured radiation pattern for +45 degrees plane at 2.5GHz 86
Fig. 5.27: Normalised measured radiation pattern for -45 degrees plane at 2.5GHz 86
Fig. 5.28: Measured axial ratio 87
Fig. A1.1: Network analyser Anritsu 37369A 98
Fig. A1.2: Network analyser Hewlett Packard 8753B 99
Fig. A1.3: Network analyser Agilent Technologies E5070B 100
Fig. A1.4: Network analyser ZVA24 Rohde&Schwarz 101
Fig. A2. 1.: Microstrip single patch 102
Fig. A2. 2: Microstrip Array 102
Fig. A2. 3: Crossed dipole antenna with tapered balun feed 103
Fig. A2. 4: Crossed dipole antenna with improved feed system 103
Fig. A2. 5: Crossed dipole antenna with improved feed system, left view 104
Fig. A2. 6: Crossed dipole antenna with improved feed system, front view 104
Fig. A 3.1: 3D Radiation pattern for microstrip single antenna 105
Fig. A3.2: 3D Radiation pattern for microstrip array antenna 105
Fig. A3.3: 3D Radiation pattern for the dual polarized antenna 106

Fig. A3.4: 3D Radiation pattern for the dual polarized antenna with improved feed system 106
Fig. A4.1: Measured radiation pattern for -45 degrees plane 107
Fig. A4.2: Measured radiation pattern for +45 degrees plane 108
Fig. A4.3: Measured gain 109
Fig. A5.1: Antenna pattern measurement set-up 110
Fig. A5.2: Free space elevated antenna range 111
Fig. A6.1: Impedance calculation 112
Fig. A6.2: Wavelength calculation 112

ACRONYMS

FITD	Finite Integration Time Domain
HSDPA	High Speed Downlink Packet Access
IEEE	Institute of Electrical and Electronics Engineers
ISM	Industrial, Scientific and Medical
LAN	Local Area Networks
LHCP	Left Hand Circular Polarization
LOS	Line of Sight
MIC	Microwave Integrated Circuit
NLOS	Non Line of Sight
OFDM	Orthogonal Frequency Division Multiplexing
OFDMA	Orthogonal Frequency Division Multiplexing Access
PCB	Printed Circuit Board
RF	Radio Frequency
RHCP	Right Hand Circular Polarization
TEM	Transverse Electromagnetic Mode
UHF	Ultra High Frequency
UWB	Ultra Wide Band
VNA	Vector Network Analyzer
VHF	Very High Frequency
VSWR	Voltage Standing Wave Ratio
WiBro	Wireless Broadband
Wi-Fi	Wireless Fidelity
WiMAX	Worldwide Interoperability for Microwave Access
WLAN	Wireless Local Area Networks
XPR	Cross Polarization Ratio

CHAPTER 1

INTRODUCTION

In the last decade, many wired Local Area Networks (LAN) communications systems have been replaced by Wireless Local Area Networks (WLAN). In July 1990, the Institute of Electrical and Electronics Engineers formed a working group (IEEE 802.11) to establish a worldwide standard for WLANs. By that time, a number of radio LAN products had been developed in the ISM (Industrial, Scientific and Medical) bands, 902-928 MHz, 2.4-2.5 GHz and 5.73-5.88 GHz. These frequency bands are unlicensed and can be used for data transmissions with some power restriction. The common name used in the commercial environment for these standards is Wi-Fi. In 1997 the first standard for WLANs was approved and in 1999 the well known standard IEEE 802.11b was published. This system operates in the frequency range of 2.4-2.5 GHz and has a bit rate of 5.5 and 11 Mbps. In the same range of frequencies, the IEEE 802.11g standard was developed, which supports a data rate of up to 54 Mbps. Other standards such as IEEE 802.11a and IEEE 802.11n have been set to operate in the 5GHz bands. In the summer of 2005 a new wireless standard was certified (3.5GHz band), 802.16-2004, otherwise, known as WiMAX. The standard 802.16 cover frequencies from 2 to 66GHz. For frequencies below 11GHz, where propagation without a direct line of sight (LOS) must be accommodated, three alternatives are provided to support non-LOS (OFDM, OFDMA and single carrier modulation). The ability to support near-LOS and non-LOS scenarios require additional physical functionality, such as the support of advanced interference mitigation/coexistence and multiple antennas. Emerging technologies like UWB, HSDPA, WiMAX mobile (802.16e), WiBro (with thousand of clients in South Korea) operate also in the 2GHz band. Wireless communication is placing new demands on antenna designs. These include dual or triple-band operation, wideband operation, polarization agility and increased gain. This report describes the results of various wireless antennas designs, simulations and measurements carried out at 2.45 GHz, which are useful in the design of communication systems compliant with IEEE 802.11, Bluetooth, Home RF, WiMAX and WiBro open wireless standard.

Many different types of antennas including dipoles, patches, and monopoles are available in the wireless market, but due to the immense growth of wireless systems and the number of users, polarization diversity will be a requirement in the future in order to increase the capacity of the cells. Leading antenna manufacturers such as Andrew Corporation or RFS. include 2.4GHz base station antennas in their catalogues but they are not dual polarized antennas. The operating frequency range for 802.11b and 802.11g (ETSI) goes from 2.412GHz (channel 1) to 2.472 GHz (channel 13), thus 60MHz bandwidth. The purpose of this project consists of obtaining a dual-polarized base station antenna with an isolation of 20dB or greater between channels and realising a return loss greater than 10dB over the frequency range above. It is also very important for the performance of the antenna that the radiation patterns are without squint and with a regular shape (20dB front to back ratio and 20dB crossed polar rejections level) over the frequency band. In terms of gain the aim for the antenna is to obtain a gain greater than 6.dBi over the full frequency range.

Because of the rapid growth in emerging wireless technologies and applications, there is an increased demand for base station antennas which fulfil the above requirements.

Wireless systems like Wibro (2.3GHz) and Wimax mobile (2.5GHz) are technologies that operate in a similar way that cellular networks like GSM or UMTS do (systems that use base station antennas).

Chapter 2 describes the most important antenna parameters as well as an introduction to dipole antenna theory and dipole feeder systems. The feed systems include various coaxial and printed baluns which provide both impedance matching and balanced-to-unbalanced transformation. This is essential to minimise feeder currents, spurious radiation and gain reduction. This chapter also introduces microstrip and substrate parameters. Chapters 3-5 present a performance evaluation of the different microstrip and printed dipole antennas that were designed and fabricated operating in the 2.4GHz band, in order to fulfil the requirements demanded by modern wireless applications. CST Microwave Studio, a 3D electromagnetic simulation software tool, based on the finite integration time domain (FITD) method, was used to model and simulate the antennas. Chapter 3 describes the design of two microstrip antennas, a single

halfwave rectangular patch antenna and a microstrip patch array. The single rectangular patch was modelled and fabricated in order to learn about the modelling accuracy. The array comprised a high gain two by two array of rectangular patchs, which were fabricated on high quality substrate. A full range of measurements were carried out. Chapter 4 describes the design of a dual-polarized directional printed antenna. The choice of dimensions and the effect of planar structures and dielectrics on the design are evaluated. The dipoles are fed using a perpendicular tapered balun structure that consists of two back to back microstrip substrates. A parasitic reflector is added in order to improve the directivity. Different substrate types were evaluated in the antenna development. Chapter 5 shows the design of a dual-polarized printed antenna (crossed-dipole) which is fed using a better balanced-to-unbalanced transformer, namely a quarter wave balun. The feeding network is a microstrip structure and it is also perpendicular to the dipoles. It also employs a parasitic reflector. The improved antenna performance is fully measured. The antenna presents both dual-linear and circular polarization capabilities. This polarization diversity is required for modern wireless systems. The low profile and the low cost are common features for these dipole structures. The final antenna fulfils the specification demanded by wireless base-stations.

CHAPTER 2

BACKGROUND THEORY

2.1 Principles of antennas

In this chapter some of the more important parameters of antennas are described. These are necessary for a clear understanding of the design process.

Input Impedance:

The antenna presents to the transmission line an impedance Z_i.

$$Z_i = \frac{V}{I} \qquad \text{Eq.2.1}$$

where V and I are the voltage and current at the antenna terminals.

$$Z_i(f) = R_i(f) + jX_i(f) \qquad \text{Eq.2.2}$$

where **¡Error! Imposible crear objetos modificando códigos de campo.** **¡Error! Imposible crear objetos modificando códigos de campo.** Resonant Antenna Eq.2.3

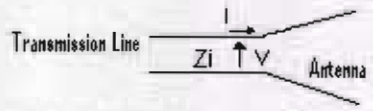

Fig.2.1: Antenna as a circuit element

At microwave frequencies the input impedance is expressed in terms of reflection coefficient, usually return loss or voltage standing wave ratio (VSWR).

Return loss

The return loss is based on the magnitude of the reflection coefficient.

The reflection coefficient Γ is defined as

$$\Gamma = \frac{Z_L - Z_0}{Z_L + Z_0} \qquad \text{Eq.2.4}$$

where Z_0 is the characteristic impedance and Z_L is the load impedance.

The return loss is usually expressed in dB and is given by

$$20\log|\Gamma| \qquad \text{Eq.2.5}$$

The voltage standing-wave ratio (VSWR) may be found using

$$VSWR = \frac{1+|\Gamma|}{1-|\Gamma|} \qquad \text{Eq.2.6}$$

Antenna isolation

Sometimes communications equipment is connected to several antennas (via several ports) in order to achieve polarization or space diversity. If the antennas are in close proximity, the isolation between the antennas (ports) becomes an important parameter. For an antenna comprising two elements, isolation can be defined as the ratio of the received power P_i at the adjacent port to the transmitted power P_{tx}. (Figure 2.2).

$$I = 10\log\frac{P_i}{P_{tx}} \qquad \text{Eq.2.7}$$

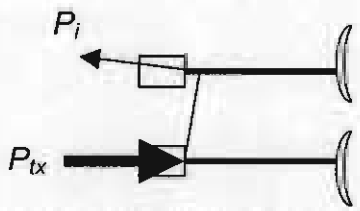

Fig.2.2: Isolation between two antennas

Bandwidth

The useful frequency range of an antenna depends, in general, on both its radiation pattern and impedance characteristics. Some narrowband antennas such as thin dipoles exhibit rapid impedance variations with frequency, while the radiation pattern changes less rapidly. However, some wideband antennas, such a biconical dipoles, exhibit impedance characteristics which are satisfactory over such a large bandwidth that the variation in the radiation pattern determines the frequency limits. Assuming no pattern degradation with frequency, the antenna impedance bandwidth is defined as the frequency limits f_1 and f_2 for which the

voltage standing wave ratio (VSWR) at the antenna feed terminal remains below an acceptable value. A commonly accepted value at microwave frequencies is a VSWR of 2:1 (Return loss -10dB).

Radiation patterns and coordinate systems

The radiation pattern of an antenna is one of its most important characteristics. The pattern is a three-dimensional representation of the field intensity with the antenna located at the origin of the spherical coordinate system as a function of the angular coordinates (ϕ, θ).

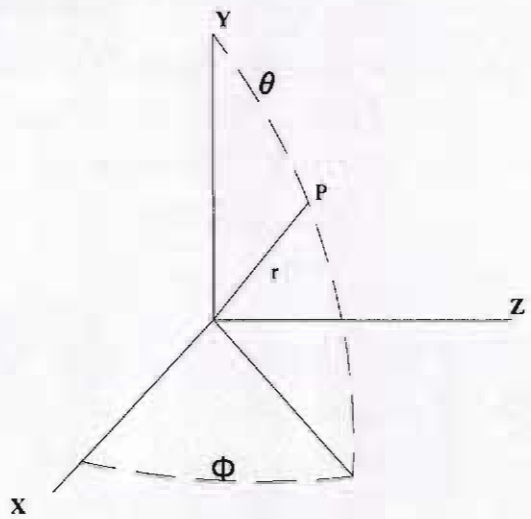

Fig. 2.3: Spherical coordinate system (ϕ, θ, r)

The patterns may be displayed with either polar or Cartesian coordinates. Polar plots are commonly used for low gain antennas such as dipoles or single element microstrip antennas. A side lobe is defined as a radiation lobe in any direction different than that the main lobe. The magnitude of the radiated power is usually normalized to maximum gain.

Gain

Antenna gain is classified into directive gain (directivity) and absolute gain. The definition of directive gain does not include input impedance mismatch losses and losses inside the antenna (e.g. ohmic losses). The absolute gain includes all

sources of loss for the antenna and is the term most often used when specifying the transmission power and link margin in real operating environments. Since the power radiated by a Hertzian dipole is concentrated in particular directions, the field in the direction of maximum radiation must be greater than that produced by an omnidirectional radiator emitting the same total power. The gain G of any given radiator may be defined in terms of the signal power received at a distant point in the direction of maximum radiation as the ratio between the maximum power received from a given antenna and the maximum power received from a reference antenna, assuming the same input power in both cases. The gain is also measured by comparing the received electric field strength between the standard gain antenna and the given antenna. The isotropic radiator is often used as the reference antenna, but it is sometimes convenient to use other reference standards, for example, the half-wavelength dipole. For a half-wavelength dipole antenna the absolute gain is G_d=2.15dBi.

Directivity

The directivity D of an antenna relative to an isotropic element is given by the relationship between the maximum radiation intensity and the average intensity of radiation.

At a certain distance from the antenna, the directivity can be expressed as the relationship between the maximum value and the average value of the Poynting vector. This relationship is unitless.

As the average value of the Poynting vector on a sphere is given for:

$$S(\theta,\phi)_m = \frac{1}{4\pi}\int_0^{2\pi}\int_0^{\pi} S(\theta,\phi)d\Omega \ (\mathrm{W/m^2}) \qquad \text{Eq.2.8}$$

The directivity can be written as:

$$D = \frac{1}{\frac{1}{4\pi}\int_0^{2\pi}\int_0^{2\pi}\frac{S(\theta,\phi)}{S(\theta,\phi)_{max}}d\Omega} = \frac{1}{\frac{1}{4\pi}\int_0^{2\pi}\int_0^{\pi} P_n(\theta,\phi)d\Omega} = \frac{4\pi}{\Omega_A} \qquad \text{Eq.2.9}$$

Polarization

The initial polarization of a radio wave is determined by the antenna that launches the wave into space. For plane waves, only the polarization properties of the electric field are specified. The plane of polarization is defined as the plane which contains the electric field vector and the magnetic field vector and is orthogonal to the direction of propagation. The tip of the electric field vector moves along an elliptical path in the plane of polarization. The polarization of the wave is specified by the orientation and shape of this ellipse and the direction in which the electric field vector traverses the ellipse. The shape of the ellipse is specified by the axial ratio, i.e. the ratio of major axis to minor axis. The axial-ratio is defined as

$$AR(\text{dB}) = 20\log_{10}\frac{\text{major axis length}}{\text{minor axis length}} \qquad \text{Eq.2.10}$$

The orientation is specified by the tilt angle, which is the angle between the major axis and a reference plane when viewed looking in the direction of propagation. The direction in which the electric field traverses the ellipse is the sense of polarization. This can be either counter-clockwise or clockwise when viewed looking in the direction of propagation.

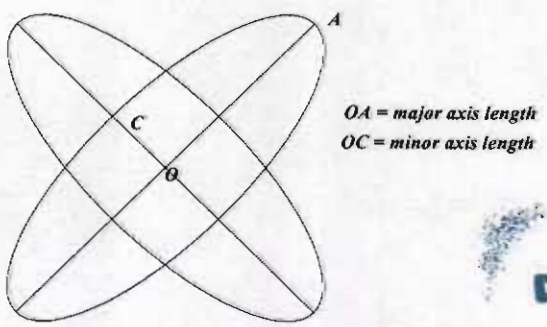

Fig. 2.4: Polarization ellipses

Cross-Polarization

Mobile communication systems traditionally use vertical polarization in the VHF (30 to 300 MHz) band because the horizontal polarization component becomes very weak at a height of 1 to 2 meters above the mobile station ground level.

Although recent terrestrial mobile communication system in the UHF band (300 MHz to 3 GHz) transmit vertically polarized waves from the base station, many obstacles in the propagation path reflect or diffract the transmitted waves and excite a horizontally polarized component. It is therefore important to know the cross polarization ratio (XPR) at a mobile terminal. The XPR is defined as the ratio between the vertically and the horizontally polarized components:

$$XPR = \frac{P_v}{P_h} \qquad \text{Eq.2.11}$$

where P_v and P_h are powers for the vertically and horizontally polarized components, respectively, at the measured site.

2.2 Dipole theory

2.2.1 Introduction

In this chapter dipole theory is described. Fundamental parameters such as input impedance and radiation patterns are examined for cylindrical and printed dipoles. A good definition of the function of an antenna was written by R. W. P. King [28]: *"the primary purpose of an antenna is to provide suitably localized and oriented paths for oscillating electric currents. The distributions in amplitude and phase of accelerated charges moving along these paths determine not only the admittance, but also all the characteristics of the electromagnetic field, including those associated with the directional properties of transmitters and receivers"*. From these words it is easy to think that one of the most important parameters to be considered for an antenna is the distribution of current. Some other very useful concepts to quote such as a radiator has a dual function of accepting energy from the transmission line and radiating it into space in desired directions or as no practical radiator can radiate uniformly in all directions, but such an omni-directional or isotropic radiator is a concept easy to visualize and it is a reference standard to which practical antennas can be related.

2.2.2 Half-wave cylindrical dipole

A very commonly used antenna is the half-wave dipole, whose length is approximately one-half of the free-space wavelength of the radiated wave. It is the longest uniform linear radiator which will support a standing wave for which all the elements of current are in phase. A half-wave dipole which is fed at its centre by means a transmission line is found to have a current distribution which is approximately sinusoidal, with a maximum at the centre and zero at the ends as shown in Figure 2.5. This type of radiator could be considered as a chain of Hertzian dipoles, therefore if the current were uniform the positive charge at the end of one Hertzian dipole would be cancelled by an equal negative charge at the opposite end of the adjacent dipole. At the extreme end of a dipole there is no current and therefore the radiation resistance would appear to be infinite when referred to the end. A cylindrical half-wave dipole is the shape most frequently used for this type of antennas.

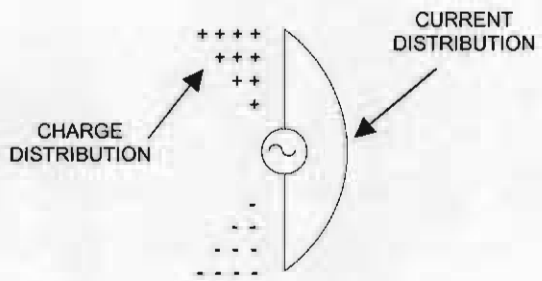

Fig.2.5: Sinusoidal current and charge distribution on halfwave dipole

Input impedance

Much of the initial analyses on the input impedance (resistance and reactance) has focused on thin cylindrical antennas. The effect and influence of the transmission lines or the junction connection to the antenna proper has not been considered in those theories. The input impedance Z_T of a center-fed cylindrical antenna is found by taking the ratio of the input or terminal voltage V_T and the current I_T at the input terminals:

$$Z_T = \frac{V_T}{I_T} = R_T + jX_T \qquad \text{Eq.2.12}$$

where R_T is the terminal resistance and X_T is the terminal reactance. Some authors including Hallen [29] and Schelkunoff [22] have presented the results of their

investigations as a series of plots of input impedance against dipole length. From these figures it can be seen that the reactive and resistive parts of the impedance vary considerably with the length of the dipole and are also somewhat dependent on the diameter of the dipole (Fig. 2.6). The important regions of the curves are those corresponding to a length of approximately half-wavelength. The input impedance, Z_{IN}, of a half-wave dipole as calculated by the induced electromagnetic fields method [36] gives the result:

$$Z_{IN} = 73.2 + j42.5\Omega \qquad \text{Eq.2.13}$$

This is the impedance at the centre of an infinitely thin dipole which is exactly a free space half-wavelength. It can be shown [36] that for a dipole of about 5 per cent less than half a wavelength, the impedance reduces to

$$Z_{IN} = 65\Omega \qquad \text{Eq.2.14}$$

This value is easier to match because it is purely resistive. In general, it has been observed that for a given wire length, the impedance variation become less sensitive as a function of frequency as the ratio $(l/2\lambda)$ decreases. Normally antennas are required to operate over a wideband of frequencies, so the variation of impedance with frequency should be as small as possible. Thus a thick dipole is desirable for wideband applications. A useful method to calculate the input impedance of a half wavelength cylindrical dipole antenna is based on the induced-emf method [22]. The reduced expression for the input impedance is given by

$$Z_i = R\left(k\frac{l}{2}\right) - j\left[120\left(\ln\frac{l/2}{a} - 1\right)\tan^{-1}\left(k\frac{l}{2} - X\left(k\frac{l}{2}\right)\right)\right] \qquad \text{Eq.2.15}$$

where Z_i is the input impedance of a centre-driven cylindrical antenna of total length l, the radius is a and the electrical length in radians $kl = 2\pi(l/2\lambda)$. $R(kl/2)$ and $X(kl/2)$ are functions that are tabulated and give values for the different lengths and wavelengths.

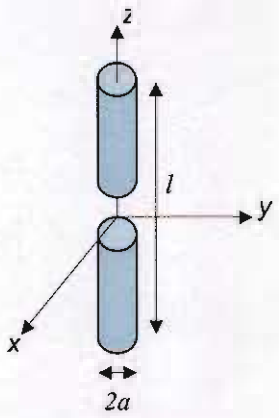

Fig. 2.6: Cylindrical dipole

Bandwidth

A very thin linear dipole has very narrowband radiation characteristics. Small changes in the operating frequency will result in large changes in its operational behaviour. In order to increase the bandwidth it is convenient to decrease the $l/2a$ ratio, thus using a larger radius.

Radiation Patterns

The pattern is essentially unaffected by the thickness of the wire in regions of high radiation. However, as the radius of the wire increases, the minor lobes diminish in intensity and the nulls are replaced by low level radiation. It has been shown [22] both experimentally and numerically that the patterns vary slightly with respect to the diameter of the antenna instead of being independent of the thickness.

2.2.3 Biconical dipoles

A common practice to construct cylindrical antennas with short conical sections at the input terminals is employed by many antenna designers. The conical sections are particularly desirable in order to reduce the shunt capacitance at the gap. The propagation in a biconical dipole can be treated as a conical waveguide which is similar in behaviour to a cylindrical waveguide. If the angles of the conical sections are small the antenna input impedance can be calculated by using Schelkunoff's theory. However wide-angle antennas are mainly used to achieve broadband operation. The angle should be chosen to be between 30° and 60° to achieve broadband characteristics.

2.2.4 Printed dipoles

A dipole may be realised on printed circuit board (PCB) and the dipole arms are therefore planar strips. The noncircular cross section may be approximated by an equivalent radius, a. As illustrated in Figure 2.7, a thin flat strip of width w may be approximated by the equivalent radius $a = 0.25w$ [29]

¡Error! Imposible crear objetos modificando códigos de campo.

Fig.2.7: Electrical equivalent radius

This concept represents in electrostatics the radius of a circular wire whose capacitance is equal to that of the noncircular geometry. Microstrip dipoles are planar structures which consist of a pair of collinear thin-strip conductors printed on the surface of a PCB. This kind of dipole is mainly used at higher frequencies where the substrate may be electrically thick due to its small size and simplicity. Thus the bandwidth may be quite broad. There are many ways to feed printed dipoles, although the radiation properties are independent of the excitation [11]. Printed antennas are widely used in mobile applications. The main antenna challenges in wireless communications systems research are to reduce the antenna size and improve performance.

The most commonly used materials in the construction of microstrip antennas are: Unreinforced PTFE, Reinforced PTFE, Fused Quartz, 96% Alumina, 99,5% Alumina, Silicon, Sapphire, Semi-Insulating GaAs. The most important electrical parameters are the dielectric constant ε_r and the loss tangent $\tan\delta$. The following criteria must be considered for substrate selection. [5]:

- Possibility of surface-wave excitation.
- Effects of dispersion on the dielectric constant and loss tangent.
- Magnitude of copper loss and dielectric loss.
- Anisotropy, in any, in the substrate.
- Effects of temperature, humidity, and aging.
- Cost.
- Mechanical requirements, such as ease of conformability, machinability, and solderability, effects of vibrations on circuit dimensions, antenna weight and ability to withstand gravitational forces.

Nonelectrical properties like Useful Temperature Range (°C), Thermal Conductivity (W/cm-K), Coefficient Thermal Expansion (ppm/K), Temperature Coefficient of Dielectric Constant (ppm/K), Minimum Thickness (mil), Machinability, Solderability and Dimensional Stability are also very important.

2.2.5 Reflector theory

Reflector-type antennas are widely used in communications systems. Conventional reflector shapes are planar (large flat sheet, small flat sheet, corner), parabolic-arc, double-curvature, paraboloid, hyperbolic, elliptical and circular. These are used to modify the radiation pattern of a radiating element.

Plane sheet reflector

The reflector is generally a parasitic element with no connection to the feedline as shown in Figure 2.8. The driven element is a half-wave dipole that is oriented parallel to the reflector and separated by a distance *S*. The size of the reflector has an important effect on the radiation pattern. The gain of a half-wave dipole antenna with reflector in free space can be approximated by [29]:

$$G(\phi) = 2\sqrt{\frac{R_{11} + R_L}{R_{11} + R_L - R_{12}}}\left|\sin(S_r \cos\phi)\right| \qquad \text{Eq.2.16}$$

where $S_r = 2\pi\frac{S}{\lambda}$, and R_{11}, R_L, R_{12} are the self resistance of the driven element, the effective loss resistance, and the mutual resistance of the driven element and parasitic respectively. From the formula it can be shown that for a reflector spacing $S = \lambda_0/2$ the gain is 0 and that a spacing of less than a quarter of wave length is desirable. In order to achieve a reasonable compromise between the bandwidth and the gain, a spacing of $S = \lambda_0/4$ is chosen.

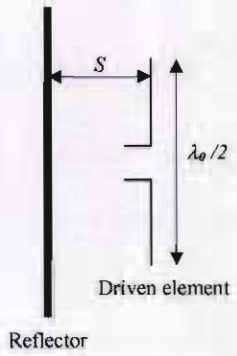

Fig.2.8: Planar reflector

2.3 Balanced and unbalanced feeder systems

2.3.1 Introduction

Input impedance of a transmission line

When a line is incorrectly terminated the input impedance is a function of the length, due to a standing wave of current and voltage.

For a lossless line, it can be shown that

$$Z_{in} = Z_0 \frac{Z_L + jZ_0 \tan(\beta l)}{Z_0 + Z_L \tan(\beta l)} \qquad \text{Eq.2.17}$$

where β is the phase constant, ($\beta=2\pi/\lambda$) and l is the line length. Resonant line sections may be used as series or parallel resonant circuits when terminated by open-circuits or short-circuits. For instance a quarterwave section terminated in a short circuit offers very high impedance at resonance and can be used in filters. Likewise a section terminated in an open-circuit offers low impedance at resonance. Hence, short circuit terminations are more common in coaxial lines and open circuits are used in microstrip and stripline.

For a line length of $l=\lambda/4$, $\beta l=\pi/2$ and

$$Z_{in} = Z_0 \frac{Z_0}{Z_L} = \frac{Z_0^{\,2}}{Z_L} \qquad \text{Eq.2.18}$$

This section transforms the impedance from Z_0 at one end to Z_0^2/ Z_L at the other end, and is known as a quarterwave transformer.

If $l=\lambda/2$, then $\beta l=\pi$

$$Z_{in} = Z_L \qquad \text{Eq.2.19}$$

For the case of $Z_T = 0$ (short circuit), it can be shown that

$$Z_{in} = jZ_0 \tan \beta l \qquad \text{Eq.2.20}$$

For line lengths $0 \leq l \leq \lambda/4$, the section offers an inductive Z_{in}

$$Z_{in} = jZ_0 \tan \beta l = j\omega L_{eq} \qquad \text{Eq.2.21}$$

For the case of $Z_T = \infty$ (open circuit), it can be shown that

$$Z_{in} = -jZ_0 \tan^{-1} \beta l \qquad \text{Eq.2.22}$$

For line lengths $0 \leq l \leq \lambda/4$, the section offers a capacitive Z_{in}

$$Z_{in} = -jZ_0 \tan^{-1} \beta l = -j\frac{1}{\omega C_{eq}} \qquad \text{Eq.2.23}$$

Balun fundamentals

Baluns are often a point of discussion and confusion and they serve many applications in RF and microwave communications. Owing to their importance, several balun (acronym for balanced-to-unbalanced transformer) designs are described in this chapter. Many analog circuits require balanced inputs and outputs in order to reduce noise and high order harmonics as well as improve the dynamic range of the circuits. Baluns are key components in many wireless communication systems for realizing components such as balanced mixers, push-pull amplifiers, antenna-feed networks and frequency multipliers.

In some microwave applications a balanced signal excitation may be required. In other applications, an unbalanced line may need to interface with balanced lines or circuits. A conventional technique for transforming back and forth between balanced and unbalanced configurations is the use of a balanced and unbalanced

transformer, typically referred to as balun. Figures 2.9 and 2.10 show unbalance to balance transitions for different technologies.

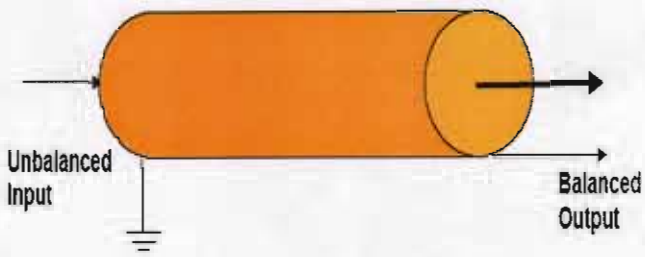

Fig.2.9: Coaxial balun

Fig.2.10: Microstrip balun

A balun is a device that presents high local impedance to radiating currents on shielded cable. The signal of a balanced circuit structure comprises two signal components with the same magnitude but 180-degree phase difference. Baluns are designed to have minimum loss and equal balanced impedances. A balun is also an impedance matching transformer that converts the impedance of one interface to the impedance of another interface. Baluns sometimes convert impedance, but that is an additional function that should be considered separately from their action. In the Figure .2.11 an unbalanced transition is shown. The coaxial cable is classified as an unbalanced line because the voltage on the outer conductor of the cable is always at zero potential.

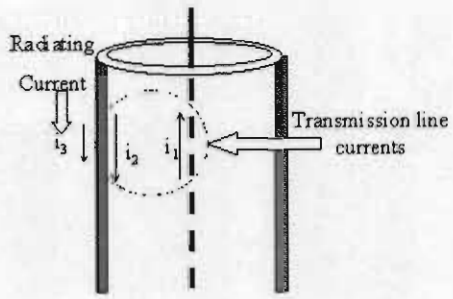

Fig.2.11: Unbalanced coaxial cable

In practice we need baluns even when feeding asymmetrical antennas (such as off-centre fed dipoles or loops), because it is not desirable for the feeder cable to become part of the antenna system and it is necessary for the current on either side of the antenna feed point to be equal. An illustration of the undesired currents that flow on the outer conductor of a coaxial cable, when feeding a dipole, are shown in Figure 2.12.

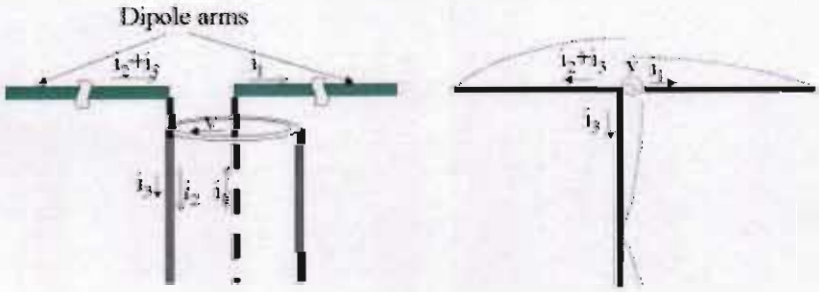

Fig.2.12: Dipole fed by a coaxial cable

A balanced antenna fed by a two-wire transmission line is a balanced system with respect to the lines, provided that the two feed points on the balanced antenna have the same orientation and placement with respect to the lines. One reason why we need a balun is because an unbalanced feed current affects the feed point impedance of the dipole antenna, which causes considerable difficulty when trying to measure the input impedance of an antenna or other device. The antenna's radiation pattern may also be adversely affected due to the asymmetrical currents as well as radiation from the radiating currents on the feed line. Wideband devices are the trend of the new wireless communications systems. To realise these bandwidths, baluns are commonly used in antenna-feed networks.

2.3.2 Microstrip balun

There are a wide-range of printed/microstrip balun topologies in use. They have the advantage of being inexpensive and easily fabricated on the printed circuit board (PCB) or Microwave Integrated Circuit (MIC) substrate. They are easy to implement and offer good performance. Some of the more important topologies and applications are now described. The simplest printed balun is the coupled line balun, also called a parallel-line balun shown in Figure 2.10. The structure is a quarter of a wavelength long at the centre frequency. It is capable of bandwidths of over an octave, provided that the coupling between the lines is high enough.

2.3.2.1 Marchand Balun

An improvement on the parallel-line balun is a printed version of the Marchand Balun. This is derived from the co-axial balun, described by Nathan Marchand in 1944. The printed version of the Marchand balun is shown in its simplest form in Figure 2.13. This is more tolerant to low even mode impedance (low coupling ratio) than the parallel line balun and has a wider bandwidth. A planar Marchand balun consists of two coupled sections, each of which is one quarter-wavelength long at the center frequency of operation.

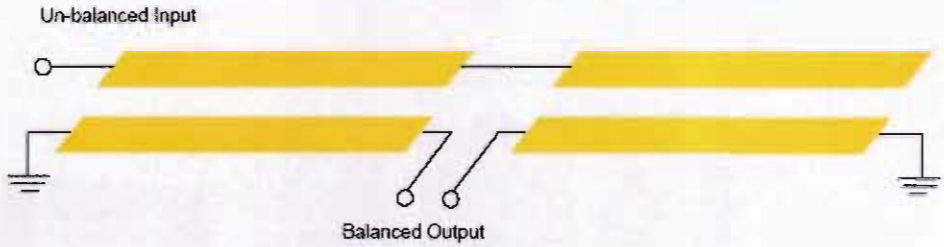

Fig.2.13: Marchand balun

The Marchand balun has a bandwidth of approximately one octave [39]. This balun has broad-band characteristics and traditionally uses coupling to achieve the 180 degree phase shift. By varying the coupling factor of the coupled sections, a wide range of impedance transforming ratios can be achieved. Different techniques are used [25] such as adding a resistive network between the balun outputs to achieve balun output matching and isolation. This class of matched balun with impedance transformation capabilities is invaluable in the design of balanced microwave circuits such as mixers, push–pull amplifiers, and frequency

doublers. An interesting application of Marchand design is a breast cancer scanner balun. The breast cancer detection system operates at a center frequency of 4 GHz and frequency range 3-5 GHz. A simplified implementation of the Marchand balun could satisfy the design criteria because the circuit must be confined to a single plane due to fabrication limitations. An improvement of the Marchand balun is carried out by using compensated coupled lines. It employs capacitive compensation to equalize or compensate the phase velocity inequality in microstrip couplers. This will increase the directivity and thus provide broadband characteristics with good isolation.

2.3.2.2 Log Periodic Balun

The design of this planar balun structure is based on the log-periodic antenna theory. With this structure the bandwidth that can be achieved is more than one octave [32]. This structure consists of several half-wave resonators with lengths that vary according to a fixed geometric ratio, τ (<1), thus forming a Log-Periodic structure.

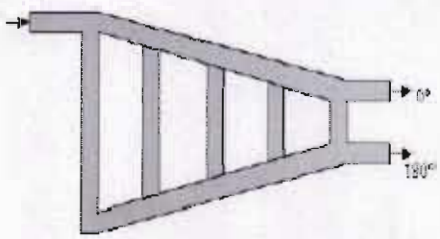

Fig.2.14: Log Periodic balun

To design a log periodic balun, the lengths of the resonators and the distances between them are related by

$$\frac{1}{\tau} = \frac{d_{n+1}}{d_n} = \frac{l_{n+1}}{l_n} = \frac{\lambda_{n+1}}{\lambda_n} \qquad \text{Eq.2.24}$$

Where, τ is the geometric ratio (<1), d is the distance between resonators, l is the length of the resonators, and λ is the wavelength. This design is suitable for applications in wireless communication circuits such as mixers, amplifiers and antennas.

2.3.2.3 Tapered balun

The tapered balun is one of the most popular types and is widely employed as a basic element of single and double balanced mixers. Tapered baluns are inherently broadband devices, due primarily to the natural potential difference between signal and ground conductors. The structure has a gradual taper in width to increase the bandwidth performance of the balun transition. There are two basic circuit implementations for the tapered balun (Fig. 2.15 and Fig 2.16).

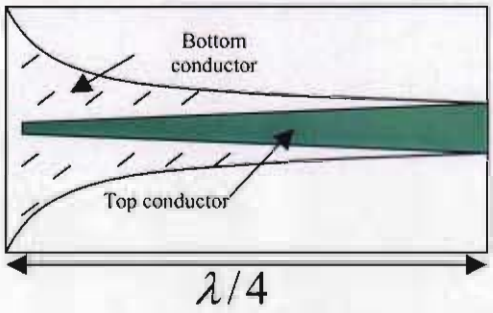

Fig.2.15: Tapered balun

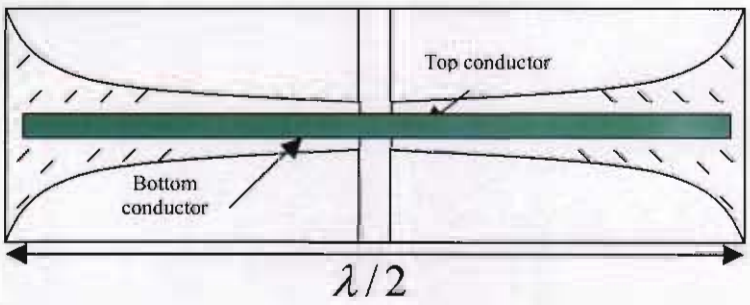

Fig.2.16: Marchand Tapered balun

The inline-tapered balun requires a gradual taper in both the top and bottom conductors' widths, and the signal potential is always between the conductors. There are many different techniques to design the taper of the conductors (logarigmic, triangular...)[29]. The balun requires the indicated lengths for proper operation and impedance-transformation properties. The Marchand tapered balun has the differential output at the centre of the structure. The design of antennas consisting of two strip dipoles, the arms of which are printed on opposite sides of an electrically thin dielectric substrate and connected through a parallel stripline is

shown in the Figure 2.17. A tapered balun is used to achieve broad bandwidth [13].

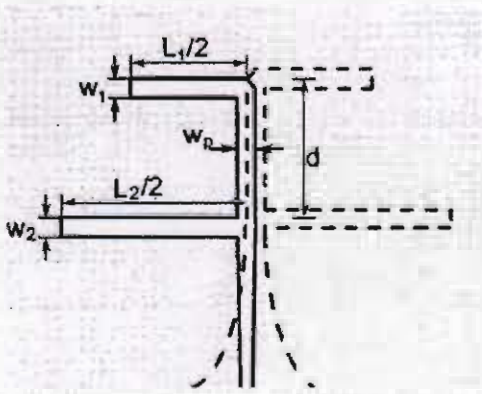

Fig.2.17: Tapered balun use in a broad-band antenna

2.3.2.4 Double Y balun

The double Y balun is a new class of miniature and wideband balun which is suitable for MMICs and wireless applications, because of the small dimensions, simple design and impressive bandwidth. The double Y balun is based on a six port double Y junction, which consists of three balanced and three unbalanced lines placed alternately around the centre of the structure. In this structure, each two opposite ports are uncoupled when the junction effects can be neglected and the other four ports are matched. A double Y balun realized using coplanar wave guide with ground plane to coplanar-strip is shown in Figure 2.18. The signal incident on the unbalanced port will be equally divided between the other four ports. Similarly, and input signal at the balanced port will also be equally divided between the four output ports, but one pair of opposite ports will be in phase opposition to the others.

Fig.2.18: Double Y balun CPWFGP – CPS

In order to make a structure which works as a balun with perfect transmission between an opposite balance and unbalanced ports, opposed pairs of lines should have reflection coefficients with opposite phases (i.e. one pair of lines should be short circuited, the other open circuited). However, parasitic resonances have been

observed in this kind of balun [44]. They depend on the length of the input transmission lines and on the specific topology of the double Y balun. They are caused by a difference in the characteristic impedances of the lines or by different electrical lengths of the open and short circuited stubs.

2.3.2.5 Radial stub balun

The radial stub balun is commonly used in hybrid and monolithic microstrip circuits. When very low impedance levels are required, the behaviour of the conventional stub degrades as a result of the excitation of higher order modes. This kind of balun provides a low input impedance level for a wide frequency band. A simple design procedure is described in [29]. The radial stub is inserted in series into the transmission line with the width of the line made as small as possible to achieve the original radial stub structure (a radial stub balun is shown in Figure 2.19). The radius is about λ/4 and the radial stub is designed as an RF shunt. This is done by fixing the dimension *Ri* and the angle α and then optimising the radius. The bandwidth increases with increase of the angle α. A radial stub behaves well for angles above 45°. The main application of the radial stub is power supply feeding.

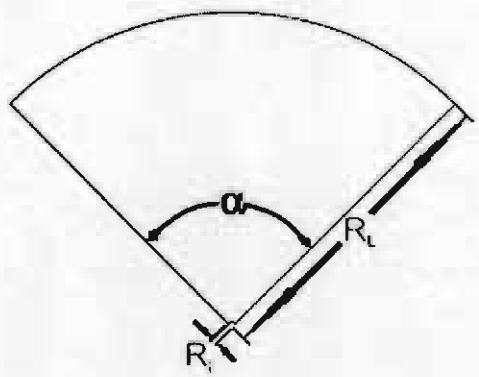

Fig.2.19: Radial stub balun

In combination with a λ/4 transformer the short circuit is transformed into an open circuit (Figure 2.20). The point the where stub joins the choke is the port where the DC supply is connected. At that position, the RF signal is short-circuited. On the other end of the choke an open-circuit is seen, so that the RF signal is not affected by the power supply feed.

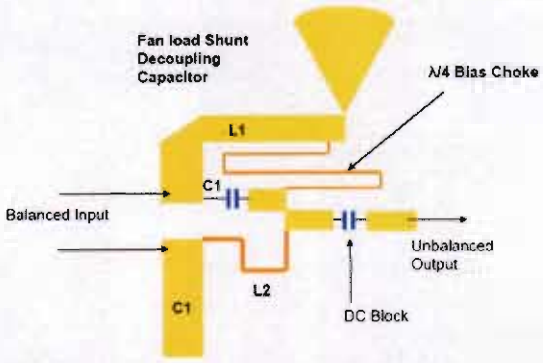

Fig.2.20: LC balun using a radial stub balun

A very common use of the radial stub balun is a transition between the coplanar stripline and a microstrip structure, where at resonance, the radial stub provides a virtual short circuit and RF continuity between the coplanar strip conductor and the microstrip ground plane.

2.3.3 Quarter wavelength balun

The "two wire" line transition is based on the well known quarter wave short circuit sleeve or "bazooka" balun. Because the balun has an electrical length of one-quarterwave, the impedance at the mouth of the cable becomes infinite, effectively suppressing the leakage current from the dipole. The "bazooka" balun operates by sliding an additional cylinder or sleeve over the outer surface of a coaxial cable. This sleeve is short-circuited to the coaxial $\lambda_0/4$ away from the feed point. A second coaxial transmission line is hence created with the new sleeve being the braid of the new line and the original coaxial outer becomes the inner of the new line. A better approach is offered by not using a sleeve, but rather creating a two wire transmission line by attaching a second wire of nominally the same diameter as the coaxial outer to the line. The characteristic impedance of a two wire line is given by:

$$Z_0 = 120 \ln\left(\frac{d}{a}\right) \qquad \text{Eq.2.25}$$

which results in higher values than for the coaxial situation. Some practical issues to consider with this type of line is the fact that the balun could now introduce asymmetry and one should position it along the braid at a position perpendicular to the two dipole arms. A practical quarterwave balun is illustrated in Figure 2.21.

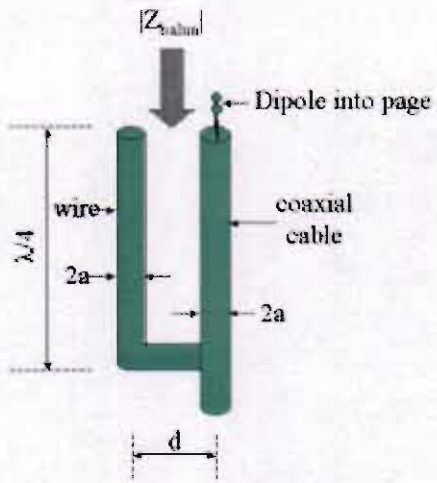

Fig.2.21: Quarter wavelength balun

Using this kind of balun to feed a dipole with the same arm dimensions, the balun is soldered to one of the dipole arms at the cable sheath. The input impedance of the dipole is modified by the loading effect of the balun, except at resonance, where it presents an open circuit. At other frequencies, the measurements are a parallel combination of the antenna and the balun impedance. This kind of balun is also used on microstrip devices. As it can be seen in the next chapters a printed dipole antenna employs a printed microstrip balun which acts as an unbalanced-to-balanced transformer from the feed coaxial line to the two printed dipole strips. The length of the dipole strip and the balun microstrip are both about a quarter wavelength. An interesting application of a microstrip quarterwave balun is illustrated in Figure 2.22, where the ground plane of the microstrip line and the dipole antenna strips are in the same plane [10]. A via-hole is used to feed the dipole as well as provide the same phase on the two dipole arms (points 1 and 2). Due to the 180° phase difference between the top strip and the ground plane of the microstrip line, feed point 2 of the printed dipole strip will have 180° phase difference with respect to feed point 1.

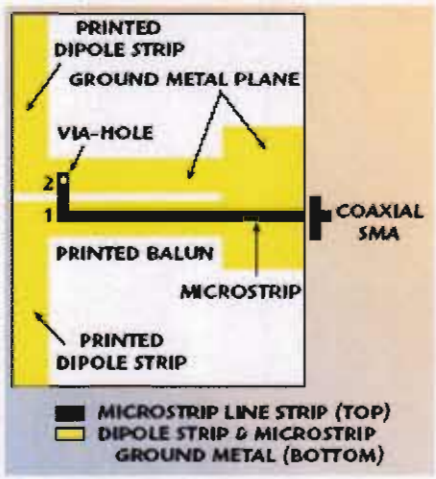

Fig.2.22: Printed dipole antenna with a quarterwave microstrip balun

2.4 Microstrip theory

One of the most popular RF transmission lines is microstrip. This kind of transmission line is commonly used primarily because it can be fabricated by photolithographic processes and is easily integrated with other passive and active microwave devices. Figure 2.23 shows the geometry of a microstrip line. It consists of a conductor of width W that is printed on a thin grounded dielectric substrate of thickness d and relative permitivity ϵ_r. If the dielectric were removed (ϵ_r=1), one could think of the line as two-wire line consisting of two flat strip conductors of width W, separated by a distance $2d$ (image theory). The behaviour of a microstrip line is special due to two main characteristics:

The presence of a dielectric

The dielectric does not fill the air region above the strip

These features determine the behaviour of the microstrip line, because some (usually most) of the field is contained in the dielectric region, concentrated between the strip conductor and the ground plane, and some of the field is in the air region above the substrate (Figure 2.24). In the case of a stripline, the fields are contained within a homogeneous region. For these reasons, microstrip line cannot support a pure transverse electromagnetic (TEM) wave. Microstrip lines support quasi-TEM waves and the phase velocity and propagation constant can be expressed as

$$v_p = \frac{c}{\sqrt{\varepsilon_{eff}}} \qquad \text{Eq.2.26}$$

$$\beta = \kappa_0 \sqrt{\varepsilon_e} \qquad \text{Eq.2.27}$$

where ϵ_e is the effective dielectric constant of the microstrip line. Since some of the field lines are in the dielectric region and some are in air, the effective dielectric constant satisfies the relation,

$$1 < \varepsilon_e < \varepsilon_r$$

and is dependent on the substrate thickness d, and conductor width W.

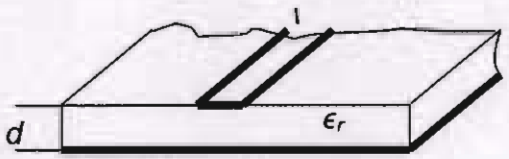

Fig.2.23: Microstrip transmission line

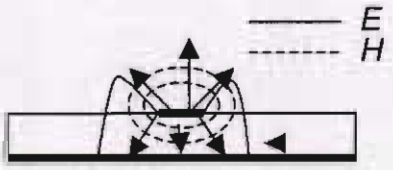

Fig.2.24: Electric and magnetic field lines of a Microstrip line

It can be shown that the effective dielectric constant and characteristic impedance are given by [37]

$$\varepsilon_{eff} = \frac{\varepsilon_r + 1}{2} + \frac{\varepsilon_r - 1}{2} * \frac{1}{\sqrt{1 + 12d/w}} \qquad \text{Eq.2.28}$$

$$Z_0 = \begin{cases} \dfrac{60}{\sqrt{\varepsilon_{eff}}} \ln\left(\dfrac{8d}{w} + \dfrac{w}{4d}\right) \rightarrow for W/d \le 1 \\ \dfrac{120\pi}{\sqrt{\varepsilon_{eff}}\left[w/d + 1.393 + 0.667\ln(w/d + 1444)\right]} \rightarrow for W/d \ge 1 \end{cases} \qquad \text{Eq.2.29}$$

For a given characteristic impedance and dielectric constant, the *W/d* ratio can be calculated as:

$$\frac{w}{d} = \begin{cases} \dfrac{8e^{A}}{e^{2A}-2} \rightarrow for W/d < 2 \\ \dfrac{2}{\pi}\left[B-1-\ln(2B-1)+\dfrac{\varepsilon_r-1}{2\varepsilon_r}\left\{\ln(B-1)+0.39-\dfrac{0.61}{\varepsilon_r}\right\}\right] \rightarrow for W/d > 2 \end{cases} \qquad \text{Eq.2.30}$$

where

$$A = \frac{Z_0}{60}\sqrt{\frac{\varepsilon_r+1}{2}} + \frac{\varepsilon_r-1}{\varepsilon_r+1}\left(0.23+\frac{0.11}{\varepsilon_r}\right)$$

$$B = \frac{377\pi}{2Z_0\sqrt{\varepsilon_r}}$$

2.4.1 Microstrip radiators

The first prototypes of microstrip antennas were developed in the early 1970's. They have been used in different applications exploiting their numerous advantages. There are many types of flat profile printed antennas: the microstrip antenna, the stripline slot antenna, the cavity backed printed antenna and the printed dipole antenna. The characteristics of these antenna types are compared in Table 2.1.

Characteristic	Microstrip Antenna	Stripline Slot Antenna	Cavity Backed Printed Antenna	Printed Dipole Antenna
Profile	Thin	Not very thin	Thick	Thin
Fabrication	Very easy	Easy	Difficult	Easy
Polarization	Linear and circular	Linear	Both linear and circular	Linear
Dual Freq. Operation	Possible	Not possible	Not possible	Not possible
Shape Flexibility	Any shape	Only rectangular	Other shapes possible	Rectangular and triangular
Spurious Radiation	Exists	Exists	Doesn't exist	Exists
Bandwidth	1-5%	1-2%	≈10%	≈10%

Table 2.1: Comparison of various flat profile printed antennas

Microstrip antennas consist of a radiating patch (copper conductor usually) on one side of a dielectric substrate (normally low, ϵ_r<10) and a ground plane on the other side. Some of the principal advantages of microstrip antennas compared to conventional microwave antennas are:

- Lightweight, low volume, low profile planar configurations
- Low scattering cross section
- Linear, circular (LH or RH) polarizations are feasable with simple changes in feed position
- Dual frequency antennas easily made
- Compatability with modular designs
- Feed lines and matching networks are fabricated simultaneously
-

However, microstrip antennas also have disadvantages such as:

- Narrow bandwidth
- Poor isolation between the feed and the radiating elements
- Possibility of excitation of surface waves
- High costs

2.5 Electromagnetic Modelling Technique

CST Microwave Studio is a specialist tool for the quick and accurate simulation of high frequency problems. It is based on a Finite Integration Technique. The Finite Integration Technique (FIT) developed by Weiland in 1977 [7] is a consistent discretization scheme for Maxwell's equations in their integral form. The resulting matrix equations of the discretized fields can be employed for efficient numerical simulations on modern PCs. The simulated structure and the electromagnetic fields are mapped to a hexagonal mesh. The mesh ensures a good compromise between the need of an accurate structure and field discretization and short simulation time. The way a structure is discretized strongly influences the accuracy of the results. In theory, the results converge against the "continuous world" results when the mesh size gets smaller and smaller until the discrete

lengths become differentials. A very fine mesh has a great number of mesh cells and with this a great number of unknowns to be solved. For smaller mesh steps sizes the time domain solver needs smaller time steps to remain stable. The time domain solver is based on an Inverse Fourier Transform Technique and calculates the development of fields through time at discrete locations and at discrete time samples. Every structure has to have at least one port where the fields can propagate into or out of the structure. At these ports, voltages and currents are monitored that are the input and output signals of the structure.

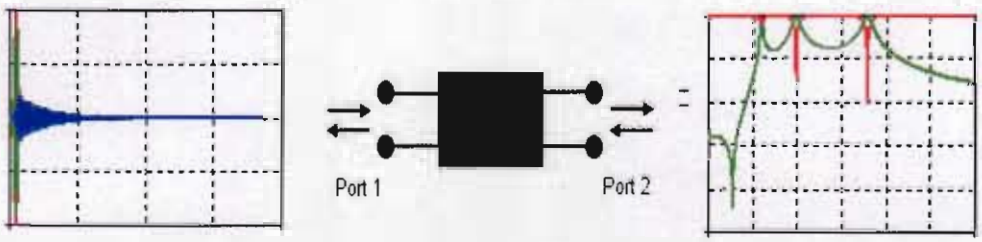

Time domain signals S-parameters derived using IFT technique

Fig.2.25 Time domain solver operation

According to these signals the transfer functions of the structure are calculated. At this stage the structure can be seen as an abstract system with input and output signals that are related by the calculated transfer functions, in our case the scattering parameters (S-parameters).

2.6 Scattering Parameters

High frequency systems have a source of signal power. A portion of this signal power is delivered to a load by means of transmission lines. Voltage, current, and power can be considered to be in the form of waves travelling in both directions along this transmission line. A portion of the signal incident on the load will be reflected. It then becomes incident on the source, and in turn reflects back from the source (if ZS $\neq$ Zo), resulting in a standing wave on the line. If a a two ports network is inserted into the transmission line, additional waves exist (Fig.2.26).

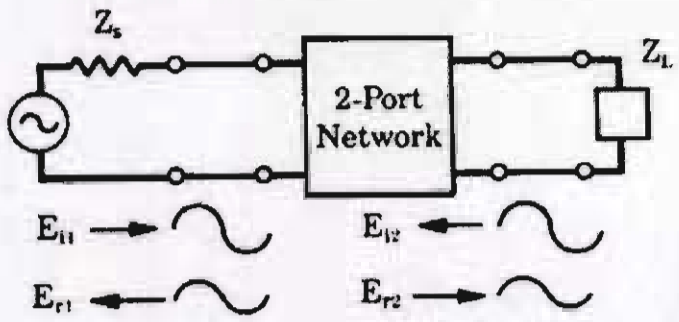

Fig. 2.26: Transmission line with a two port network

In order to relate these four travelling waves, some parameters set are defined. H parameters are presented as follows:

$$V_1 = h_{11} I_1 + h_{12} V_2$$
$$I_2 = h_{22} I_1 + h_{21} V_2 \qquad \text{Eq.2.31}$$

$$V_1 = E_{i1} + E_{r1}$$
$$V_2 = E_{i2} + E_{r2} \qquad \text{Eq.2.32}$$

$$I_1 = \frac{E_{i1} + E_{r1}}{Z_0} \quad I_2 = \frac{E_{i2} + E_{r2}}{Z_0} \qquad \text{Eq.2.33}$$

By substituting the expressions for total voltage and total current Eq 2.33 on a transmission line into this parameter set, we can rearrange these equations such that the incident travelling voltage waves are the independent variables; and the reflected travelling voltage waves are the dependent variables Eq 2.34.

$$E_{r1} = f_{11}(h) E_{i1} + f_{12}(h) E_{i2}$$
$$E_{r2} = f_{21}(h) E_{i1} + f_{22}(h) E_{i2} \qquad \text{Eq.2.34}$$

The functions f_{11}, f_{21} and f_{12}, f_{22} represent a new set of network parameters relating travelling voltage waves rather than total voltages and total currents. In this case these functions are expressed in terms of H-parameters. They could have been derived from any other parameter set. This new parameter set is called "scattering parameters," since they relate those waves scattered or reflected from the network to those waves incident upon the network. These scattering parameters will commonly be referred to as S-parameters. If we divide both sides of these

equations by Zo, the characteristic impedance of the transmission line, the relationship will not change. It will, however, give us a change in variables.

$$a_1 = \frac{E_{i1}}{\sqrt{Z_0}} \quad a_2 = \frac{E_{i2}}{\sqrt{Z_0}}$$
$$b_1 = \frac{E_{r1}}{\sqrt{Z_0}} \quad b_2 = \frac{E_{r2}}{\sqrt{Z_0}} \qquad \text{Eq.2.35}$$

The square of the magnitude of these new variables has the dimension of power. |a1|2 can then be thought of as the incident power on port one; |b1|2 as power reflected from port one. The new set of equations relates these four waves in this way:

$$b_1 = S_{11}a_1 + S_{12}a_2$$
$$b_2 = S_{21}a_1 + S_{22}a_2 \qquad \text{Eq.2.36}$$

The S-parameters are measured as follows:

For S11, it is terminated the output port of the network and measure the ratio b1 to a1

$$S_{11} = \left.\frac{b_1}{a_1}\right|_{a2=0} \qquad \text{Eq.2.37}$$

Terminating the output port in an impedance equal to the characteristic impedance of the transmission line is equivalent to setting a2 = 0, because a wave incident on this load will be totally absorbed. S11 is the input reflection coefficient of the network. Under the same conditions, it can be measured S21, the forward transmission through the network. This is the ratio of b2 to a1

$$S_{21} = \left.\frac{b_2}{a_1}\right|_{a2=0} \qquad \text{Eq.2.38}$$

This could either be the gain of an amplifier or the attenuation of a passive network. By terminating the input side of the network, it is set a1 = 0. S22, the output reflection coefficient, and S12, the reverse transmission coefficient, can then be measured:

$$S_{22} = \left.\frac{b_2}{a_2}\right|_{a1=0} \quad S_{12} = \left.\frac{b_1}{a_2}\right|_{a1=0} \qquad \text{Eq.2.39}$$

CHAPTER 3:

STUDY OF MICROSTRIP PATCH ANTENNAS

3.1 Introduction

In this chapter the design, modelling and fabrication a microstrip patch array antenna for the 2.45 GHz Industrial, Scientific and Medical (ISM) band is described. This band is currently allocated to wireless applications employing the IEEE 802.11b, g and Bluetooth standards. The microstrip antenna is known for narrow bandwidth, but it is the first antenna investigated here because it has a well known performance and is used primarily as an evaluation of the modelling (including the electromagnetic solver software) and measurement techniques. Firstly, the design of a single patch antenna is carried out to determine appropriate dimensions and learn about the modelling accuracy. Initially, an empirical method is used to determine the patch dimensions; in this case the antenna is a half-wave rectangular patch. Finally an electromagnetic solver is used to model the antenna and optimise the results. An array of four microstrip patches is also developed for increased gain. The return loss, input impedance, bandwidth, gain and radiation patterns are the main parameters examined, both experimentally and numerically.

3.2 Single patch design

An empirical method is used [3] to find initial patch dimensions. The dimensions required are the patch length L, the width w and the thickness h. As the patch is square, w and L will have the same value, as shown in Figure 3.1. The dielectric substrate chosen for the antenna is Rogers RT/duroid 5870 because of the features; very low electrical loss for reinforced PTFE, good isotropy, uniform electrical properties over frequency and excellent chemical resistance. The dielectric constant of this laminate is uniform from panel to panel and is constant over a wide frequency range. We have used a laminate of h =3.18mm and a relative permittivity of $\varepsilon_r = 2.33 \pm 0.02$ with a loss tangent of $\tan\delta$ =0.0012. These were chosen because low permittivity and large thickness, yield a high radiation

efficiency (98%). If the relative permittivity is large and h is thin, then the efficiency could be as low as 50%. Hence values of h and ε_r are chosen; 3.18mm and 2.33 respectively. Obtain a value for L, an iteration process is carried out. The first value of L is obtained using Equation 3.1.

$$L = \frac{c}{2f_0\sqrt{\varepsilon_r}} \qquad \text{Eq.3.1}$$

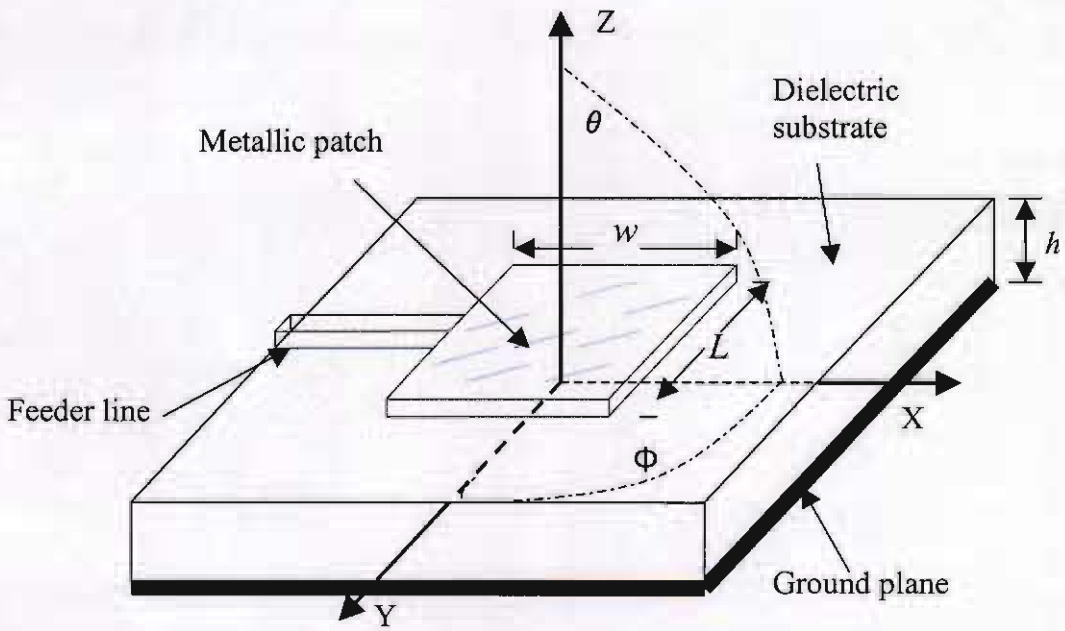

Fig.3.1: Single patch antenna and coordinate system

Using 2.45GHz as the frequency f, L = 40.1mm. Now the effective relative permittivity is calculated using

$$\varepsilon_{eff} = \frac{\varepsilon_r + 1}{2} + \frac{\varepsilon_r - 1}{2}\left(\frac{1}{\sqrt{1 + 12h/L}}\right) \qquad \text{Eq.3.2}$$

Therefore ε_{eff} = 1.66, so the value of the fringe factor ΔL can be found using Equation 3.3

$$\Delta L = 0.412h\frac{(\varepsilon_{ff}+0.300)(w/h+0.262)}{(\varepsilon_{ff}-0.258)(w/h+0.813)} \qquad \text{Eq.3.3}$$

Since w=L, then $\Delta L = 1.75$. Now the new value of L is given by

$$L = \frac{c}{2f_0\sqrt{\varepsilon_{eff}}} - 2\Delta L \qquad \text{Eq.3.4}$$

hence L was found to be 37mm.

3.3 Simulation of microstrip patch

Simulation of the patch antenna using the above dimensions is carried out using a full-wave (uses all 6 Maxwell's equations) electromagnetic solver CST Microwave Studio. A single patch is simulated using the dimension previously calculated L and the parameters of the chosen substrate on a ground plane of size 100mm x 100mm. Initially we determined the patch edge impedance. This yielded a value of 319 + j0.1Ω for the edge at a frequency of 2.439 GHz (Fig.3.2). A quarter wave matching section with Z_o = 126.29Ω is then used to reduce that impedance to 50Ω. The free-space wavelength for 2.45GHz is 122mm so the quarter wave length is 30.6mm and an electrical quarterwave in the substrate is 20.05mm, which is the required length of the transformer section. Figure 3.3 illustrates the simulated return loss of the patch with the matching section. The return loss was greater than 10dB over the frequency range 2.444 GHz to 2.504 GHz.

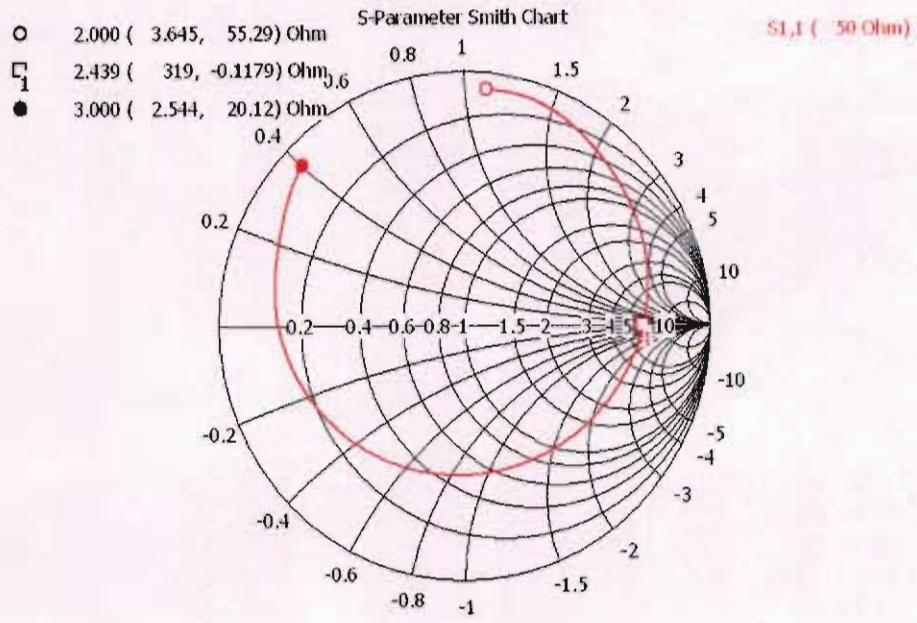

Fig.3.2: Smith Chart showing the impedance at the edge of the patch

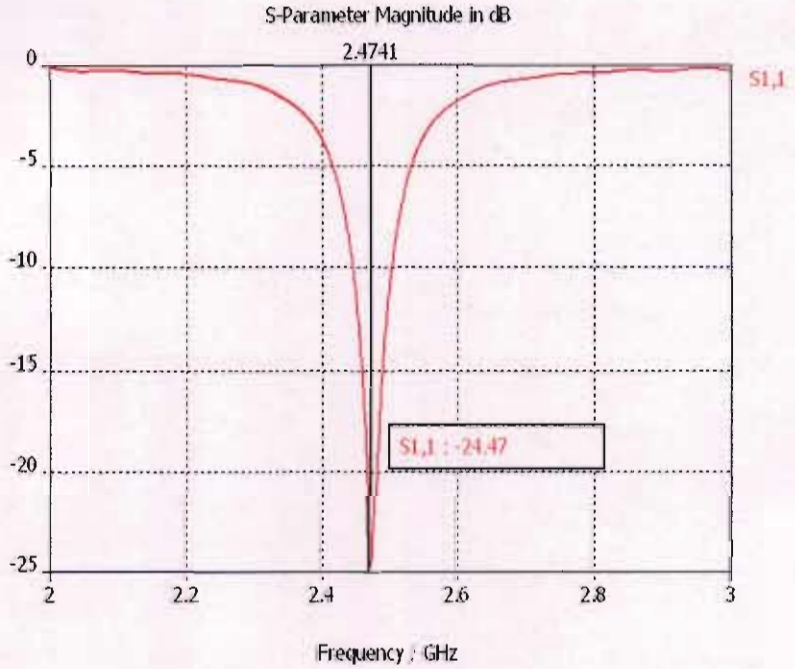

Fig.3.3: Simulated Return loss versus frequency for the patch with matching section

3.4 Fabrication and Measurements

The antenna was then fabricated by exporting the 2D shape of the designed element as a DXF file from the EM solver. This file is input to a CAD package, which in turn, is transferred to the the LPKF milling machine, which cuts the patch antenna. To feed the antenna an SMA launch connector is soldered at the end of the feed line. The S11 is measured using a Rohde and Schwarz vector network analyser (VNA) as shown in Figures 3.4 and 3.5. The radiation pattern is also measured using the VNA and a turntable (see appendix A5). Figure 3.4 illustrates the behaviour of the return loss between 2 and 3 GHz.

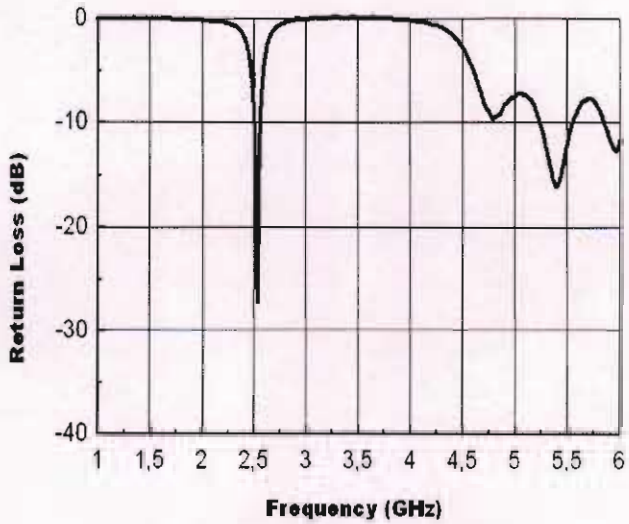

Fig.3.4: Measured Return loss over wide band (1-6 GHz)

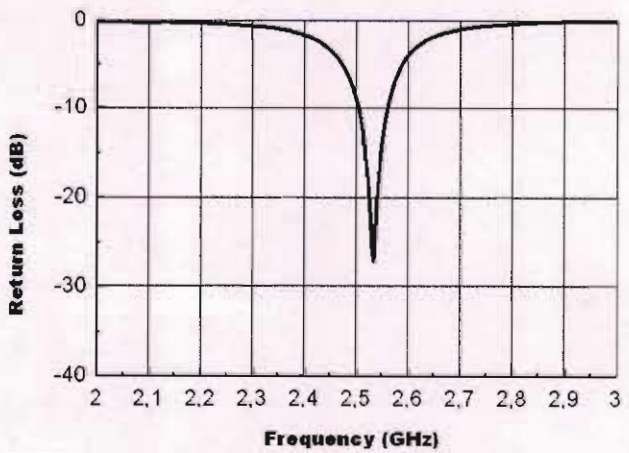

Fig.3.5: Measured Return loss versus frequency for the single Patch

3.5 Optimisation

In Figure 3.5 it can be seen that the resonant frequency doesn't quite agree with the simulated value. The measured value is 2.53GHz. The difference is 60MHz which is a percentage of 2.44%. To avoid this discrepancy the dimension of the patch is increased slightly to get a lower resonant frequency. Now the patch sides have L=37.8mm. In the Figures 3.6 and 3.7 we can observe that the measured radiation patterns are in good agreement with the simulated ones. As can be observed, the shape of the patterns is somewhat different behind the ground plane, but that is not critical in this case. These differences can be caused by radiation from the feedline or connectors, which are not modelled. In both plots the gain is normalised. In the simulation we got a gain of 7.5 dBi and experimental plots have been normalised to this value.

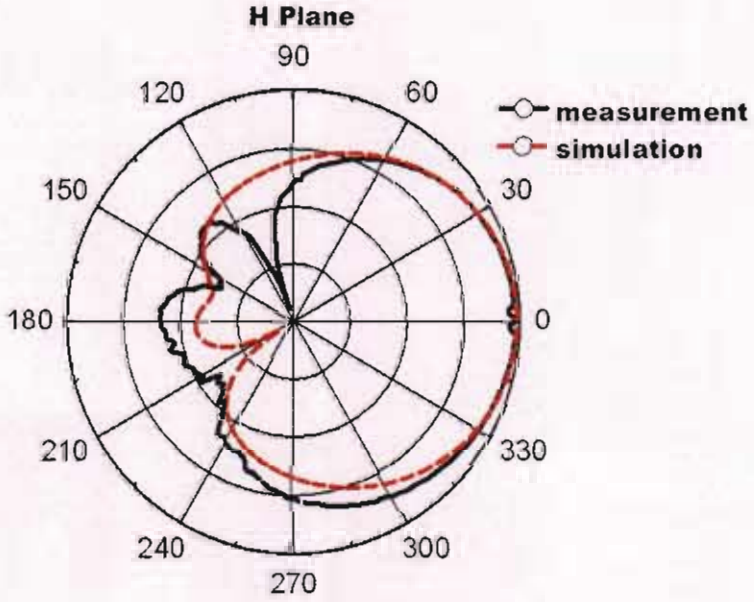

Fig. 3.6: Radiation pattern for single patch, E-plane (ZX-plane)

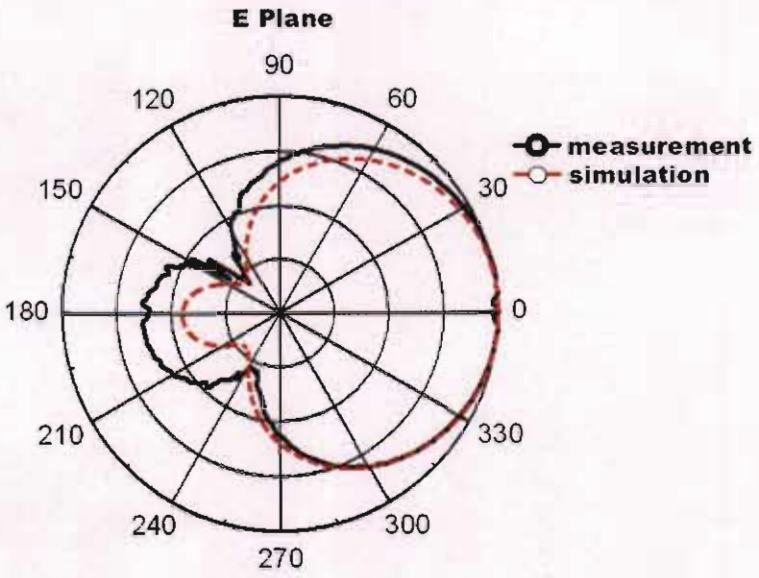

Fig.3.7: Radiation pattern for single patch, H-plane (ZY-plane)

3.6 Array Design

The array consists of four single patch elements, fed with equal phase. All of them have the same dimensions (37.8mm per side). The substrate is the same that we used for the single patch except the ground plane size is 150mm x 150mm. The structure of the antenna consists of 2 x 2 patches, as can be seen in Figure 3.8.

3.7 Array Spacing

The spacing between the patches needs to be identical; the symmetry is required because the radiation pattern and the return loss are sensitive to the spacing. If the distance *d* between two patches is $d \geq \lambda_0$, there can be problems with undesirable grating lobes in the radiation pattern, and for maximum gain, the spacing *d* should be equal to $0.5\ \lambda_0$. We chose $0.6\lambda_0$ which achieves high gain and allows adequate spacing for feed lines.

$$D=0.6\lambda_0$$

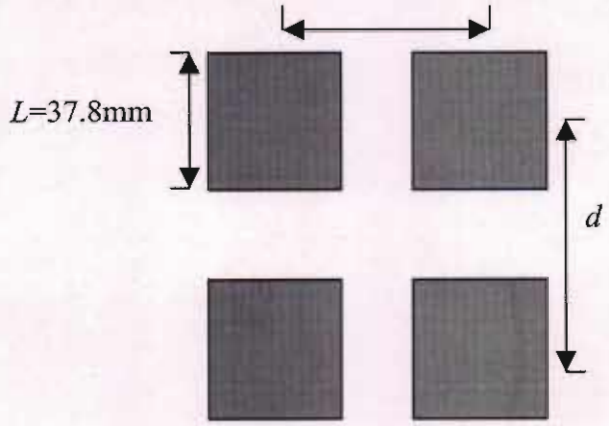

Fig.3.8: Dimensions and array spacing

3.8 Calculation of the feed lines

Different sections of feed lines are used to feed the patches. The 319 Ω edge impedance was reduced to 100 Ω using a quarter wave section of Z_0 = 178.60 Ω (the same line is used in the four patches). The 100Ω lines are combined for two patches, to make a 50Ω impedance. This is raised to 100Ω again by a quarter wave section of Z_0 = 70.71 Ω. Then the 100Ω are combined at the centre to produce a 50Ω input impedance. Figure 3.9 illustrates the modelled array with its feed lines. The dimensions have been calculated with the electromagnetic solver software (see appendix A6).

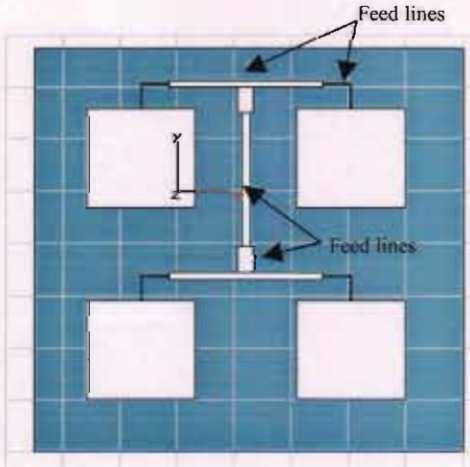

Fig.3.9: Modelled microstrip array and different feed lines

3.9 Simulation and fabrication

CST Microwave Studio was also used to simulate the array. The different line lengths and widths required were calculated using the solver. (see appendix A6). The primary purpose of the simulations was to identify the optimum feeding system and the optimum feed point. Different configurations were tested. As we can see in Figure 3.10, the antenna is well matched at 2.41 GHz. A discrepancy between the simulation and the measurement still exits.

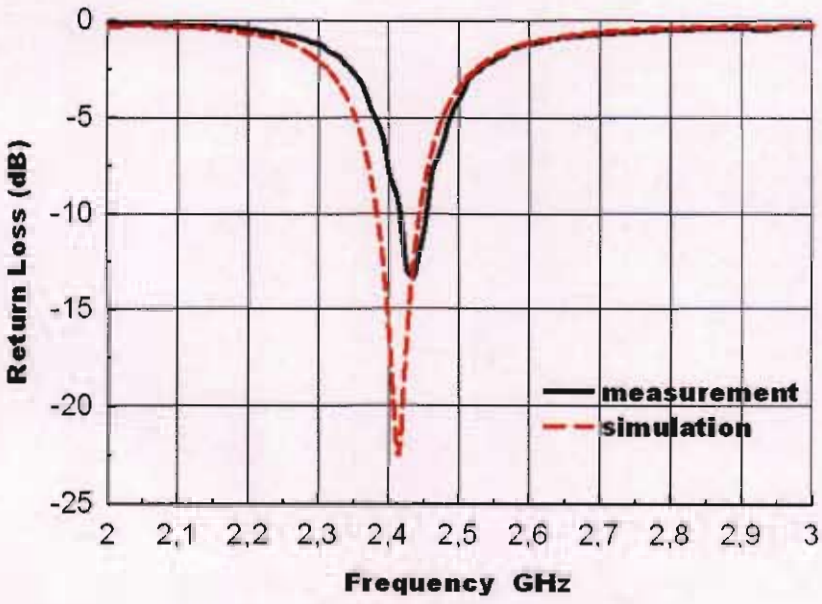

Fig.3.10: Return Loss for the microstrip array

The antenna has been fabricated using the same process that it was used for the single patch. An SMA connector was used to feed the antenna. In the Figure 3.10 we can observe that the measured return loss is somewhat poor if we compare it to the simulated value. But in this case the resonant frequency 2.434GHz is very close. The secondary purpose is to compare the radiation patterns obtained by simulation and measurement. The radiation patterns are normalised to maximum gain (Fig. 3.11 and Fig.3.12). In the simulation we obtained a gain of 12.49 dBi.

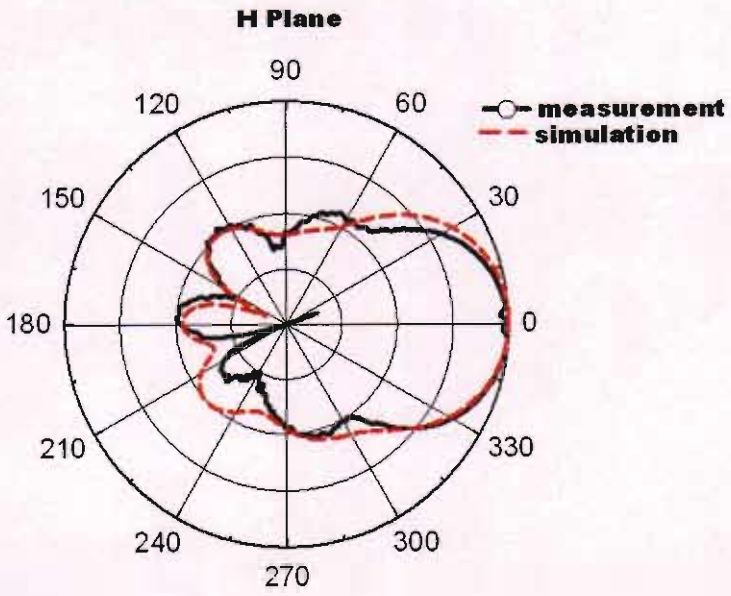

Fig. 3.11: Radiation pattern for 2x2 array, E-Plane (ZY-plane)

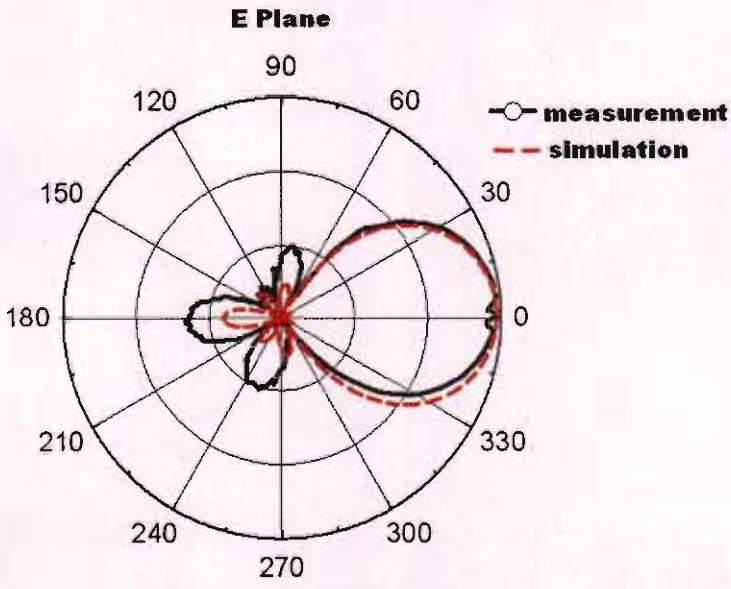

Fig.3.12: Radiation pattern for 2x2 array, H-plane (ZY-plane)

The plots show good agreement between simulated and measured results. The front-to-back ratio is greater than 20 dB in both planes, which realises a highly directional antenna array.

3.10 Gain Measurement

The absolute gain method [14] is used to calculate the gain of the antennas (single patch and array). To use this method, two identical single patch antennas are built with the dimensions that we obtained in the optimisation (see 3.4). Figure 3.13 illustrates the system used to measure the gain.

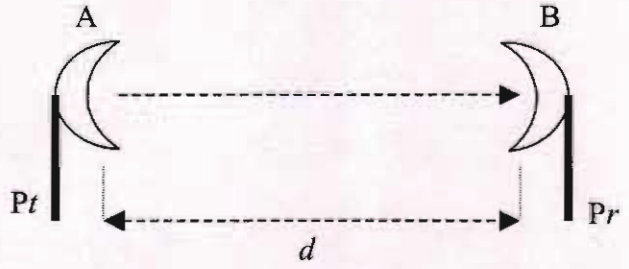

Fig. 3.13: Two antenna system for the measurement of antenna gain

The gain is given by

$$G_A = G_B = \frac{1}{2}\left[20\log\left(\frac{4\pi d}{\lambda}\right) - 10\log\left(\frac{P_t}{P_r}\right)\right] \qquad \text{Eq.3.5}$$

where G_A and G_B are the antenna gains expressed in dBi, P_t and P_r are the transmit and receive powers expressed in Watts and d is the distance between both antennas. To get the ratio between P_t and P_r, we measured the S_{21} parameter with the network analyser. The value that we obtained is just the ratio between the powers. The distance that we used was $d = 0.6$m and $\lambda = 0.122$ for 2.45GHz.
Taking in account the feeder loss, the equation is

$$G_A = G_B = \frac{1}{2}\left[20\log\left(\frac{4\pi d}{\lambda}\right) + L_{feeder} - 10\log\left(\frac{P_t}{P_r}\right)\right] \qquad \text{Eq.3.6}$$

where the measured feeder loss was $L_{feeder} = 5.5$dB

The gain is found to be 6.45dBi. There is a small difference (0.4 dB) between the calculated value, based on measurement and the simulated value, which is 6.85 dBi. This discrepancy is mainly due to the reflections in the measurement set-up, as a far-field anechoic chamber was not available. To measure the gain of the

microstrip array we just substitute one of the antennas in the system (Fig. 3.12) with the array and we used Equation 3.7

$$G_A = \left[20\log\left(\frac{4\pi d}{\lambda}\right) + L_{feeder} - 10\log\left(\frac{P_t}{P_r}\right) - G_B \right] \qquad \text{Eq.3.7}$$

where G_A is the gain of the array and G_B is the known gain of the single patch, 6.45dBi. Then the gain is G_A = 12.57dBi. The simulated value was 12.5dBi, so the agreement with measurement is very good.

3.11 Conclusion

The results obtained show that the microstrip antenna is suitable for narrowband wireless communications, with the 2.4-2.5 GHz bandwidth achievable with a single patch element. However, the laminate is costly and if higher directivity is needed, the bandwidth is not realisable when an array is used, which also has implications for manufacturing tolerances. It is also important to highlight that dual polarization is hard to achieve using patches. That is because it is very difficult to define the suitable place for the feeding points and isolate them, thus it would be hard to obtain reasonable input impedance and good isolation results. Due to the limitation of bandwidth, cost and isolation for these microstrip antennas, no further work on the microstrip antenna will be carried out.

However, very good agreement has been obtained between experimental and simulated work, which validates the modelling software and measurement techniques involved. With this the main objectives of this chapter have been covered and in the next chapters CST will be used to design the antennas

CHAPTER 4:

CROSSED DIPOLE ANTENNA

4.1 Introduction

Polarization agility is desirable for modern wireless communications. Two crossed elements make possible the application of polarization diversity in order to reduce the deep fades that may affect the signal envelope. Because different linear polarizations reflect and penetrate surfaces differently depending on the angle of arrival and material type, the most effective way to propagate or penetrate inside buildings is to use a dual or a circular polarized antenna. This allows for more continuous coverage in indoor environments than a purely linear polarized signal, and significantly increases the probability of maintaining the link, so that is the main reason to design this kind of antenna. Wire antennas are probably the simplest types of antennas, and most of the earliest antennas (e.g., used by Hertz and Marconi) were of this type. Wire dipoles and monopoles mounted on a ground plane are most commonly used at lower frequencies (HF to UHF) and have relatively low gains. On the other hand, printed antennas are a relatively new type of antenna consisting of printed conductors on a microstrip or similar type of substrate, and are thus compatible with planar microwave circuit technology. Printed antennas usually operate at microwave frequencies and have low gains. To get a good performance from a dipole, it should be resonant. This requires the dipole to be slightly less then half a wavelength long.

4.2 Initial theory and design

Initially the theory based on the wire dipole is used. This theory [29] states that for a cylindrical dipole, the dipole length for the first resonance is given by

$$L = 0.48A\lambda_0 \qquad \text{Eq.4.1}$$

where L is the length of the wire dipole, λ_0 is the free-space wavelength, r is the radius of the dipole and A is the length-to-radius parameter for the dipole given by

$$A = \frac{L/r}{1 + L/r} \qquad \text{Eq.4.2}$$

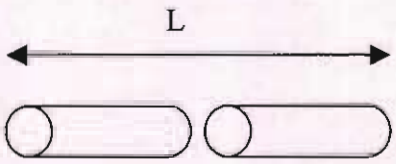

Fig. 4.1: Length of a dipole

The frequency of operation is 2.45 GHz, so the wavelength for that frequency is 0.122m. Supposing that A is 1, the length is 0.06m (60mm), this approximation is used when the wire is very thin (the radius is very small). For a thick wire, $A<1$ and, using a radius of 0.5mm, it is obtained $A=0.9917$, hence L = 0.05950m from Equation 4.1. In our case the conductor is not circular so it is necessary to take an equivalent radius, [6] for a thin flat sheet of width, W, the equivalent radius is given by

$$r = \frac{W}{2\pi} \qquad \text{Eq.4.3}$$

The selected length is W= 6.24mm, then r_{eq} is 0.9931mm. Using that value in Eq.4.2, it is obtained A = 0.9837, hence the length becomes 0.0590m from Eq.4.1.

4.3 Modelling of printed dipoles

Strip dipoles printed on electrically thin low-permittivity substrates behave similarly to ordinary dipoles. Working with planar antennas and following the theory of equivalency between wires and planar structures, the size of the antennas has to be modified.

4.3.1 Simulation: Printed strip dipole

As in chapter 3, CST Microwave Studio was employed to model and simulate the antenna. Figure 4.2 shows a dipole printed on a substrate with a relative permittivity of 4.3 (FR4) which is centre-fed. The width of the dipole is 6.2mm

and the length is 19mm per "arm". The thickness of metallization for the dipoles is 0.035mm and the substrate thickness is 1.524mm.

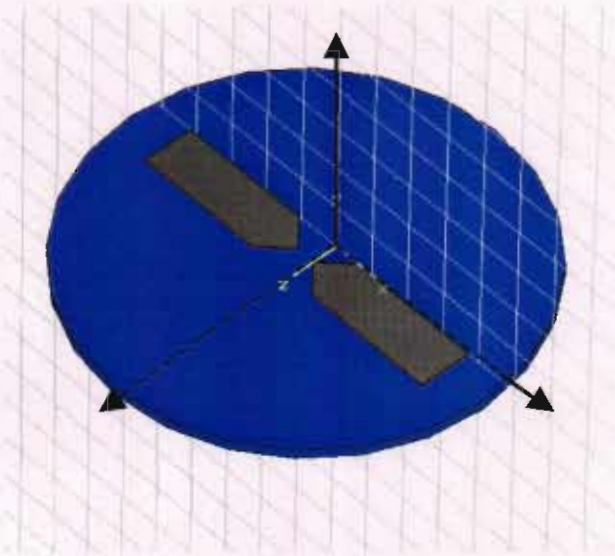

Fig. 4.2: Single printed dipole

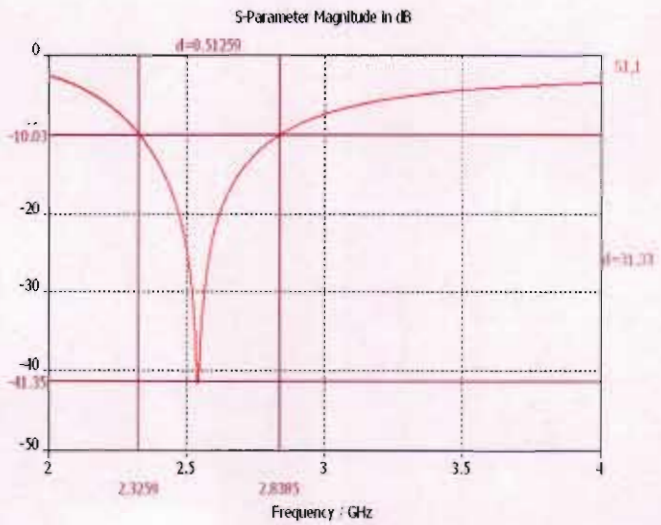

Fig.4.3: Simulated return loss vs frequency for single printed dipole

Figure 4.2 shows the return loss plot for the dipole over frequency (2GHz to 4GHz). The return loss was –41.35dB at 2.54GHz and the bandwidth was 500MHz (2.32GHz to 2.83GHz). Both results meet the specifications and they allow us to go on with the next steps.

4.3.2 Dual polarized dipoles

To obtain dual polarization, a pair of orthogonal dipoles is modelled as illustrated in Figure 4.4. Both dipoles have two arms completely equal and the four arms are symmetrical and orthogonal. Both dipoles are feed across the centre gaps. Observing S11 in Figure 4.5 and comparing with results for S11 for a single dipole, it is noticeable that the return loss is worse and the resonant frequency is somewhat shifted. The isolation between ports, S21 is very poor at the resonant frequency, which means coupling between orthogonal dipoles has to be reduced.

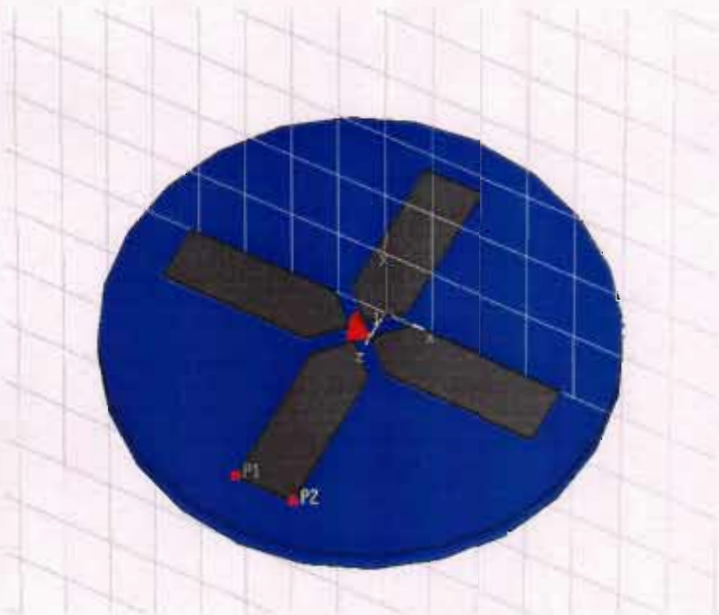

Fig.4.4: Orthogonal dipoles

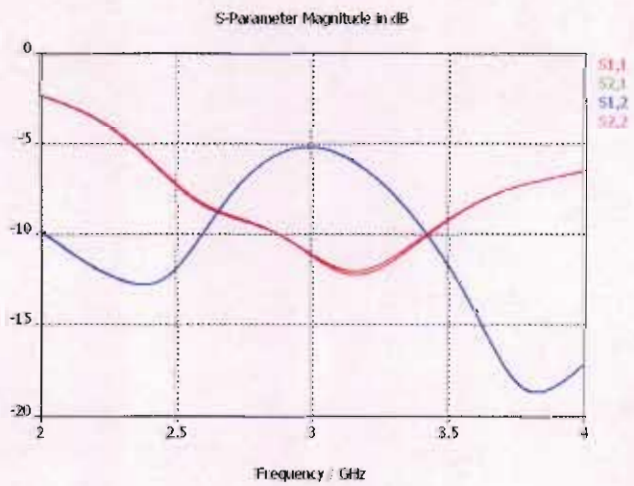

Fig.4.5: Simulated return loss and isolation vs frequency for orthogonal dipoles

4.3.3 Addition of a reflector

To improve these parameters and to achieve the desired radiation pattern, a reflector was introduced $0.2\lambda_0$ from the rear of the substrate. The results were still poor. Parameters such as, reflector-to-dipole spacing, dipole length and substrate thickness, were varied. The results have improved a little, but a poor isolation and bad return loss are obtained (Figure 4.7). Different kind of variations such as increasing the gap between the dipoles was undertaken, but the results were still poor. The final dimensions of the reflector are 127 x 127mm square and with 1mm of thickness which is symmetrical with respect to the centre of the dipoles.

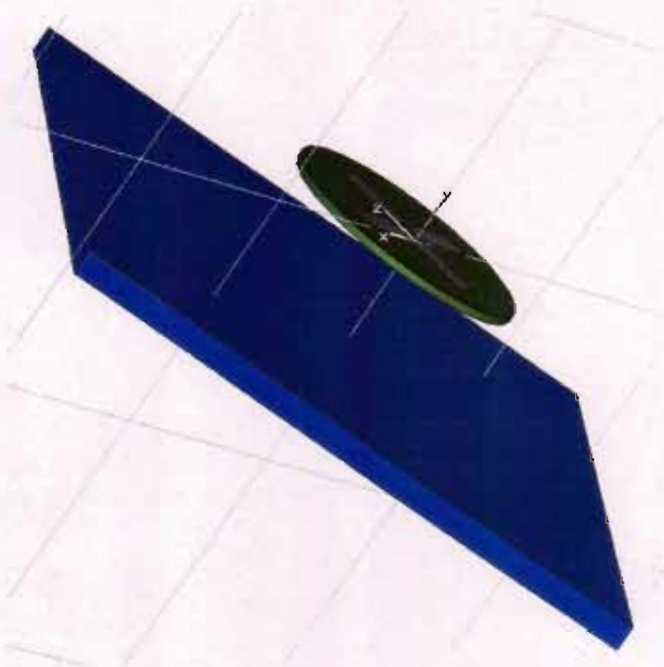

Fig. 4.6: Orthogonal dipoles & reflector

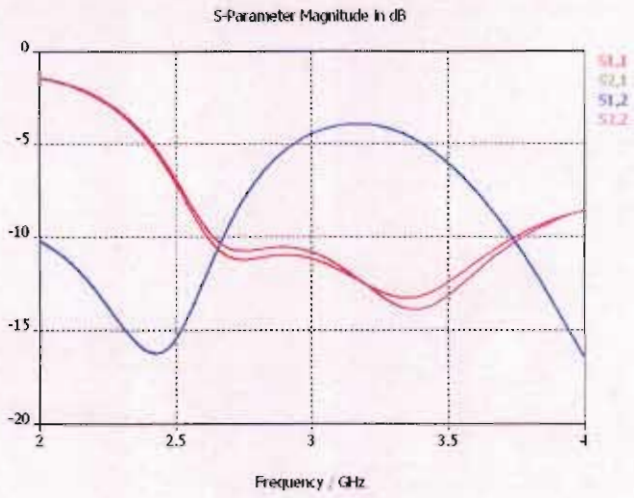

Fig. 4.7: Simulated return loss and isolation for orthogonal dipoles & reflector

More than 1GHz of bandwidth is obtained taking in account the values with return loss greater than 10dB. The impedance at 2.4GHz, is 21.29 – j0 Ω. It can be seen that Figures 4.5 and 4.7 present the same result for S21 and S12 (something reasonable), that is the reason why just S12 is shown.

4.3.4 Addition microstrip feeders

In this stage of the simulation, in order to improve the results suitable matching feeders were used. Initially the type of matching system had to be chosen and due their simplicity microstrip feeders were chosen.

A balun feeder system is necessary to work with the balanced dipole antennas. There are different ways to develop a balun with microstrip as it can be seen in chapter 2. Triangular taper was selected [29] because this offers a wide bandwidth and was suitable for our structure. Two microstrip feeders with a length of λ_0 were designed. This length was used because the first null for the reflection coefficient magnitude response [29], βL, occurs at $\beta L = 2\pi$. From Equation 4.4

$$\beta = \frac{2\pi}{\lambda} \qquad \text{Eq.4.4}$$

then L is equal to λ.

The microstrip feeders were printed on a substrate with ϵ_r of 4.2 and 0.762mm of thickness (GML 1000), substrate designed for wireless communications, the dielectric constant is low and stable when used over broad temperature and

humidity operating ranges). The low value of thickness helps to reduce radiation from the feeders lines.

Figure 4.8 shows the feeder printed on the substrate. Both feeders have the same dimensions. The taper has to transform 21.29 Ω to 50 Ω. These widths are calculated with CST Microwave Studio (see appendix A6). It is obtained a value of 4.7mm for 21 Ω, impedance at 2.45GHz and 1.8mm for 50Ω. The feeders' metallization thickness is 0.035mm.

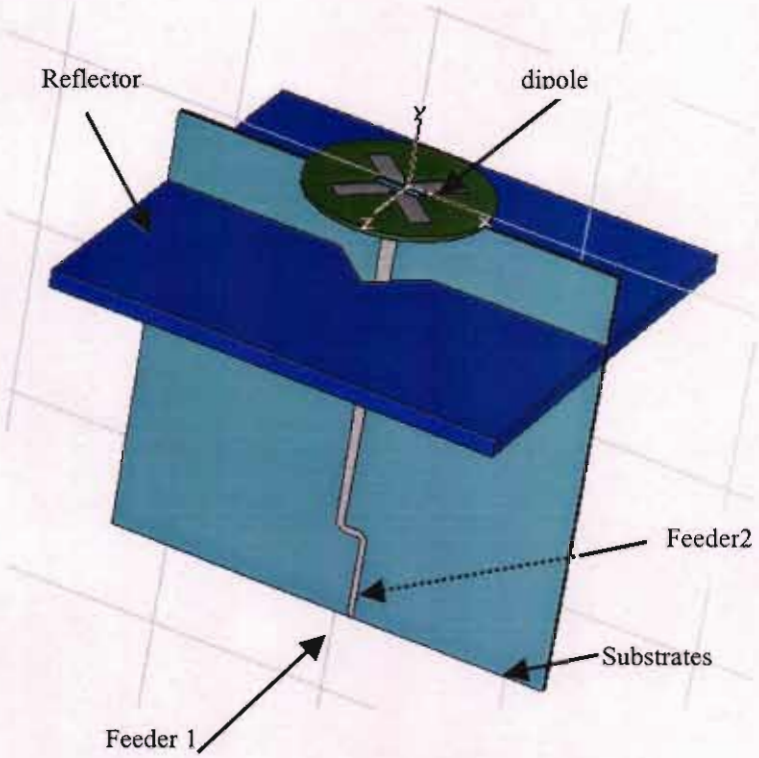

Fig. 4.8: Dual polarized antenna, microstrip feeders

The ground plane for these feeders is a stripline and is shown in figure 4.9. This acts as part of the balun. The stripline is located between the two substrates (GML 1000). It is connected to the dipoles through a brick or via. The stripline has also a similar path to the feeders close to the dipole.

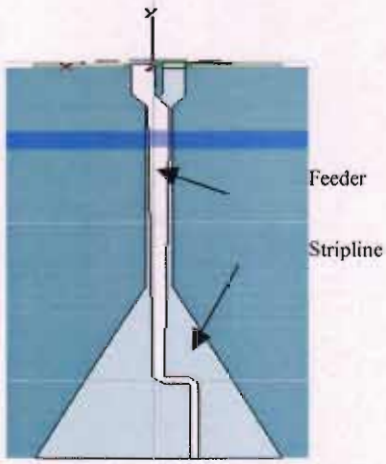

Fig. 4.9: Stripline , Plane XY

4.4 Simulation and manufacturing

Finally the antenna was built (see appendix A2) with the same process that was used in the chapter 2. In this section some measurements (where one port is terminated) are compared with the results obtained from the simulation. Figures 4.10 and 4.11 show the return loss and the isolation of the antenna. Unfortunately the agreement is again poor. Figure 4.10 presents a bandwidth of 1GHz (from 2.025GHz to 3.09GHz) which was achieved by simulation and a bandwidth of 450 MHz (from 2.1GHz to 2.55GHz) obtained by measurement. These results are acceptable because in both cases a wideband of operation was obtained. This discrepancy between them is due to the complexity of the antenna. As expected, the isolation between the ports is still very poor. To measure the isolation a different procedure was used. In Figure 4.11 it can be observed that the measured isolation is a little worse than in the simulation. At 2.45GHz, a value of 5dB is obtained.

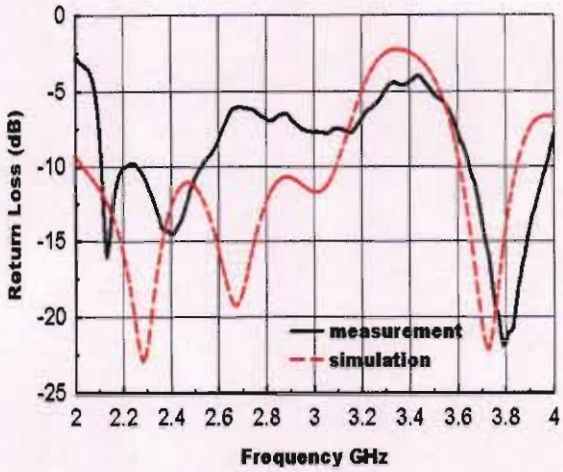

Fig.4.10: Return Loss for the dual polarized antenna

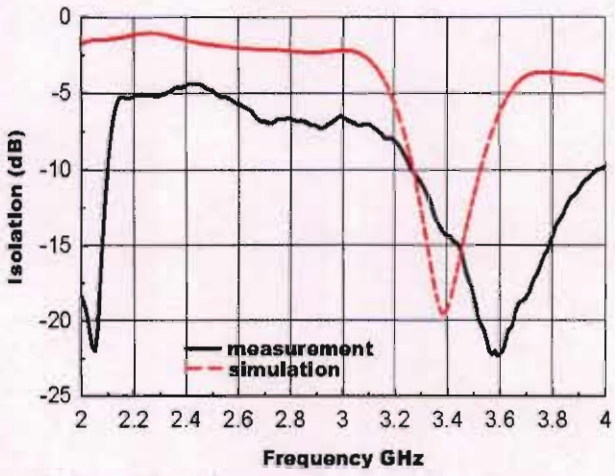

Fig. 4.11: Isolation for the dual polarized antenna

4.4.1 Radiation patterns and gain measurements

Radiation patterns are illustrated in figure 4.12. Both patterns are normalised to the maximum gain. In the simulation a gain of 7.5dBi was obtained. The simulated radiation efficiency is 87%.

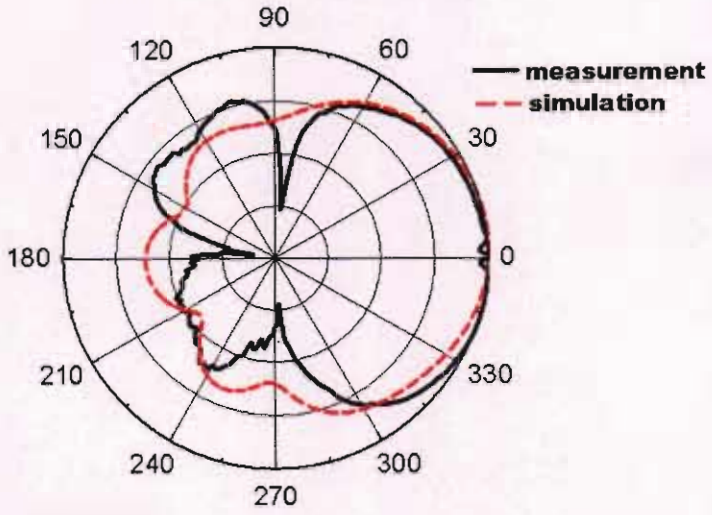

Fig.4.12: Radiation pattern for dual polarized antenna. H plane (ZX)

Figure 4.13 shows the squint obtained in the simulation. The main lobe direction is at 7 deg, so the squint at 2.4GHz is 7deg. This squint was found to be frequency dependant because at 2.6GHz it has the main lobe at 1 deg and at 2.8GHz the main lobe is at -3 deg.

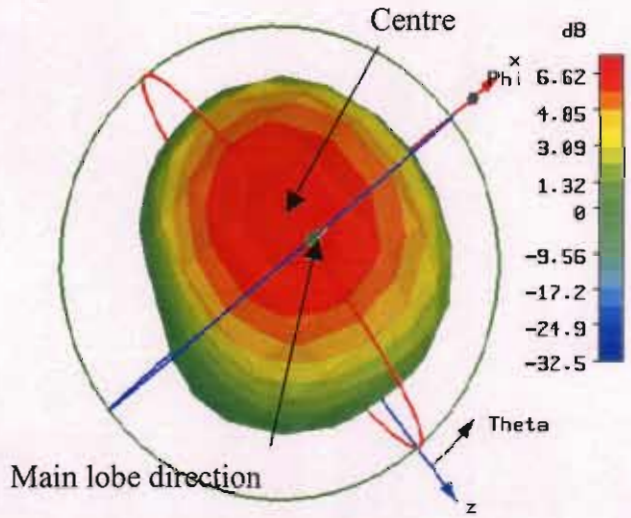

Fig.4.13: 3D Radiation pattern for dual polarized antenna. Illustrating the squint

The substitution method was used in chapter 2.9 has been used to measure the gain of the antenna. Then, using the Equation 2.6, where L_{feeder} = 5.5dB, d is 0.6m, G_B is 12.5 dBi and G_A is the unknown gain. Therefore the gain of the dual polarized antenna is 4.5 dBi.

4.4.2 Optimisation

A second design was carried out to improve the results. Initially it was thought that phase differences in the feed lines might be the reason for the squint. Then the microstrip feeders were redesigned. The feeders' length and the ground plane size were reduced (see Figure 4.14).

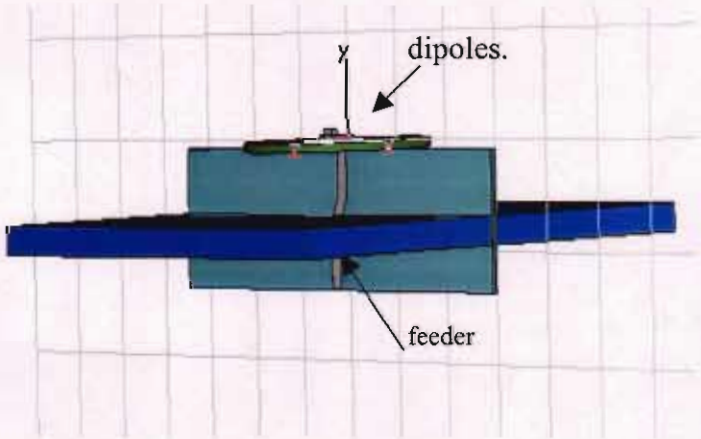

Fig. 4.14: New design of the dual polarized antenna

Initially, the length of the feeders and the ground plane was established to 0.35λ. The isolation did not improve and the resonant frequency was not in the correct frequency range. To move the resonant frequency the lengths of the dipoles were changed. After some tests with different lengths it was demonstrated that the taper balun wasn't working. The feeders were behaving like part of the antenna, and contributed to the radiation. After some rework, the feeder length was set to 0.2λ. The results for these dimensions are shown in figure 4.15 and 4.16. In the return loss (Figure 4.15) a bandwidth of 350MHz (from 2.25GHz to 2.6GHz) was achieved. As can be seen in Figure 4.16, the poor isolation has not been improved. That is due to the strong coupling between the ports.

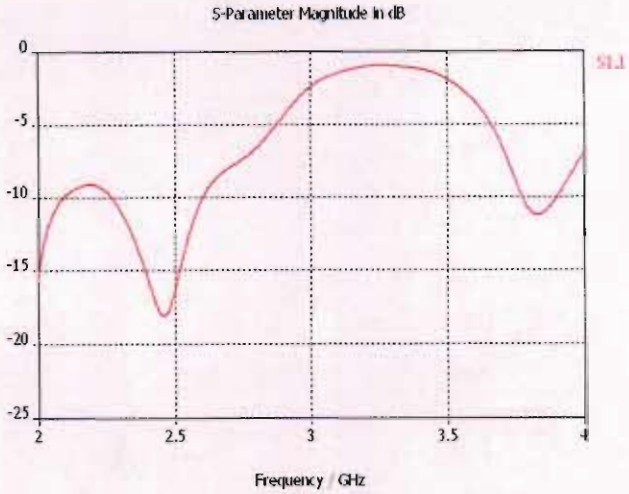

Fig.4.15: Simulated return loss for the new dual polarized antenna

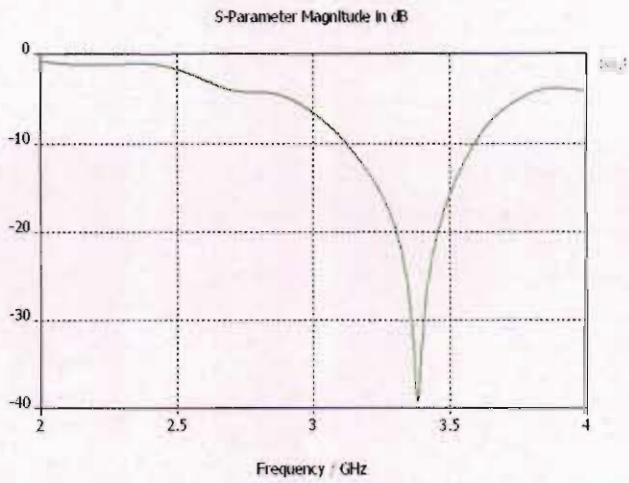

Fig.4.16: Simulated isolation for the new dual polarized antenna

The other important parameter in this chapter is the squint. With the new design the squint has been removed at 2.4GHz. Figure 4.17 illustrates the 3D radiation pattern of the new design. The main lobe direction is at 0 deg. A simulated gain of 8.25dBi was obtained.

Main lobe direction

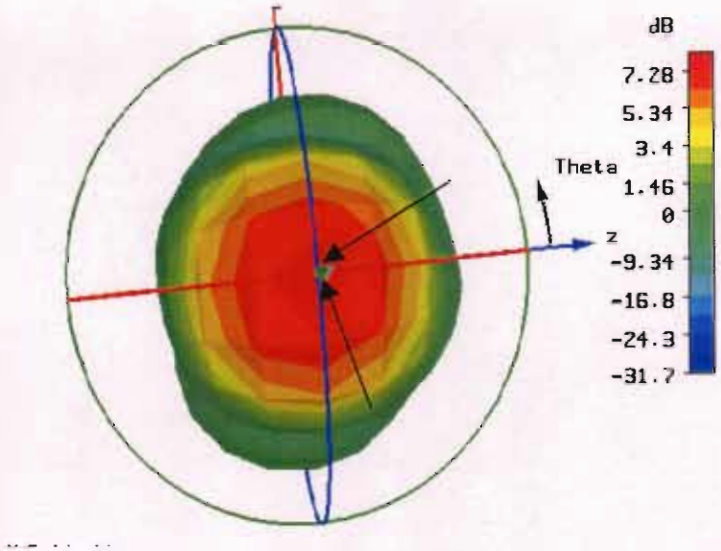

Fig. 4.17: 3D Radiation pattern for dual polarization antenna. No squint

The optimization of this performance is based on the reduction of the antennas size, something very important in terms of material cost and visual impact, and in the disappearance of the squint, thus the radiation patterns are optimum for base station requirements.

It should be mentioned that there were many problems with simulation, due to the orthogonal nature of the antenna. The software CST Microwave Studio has a special way to set the mesh (see appendix A7). CST uses two different coordinate systems, a global system and a local coordinate system. The local system (see appendix A7) was used to model the antenna, and the dipoles were oriented using this coordinate system. Many days were spent trying to set proper meshing parameters (increasing the number of cells or varying the lines per wavelength). Finally it was noticed that the problem was that the ports should be orientated in the direction of the global coordinate system (XYZ) because the mesh plane can only be oriented in those directions. To correct the problem and in order to run the simulation, the antenna was re-oriented by 45 degrees. However, it was decided to investigate another feed method for the crossed dipole, in order to achieve better isolation.

4.5 Conclusion

In this chapter a tapered balun was selected to feed the crossed dipole antenna. The dipole itself is fabricated of low-cost laminate which offers a small amount of

miniaturisation due to the relative permittivity. It has been demonstrated experimentally in this chapter that this feeding network yields very poor isolation. The obtained bandwidth is much greater than the desired bandwidth which has been described in chapter 1. Unfortunately the isolation doesn't match with the objectives. This resulted in a poor antenna performance in that squint exists in the radiation pattern, due to a phase offset between dipoles due the feedlines radiating. The poor isolation was a contributory factor. This led to significant inefficiencies making this antenna uncompetitive. There are other options for the feed network, which need to be investigated and these are discussed in Chapter 5.

CHAPTER 5:

CROSSED DIPOLE ANTENNA WITH IMPROVED FEED SYSTEM

5.1 Introduction

This chapter describes the steps taken to improve the performance of the crossed dipole element developed in Chapter 4. The main objectives of this investigation (see Chapter 1), were to obtain a reasonably wideband element (more than 100MHz bandwidth), with good isolation (better than 20dB) between ports and high gain (approx 7dBi). A low profile and low cost are also necessary. Various simulations and models were evaluated before a fabricated version was realized. A different balun system is adapted to the desired structure

5.2 Modelling

5.2.1 Substrate effects

The finite integration time-domain technique using CST Microwave Studio was used to simulate the structure. Figure 5.1 and Figure 5.2 show the performance of a dipole printed in free space and on substrate. Different dielectric constants (three different permittivity values, ϵ_r = 2.3, ϵ_r = 3.2 and ϵ_r = 4.3) and five different substrate thicknesses (h = 1mm, h = 0.8mm, h = 1.6mm, h = 2mm and h = 3mm) have been simulated varying the length of the dipole (l = 48mm, l= 44mm, l= 42mm, l= 40mm and l= 36mm). The length of the gap, g, is 6 mm.

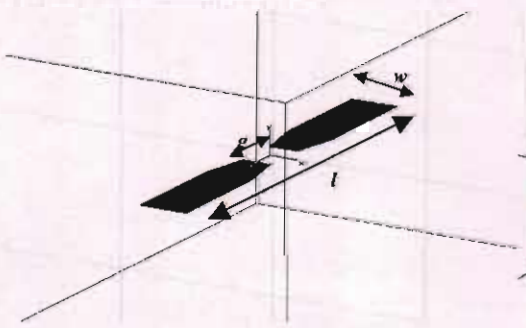

Fig.5.1: Half-wave dipole printed in free space

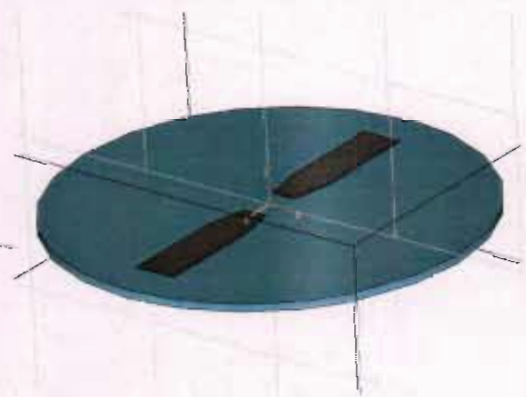

Fig.5.2: Half-wave dipole printed on substrate

The influence of the relative permittivity of the dielectric substrate on the dipole resonant frequency was investigated. It can be seen from Figure 5.3, that at 2.45 GHz, the overall dipole length is reduced from 49 mm in free-space to 41 mm when printed on 1 mm thick FR4 (standard PCB material) substrate (ϵ_r=4.3) which has a loss tangent of 0.2 (see Appendix 8 to check the obtained results for other thicknesses). The dielectric effect increases the electrical length. It also reduces the bandwidth of the dipole as shown in Figure 5.4. It can be seen that maximum bandwidth is achieved in free-space. The bandwidth achievable when printed on a laminate of relative permittivity 4.3 is 370 MHz, according to simulated results. This is somewhat less than the free-space value, but the reduced size is necessary.

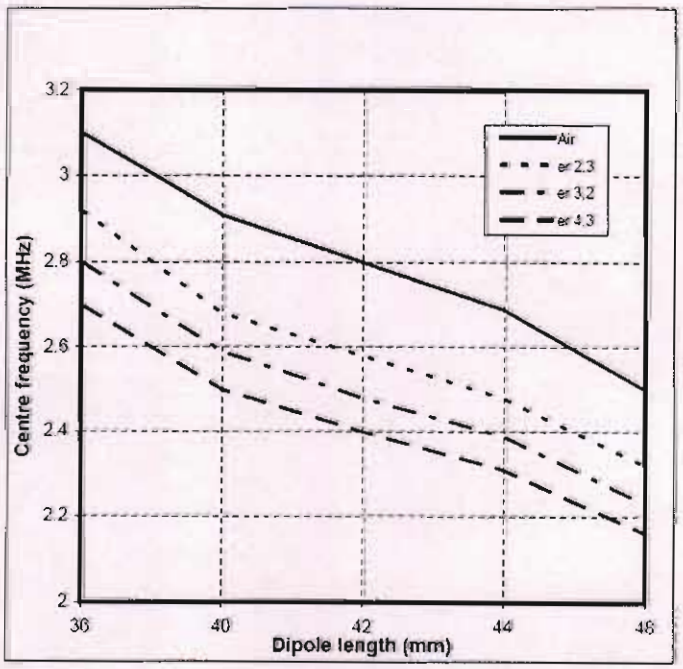

Fig. 5.3: Centre frequency versus dipole length (l) for different substrate permittivity.

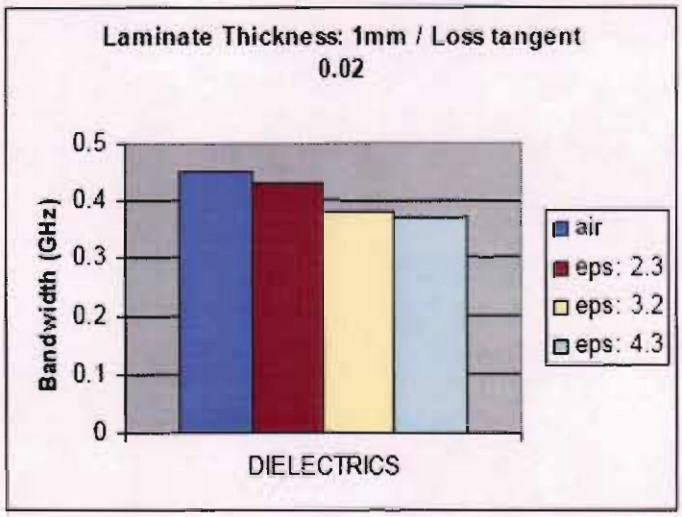

Figure 5.4. Effect of printing the dipole on dielectric laminate (1mm thick) versus impedance bandwidth, for different values of relative permittivity.

5.2.2 Single printed dipole

As it has been shown in Chapter 2, microstrip is a structure that supports different configurations. A quarterwave balun is one of them. This kind of feeding network was selected due to its proven performance and features. This network offers the possibility of designing each feeder varying just a minimum number of parameters. Initially a single dipole was modelled. Figure 5.5 shows the dimensions and the configuration of the first model, where one printed dipole is fed using a quarter wavelength balun. At 2.5GHz and using a substrate of relative permitivity equal to 3.2, the electrical quarter wavelength ($\lambda/4$) is 16.76mm. The dipole is printed on a substrate with permittivity of 4.3 and 1mm of thickness, the dipole arm length (l) is 17mm and the gap (g) is 6mm. As it can be seen in Figure 5.5 and 5.6, the feeding structure consists of two vertical elements connecting each dipole with the ground plane (a rectangular hole was realized in the substrate in order to facilitate the connection). Each vertical element comprises a shorting strip feeder. This type of balun is based on the well-known resonant line section terminated by short circuit. Its double purpose is to transform the unbalanced current distribution of the input transmission line into the balanced one of the dipole while an impedance match is provided. The connection betweens the dipoles and the ground plane is done at 17mm from the dipole, what means that the grounding is at $\lambda/4$ distance. The width of the strip feeder is 2mm that

corresponds to an impedance of 50Ω and the feeding point is at 25mm from the dipole (Figure 5.6).

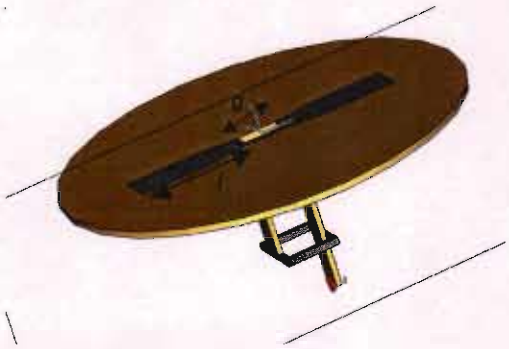

Fig. 5.5: Quarter wavelength balun structure

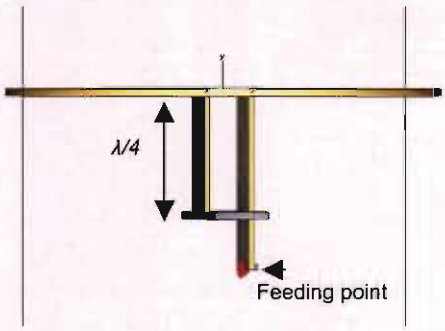

Fig. 5.6: Quarter wavelength balun structure

Figure 5.7 presents the simulated results for the return loss obtained using CST MWS. As it can be observed, the dipole is resonating around the frequency band of 2.5GHz which is the desired frequency but the return loss is poor. It needs to be greater that 10 dB over a wider frequency range. Different modifications and variations are modelled and tested in order to achieve a better reflection coefficient. Figure 5.8 shows the improvement obtained due to the optimization of the feeder width. The width of the feeder strip is 0.8mm which corresponds to a 81.3Ω line ($\epsilon_r = 3.2$), a high impedance line. The other parameters are identical to the first model.

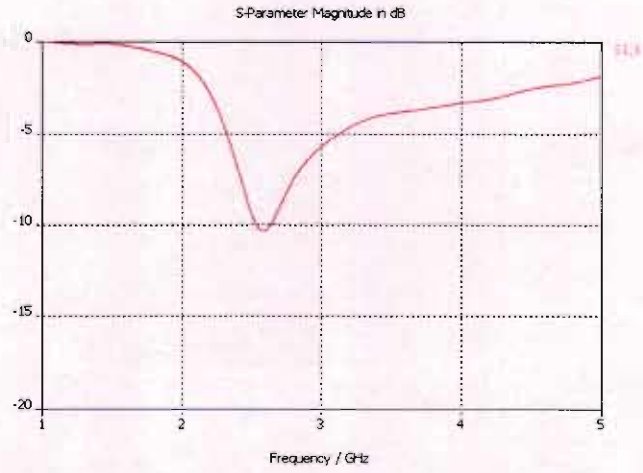

Fig. 5.7: Return loss for a single dipole using a quarter wavelength balun

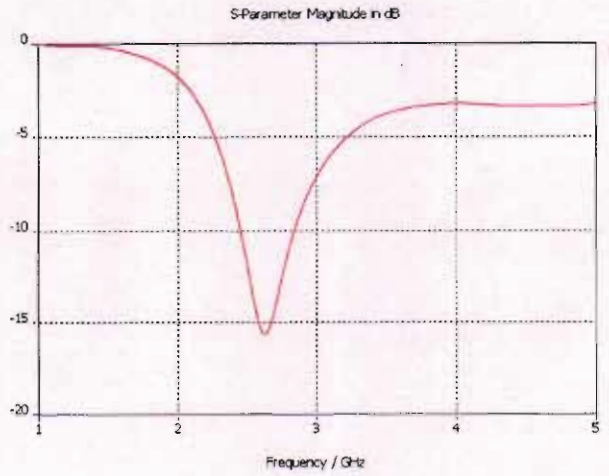

Fig. 5.8: Return loss for a single dipole using an optimized quarter wavelength balun

5.2.3 Crossed printed dipoles

In this section, a printed crossed-dipole antenna is designed and modelled using the quarterwave balun. An identical dipole was orthogonally added to the single dipole printed structure. A bigger hole was realized to permit the connection of the second dipole balun. Figure 5.9 shows the way of how the grounding of both dipoles was modelled. As it can be seen in the Figure a metal square ring makes possible the short circuit and thus the balun operation. The short circuit is located at $\lambda/4$ distance from the dipole. The strips used to feed the dipoles are 1mm thick, the width of the four microstriplines is 3.6mm and the feedpoint for both dipoles is 25mm from the dipole. The strip feeders are connected to the dipoles through perpendicular conducting bridges that are positioned at different heights.

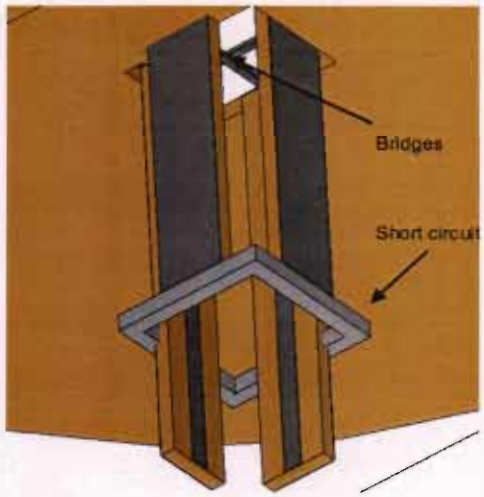

Fig. 5.9: Feeding structure for crossed dipoles

Figures 5.10 and 5.11 show the simulated return loss and the isolation respectively. The differences obtained between S11 and S22 in both figures are due to the bridges location. It is the only place where the structure is not symmetrical. In both Figures it can be observed that a resonance appears at 2GHz in the second port, this is due to an error in simulation. The return loss obtained is good around the required frequency band and the isolation achieved is considerably when the tapered balun is used (Ch 4). It can be seen in Figure 5.10 that the measured 10dB return loss bandwidth obtained is greater than 340 MHz.

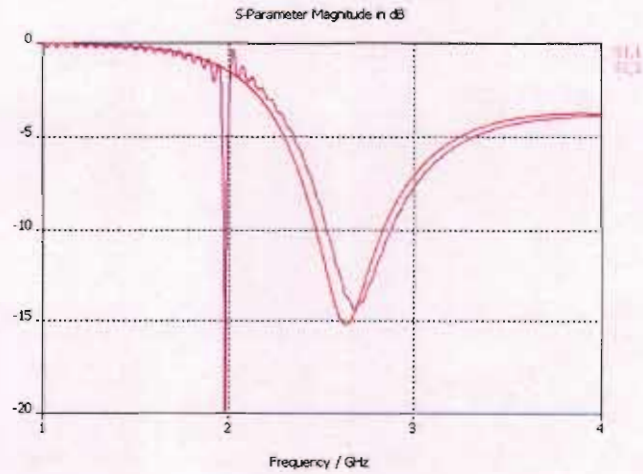

Fig. 5.10: Return loss for crossed dipoles using a quarter wavelength balun

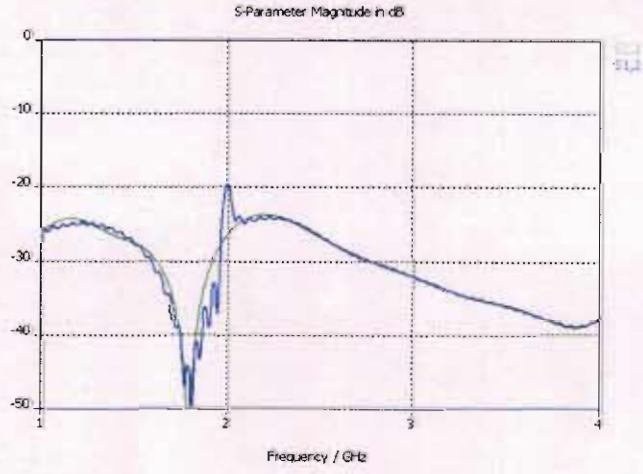

Fig. 5.11: Isolation for crossed dipoles using a quarter wavelength balun

One of the objectives of this design consists of achieving a directional antenna. To obtain directivity a parasitic reflector (35mmx35mmx2mm) is centrally added at the base of the structure at $\lambda/4$ distance from the dipole. The parasitic reflector

was not connected to the short circuit of the feeders in the first simulated model (Figure 5.12).

Fig. 5.12: Parasitic reflector centrally mounted

The return loss deteriorated and a bandwidth of around 150MHz was obtained. A different model was simulated where the parasitic reflector was located at 18mm distance from the dipoles, 1mm lower than the short circuit. The results achieved with the modified model improved the return loss results (bandwidth greater than 200 MHz). Figures 5.13 and 5.14 show the obtained results. It can be observed that the resonance is centred at 2.5GHz.

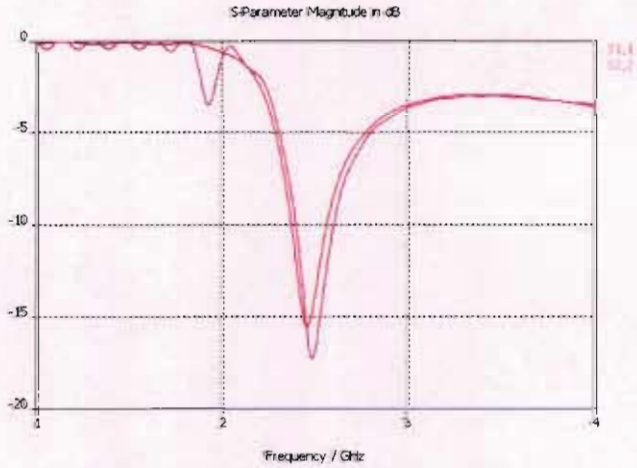

Fig. 5.13: Return loss for crossed dipoles and a parasitic reflector using a quarter wavelength balun

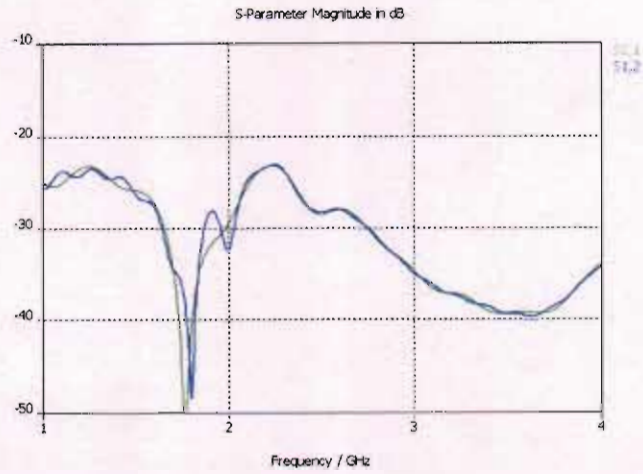

Fig. 5.14: Isolation for crossed dipoles and a parasitic reflector using quarter wavelength balun

Various changes to the geometry of the feed network were made to improve the bandwidth and isolation. The substrate of the feedlines was changed, a dielectric with a relative permittivity of 4.3 was chosen. Then, the reflector separation was reduced, as was the short circuit, specifically at 14.75mm because the $\lambda/4$ for the new permitivity is 14.75mm at 2.45GHz. The feeder strip was substituted by a transformer realized by employing different strip widths, with the objective of achieving the best feeding network to match the input impedance of the dipoles. By observing results of the scattering parameters S11 and S22 in the simulated Smith chart the relationship between the different parts of the transformers lines was clarified. Fig 5.15 illustrates a model where most of the elements have been hidden in order to show just the transformer lines clearly. The transformer consists of two parts, the first one is 1.6mm width that corresponds to 50Ω line (ϵ_r = 4.3) and the second one is 2.4mm thick which corresponds to 38Ω line, thus a transformer that transforms 50Ω to 28.8Ω. The junction of both lines is done at $\lambda/4$ from the dipoles. In Chapter 2 it has been explained that the impedance of a short and thick dipole is smaller than that of a thin dipole with the same overall dimensions. Using that feeding network a very good resonance was obtained at 2.5GHz but also a very narrow bandwidth, therefore the design was not approved.

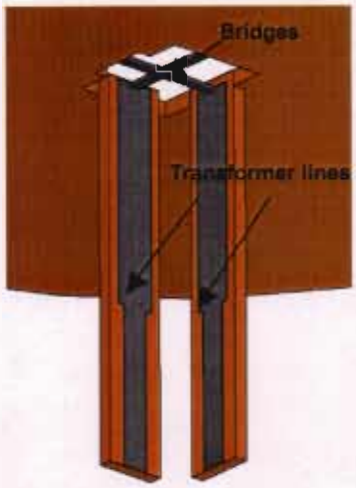

Fig. 5.15: Transformer lines

The next parameter investigated was the dipoles shape. Many different shapes were simulated and evaluated. Variations on the crossed dipole shape were made to increase the bandwidth as shown in Figure 5.16 and 5.17. All the modifications, variations and simulations realized on the antenna structure provided a valuable background understanding which led to the final stage. The triangular shape (Fig. 5.16) was evaluated because it is one of the most famous shapes for printed dipoles due to its good behaviour with wideband performances. The biconical antenna is used in Electromagnetic Compatibility (EMC) and radiation pattern measurements and that is because its recognized wideband behaviour and accuracy. Knowing that and trying to reproduce the same effects in the investigated antenna, the biconical shape (Fig. 5.17) was adapted to a planar printed scenario (the classical biconical antenna is either solid or made with wires and it is three-dimensional).

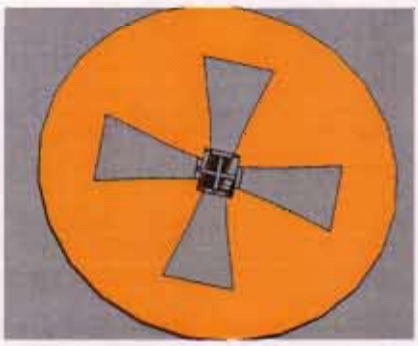

Fig. 5.16: Triangular shape

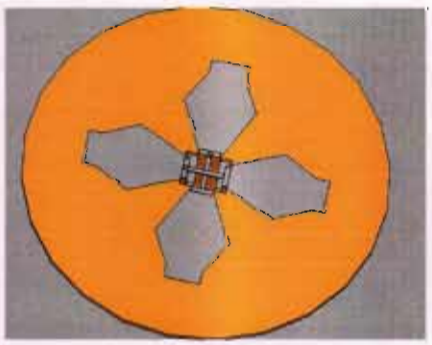

Fig. 5.17: Combined shape

5.3 Final design

In order to drive the design to its final stage, a few parameters were finally changed. The experience obtained over the previous chapters and sections has been invaluable. First of all, the size of the parasitic reflector has been increased. With this variation the antenna achieves higher gain, a better front to back ratio and return loss. The final separation between reflector and dipole is 14.75mm. In order to maintain a good isolation, many efforts were invested in the design of the new shape of the dipoles. In order to avoid coupling between both dipoles, the angle of the wing-shape was carefully modelled. Finally, as shown in Figure 5.18, orthogonal and symmetrical dipoles were designed. The antenna is modelled using a circular piece of FR4 laminate of 1mm thickness and radius r=30 mm. The relative permittivity is 4.3 in this frequency range. The dipole wing length l =17mm, the gap between dipole wings g = 6mm. The maximum width of the wing w= 12mm, which occurs at a distance $l2$ =6.3mm from the end of the wing.

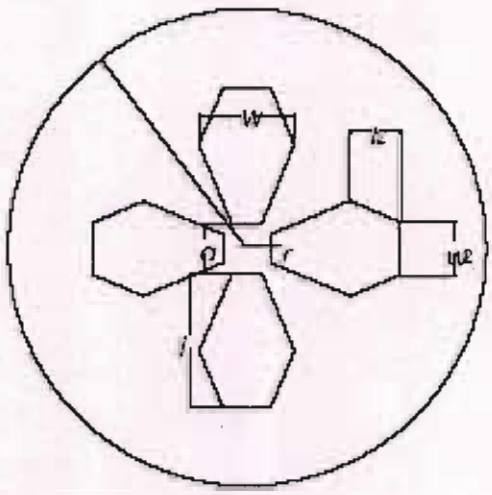

Fig. 5.18: Geometry for the printed crossed-dipole antenna

Matching between the dipoles and the feeding network was necessary to ensure a good result for the return loss. For that reason the investigation of the proper feeder performance was one of the main parts of the final design. A 4mm strip was selected (the feeder impedance has decreased to 26Ω using a dielectric with relative permittivity of 4.3) and that is due the lower impedance of the new dipole

shape. The feeding point is now located at 30.35mm distance from the dipoles. Figure 5.19 shows the final model.

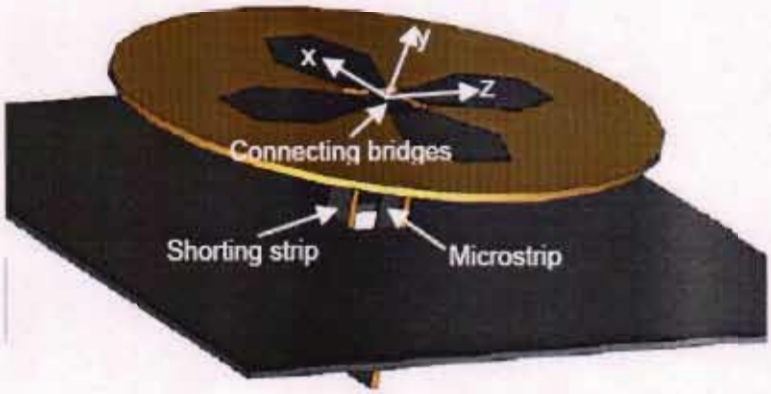

Fig. 5.19: Final model and coordinate system

Once that the variations and the modifications have been explained and the final dimensions have been defined, the results achieved with the final model are presented in Figures 5.20 and 5.21.

Fig. 5.20: Simulated return loss for the final design

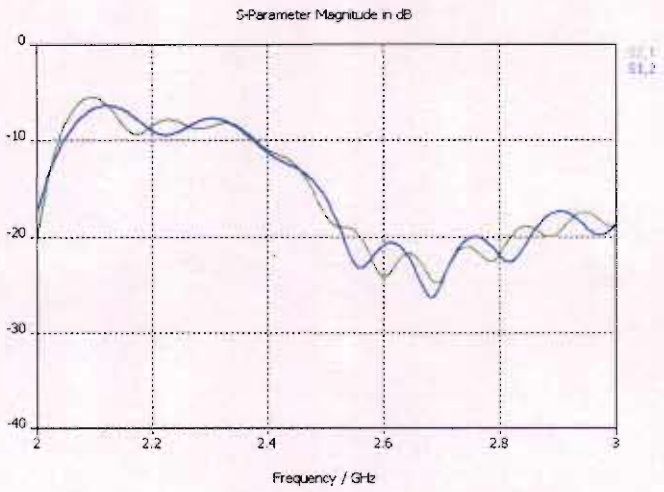

Fig.5.21: Simulated isolation for the final design

It can be seen in Figure 5.20 that the return loss is not the same for both dipoles. That is caused by the asymmetry that the bridges introduce into the performance. In both cases the bandwidth result is greater than 230MHz for a 10dB return loss (from 2.45 to 2.72 GHz for S11 and from 2.45 to 2.68GHz for S22). The simulated isolation is better than 13dB from 2.45 to 2.53GHz and better than 20dB from 2.53 to 2.8GHz. These results guarantee no coupling between the dipoles in a real operation scenario. As it can be observed the obtained bandwith is somewhat smaller than that obtained in the previous chapter; this is due to the compromise that must be made between wideband return loss and the isolation. The isolation is significantly improved compared to that in previous chapter. The simulated radiation patterns are shown in Figure 5.22 and 5.23. The dipole that is oriented to Z axis corresponds to -45 degree port and the dipole the dipole that is oriented to X axis corresponds to +45 degree port.

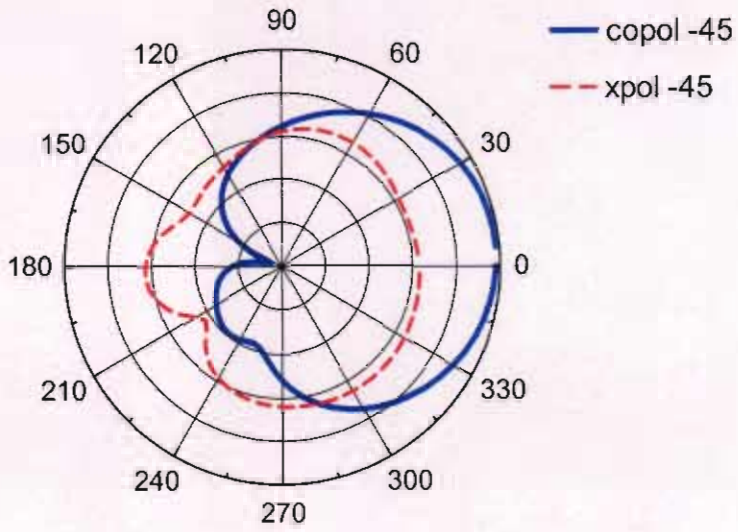

Fig. 5.22: Normalised simulated radiation pattern for -45 degrees plane at 2.5GHz

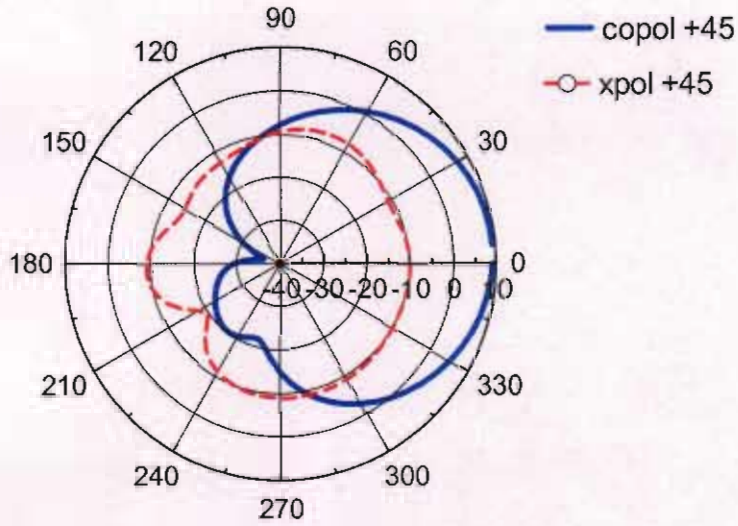

Fig. 5.23: Normalised simulated radiation pattern for +45 degrees plane at 2.5GHz

Figure 5.22 and 5.23 show the copolar and crosspolar normalised radiation patterns, where a gain of 9.3dBi (with the maximum at 0 degrees, therefore no squint) was obtained in both ports. From the Figures it can be observed that the front-to-back ratio is better than 30dB. The copolar beamwidth is 61.1° for the +45 port and 60.5° for the -45 port. The total efficiency and the radiation efficiency are 0.877% and 0.947% for -45 port respectively and 0.889% and 0.963% for +45 port. The linear cross-polarization rejection levels are better than 20dB on boresight on both ports. In order to summarize, a good bandwidth,

reasonable isolation and good radiation parameters were obtained. The antenna is now fabricated.

5.4 Fabrication and measurements

In this section, features and dimensions of the fabricated prototype are presented. The antenna was fabricated by exporting a 2D DXF file from the EM solver, then the file is input to a CAD package, which in turn, is transferred to the LPKF milling machine, which mills the patch antenna on the laminate. The feedlines are then cut and milled. Two SMA launch connectors are soldered at the end of the feeder lines. The measured results obtained with the prototype antenna are also shown.

Fig. 5.24: Photograph of the fabricated antenna

The antenna is fabricated on a circular piece of FR4 laminate of 1mm thickness and 4.3 of relative permitivity. The dimensions are the same that were used in the simulation (Fig. 5.18). A parasitic planar reflector of 70 x70 x 1mm was soldered to the feeders' strips in order to short the ground. Each vertical element comprises a shorting strip and an impedance transformer realized by using a FR4 laminate of 0.8mm thickness and a permitivity of 4.3. The return loss and the isolation were measured using an Agilent Technologies vector network analyser (VNA) (appendix 1). It can be seen in Figure 5.25 that the measured 10dB return loss (S11 and S22) is achieved from about 2.25 GHz to 2.7 GHz, yielding an impedance bandwidth of greater than 450 MHz (more than 18% fractional impedance bandwidth) for both ports. The measured isolation (S12 and S21) is

better than 20dB for most of the bandwidth, i.e. from 2.35 GHz to 2.55 GHz. This includes the wireless ISM band (2.40 to 2.488GHz). Comparing with the results obtained in the simulation it can be observed that the measured impedance bandwidth is wider, moreover the resonance is not as deep. The isolation result is also better than the simulated one, but in this case agreement between them is reached. In this case the measured values outperform the simulated ones. This occurs because the feeding point location is a very sensitive parameter that in the simulation corresponds to a very small point and in the fabricated prototype corresponds to a couple of millimetres diameter and for the inner of the SMA connector depends on the drilling and soldering procedures. Therefore the slightly different result was caused by the inaccuracy of the fabrication.

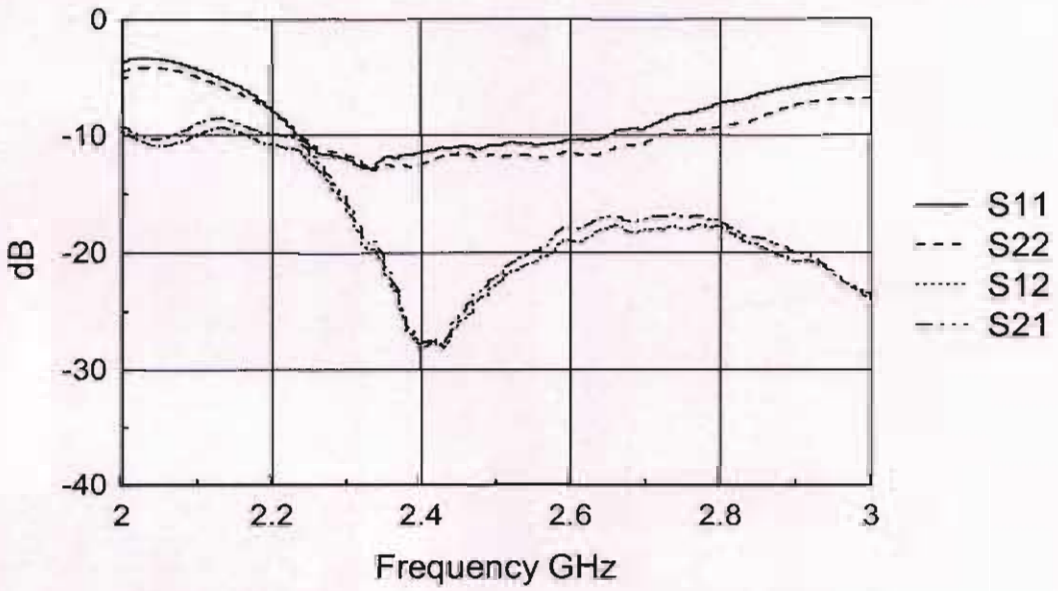

Fig. 5.25: Measured impedance bandwidth and isolation between ports for the crossed dipole antenna

The radiation patterns were measured in an anechoic chamber at 2.45 GHz for both polarizations. Figure 5.26 shows the measured pattern for the -45 degree plane, while the -45 degree plane is shown in Figure 5.27. The linear cross-polarization rejection levels are better that 20 dB on boresight and the front-to-back ratios are in excess of 20 dB for both planes. The patterns are normalised to maximum measured gain, which was 6.5dBi for both polarizations. A 10 dB per division scale is used. The gain was measured with a calibrated pyramidal horn antenna (see appendix 4).

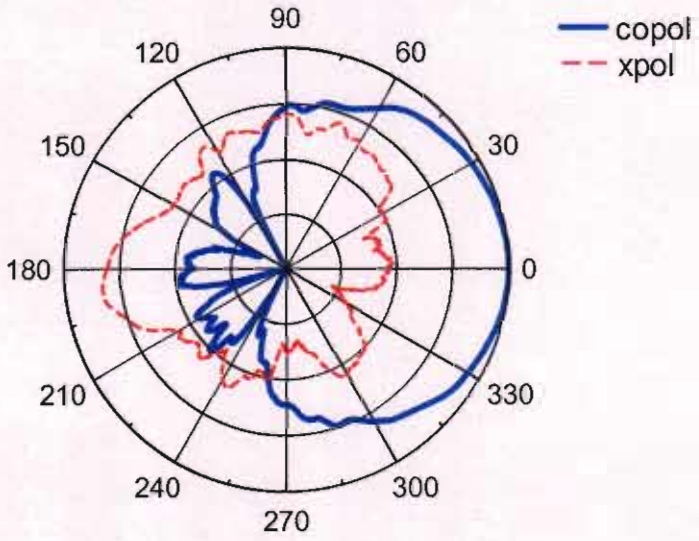

Fig. 5.26: Normalised measured radiation pattern for +45 degrees plane at 2.5GHz

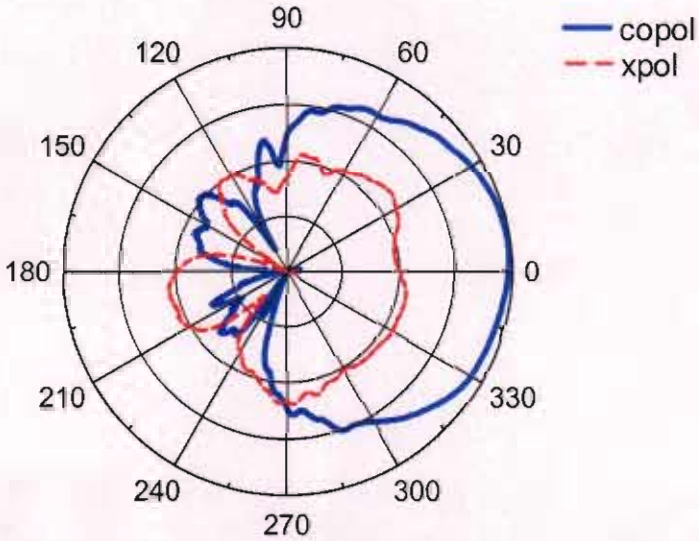

Fig. 5.27: Normalised measured radiation pattern for -45 degrees plane at 2.5GHz

5.5 Dual polarization and circular polarization capabilities.

The element can now provide 2 independent orthogonally polarized signals. Circular polarization can also be achieved by exciting each dipole port with equal magnitude, but with a phase difference of 90 degrees, depending on whether right-hand circular polarization (RHCP) or left-hand circular-polarization (LHCP) is required. A spinning dipole is often used to examine the axial-ratio performance for circularly-polarized antennas. The spinning dipole was excited by one port of

the Rohde & Schwarz ZVA24 vector network analyser and port two is connected to the antenna. The analyser is frequency swept and the antenna response is shown in Figure 5.28. It can be seen that the axial ratio (S21, in this case) is less than 4 dB from 2.4 GHz to 2.63 GHz. The spinning dipole pattern shows good circular polarization at 2.5 GHz over a wide beamwidth in Figure 5.29.

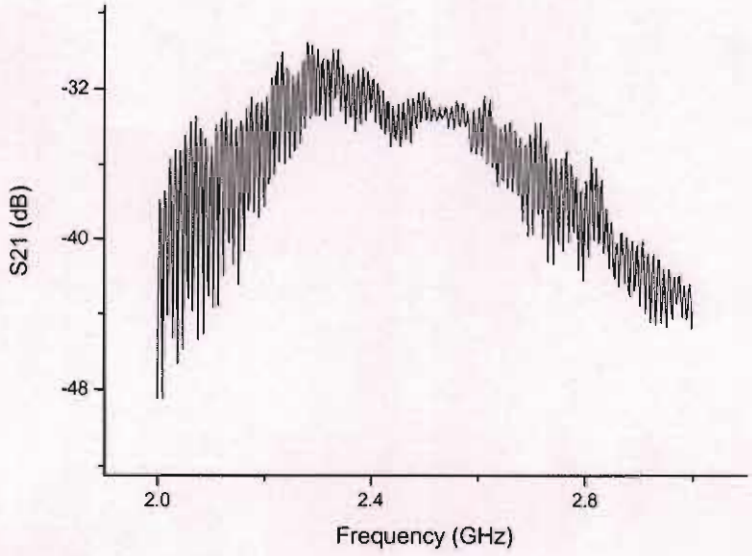

Fig. 5.28: Measured axial ratio

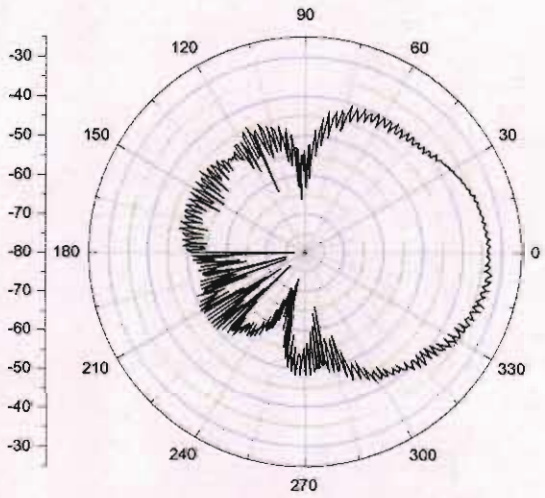

Fig. 5.29: Measured spinning dipole radiation pattern.

5.6 Conclusion

In this chapter the design and the fabrication of a dual polarized base station antenna fed by a perpendicular quarterwave balun has been described. Valuable

expertise has been acquired evaluating the different relative permitivities of the dielectric substrate and examining these effects on the antenna dimensions and on the final performance (as the reduction of the dipole length, hence the reduced size of the antenna). In order to follow a step by step procedure, a single dipole fed by the chosen feeding technique, the quarter wave balun, was investigated. The width of feeding tracks and the grounding location was optimized in order to obtain a wideband return loss. A second orthogonal dipole was added to the structure to achieve dual polarization with good isolation. A parasitic reflector was introduced and the directivity was obtained. Good isolation, bandwidth and gain were achieved but several modifications were carried out in the different parameters (permitivity, tracks width...) in order to optimise performance. An optimized dipole shape was tested and superior return loss characteristics were obtained due to the enhanced matching. This optimized structure was fabricated and tested and the desired results were achieved experimentally. Radiation patterns were measured in an open range and patterns suitable for a base station antenna were achieved over the full frequency range. Circular polarization capabilities were also examined and good results were obtained.

CHAPTER 6:

CONCLUSION

In this thesis two different types of antennas have been investigated, microstrip patch antennas and printed dipole antennas. Both a single halfwave rectangular patch and a microstrip patch array were developed using microstrip radiators and feed techniques. For the microstrip antennas RT/duroid 5870 was the chosen substrate. It was selected due to its good stability of ε_r and tolerance of parameters such as ε_r, $\tan\delta$ and anisotropy. Very good agreement between the simulated and measured results was obtained for the single rectangular patch and the array. For the single patch, results were predictable. For the array, a good gain (12dBi) and reasonable impedance bandwidth (-14dB return loss from 2.4 to 2.5GHz) were achieved and therefore the performance would be suitable for wireless communication systems. The horizontal and vertical planes were also measured for both antennas and the achieved results present proper patterns for access points in WiFi networks. In both cases low profile was achieved. However, the disadvantage of these antennas is the high cost of the substrate. Using a cheaper substrate would decrease the radiation efficiency and hence the antenna gain. The bandwidth may also be reduced. In order to keep costs down and to obtain features like dual and circular polarization capabilities, another design was investigated.

Two crossed dipole printed antennas with different feeding networks were also developed. All were empirically designed, simulated and tested in the frequency range of 2.45GHz. For the simulation all the antennas were modelled and evaluated with CST Microwave Studio, a 3D electromagnetic simulation software based on the Finite Integration Time Domain (FITD). It should be mentioned that substantial efforts were realized in order to set the meshing parameters correctly (increasing the number of cells or varying the lines per wavelength) and to orientate the ports, because they should be placed in the direction of the global coordinate system (XYZ). .Fabricated antennas were tested and measured using high class vector network analysers and patterns were measured both in indoor

and outdoor test ranges. Multiple types of substrate with different permittivity were been used in the antenna designs.

The dual polarized antenna with tapered balun feed proved to be very complex. For this antenna the low-cost FR-4 laminate was used, a low frequency substrate for the dipoles and GML 1000 was used for the feed lines (a perpendicular structure that consists of two back to back microstrip substrates). A tapered balun was added to improve the matching. The bandwidth obtained (350 MHz in the measurement) is acceptable for wireless applications. The isolation results were very poor from the beginning of the design and despite many optimizations and much effort, the balun failed to achieve the required performance. Squint was found in the radiation pattern of the antenna. This squint problem was very hard to avoid and an in-depth investigation was carried out. The antenna pattern was measured at different frequencies and it was observed that squint was frequency dependent. Thus there was a phase differences between the two dipoles ports, caused by the asymmetry of the feeding tracks. In order to solve the problem the antenna was redesigned to be totally symmetrical in all respects. This reduced the squint somewhat but the port-to-port isolation was still poor. In this stage of the project it was confirmed that the baluns were not operating and were resonating as part of the dipoles. The tapered balun feed network did not work as was expected, hence, it proved to be a bad choice to provide dual polarization over a wide bandwidth. After some changes the squint disappeared but the isolation was still poor.

With the goal of improving the performance of the dual polarized printed antenna, a different feed network was developed. It is also a perpendicular structure and it consists on a quarterwave balun which was selected due to its proven performance and features. In this antenna FR4 was used for the dipoles and for the feed lines because of the low cost of this material.

Good results for isolation and return loss were obtained on the first simulation run. However, by optimising the dipole wing geometry and the dimensions, a wide bandwidth was achieved (greater than 230MHz for a 10dB return loss), without significant degradation of port-to-port isolation, crosspolar performance,

gain or circular-polarization performance. The return loss (S11 and S22) was measured over a frequency range from 2.25GHz to 2.7GHz and was yielded more than 18% fractional impedance bandwidth. The measured S12 and S21 values (in the measured isolation) were better than 20dB from 2.35GHz to 2.55GHz (most of the bandwidth, including the wireless ISM band, 2.40 to 2.48GHz). The patterns were also measured and either +45 as -45 patterns obtained competitive results over the frequency range. The front to back ratio was better than 20dB (very important parameter for a base station antenna). The crossed polar rejection was also better than 20dB on the boresight, something which confirms desirable behaviour of the dual polarization and therefore the diversity. The antenna has a gain of 6.5 dBi, over the frequency range of 2.2GHz to 2.7 GHz, for linear polarizations. The antenna produced circularly-polarized waves with an axial ratio less than 4 dB, from 2.4 GHz to 2.63 GHz. The measured port-to-port isolation is greater than 20 dB over this range.

Another important feature to highlight is the small dimension of the antenna, something that nowadays gains importance due to the visual impact sensitivity which exists in society. Therefore thanks to the low profile, the cost of the antenna is lower and that would help in a fabrication process.

A possible further improvement in performance may be possible by optimizing the feed line and the balun transformers. This could yield a small increase in bandwidth and gain. The emerging communication standards (802.11n, 802.16d, 802.16e, WiBro...) will require polarization diversity and high gain base station antennas. The low-cost and low profile of the proposed antennas fulfil some of the requirements that the current market demands. Future work would involve arraying these elements and developing a feed network for polarization agility.

REFERENCES

[1] Arai, H., *Measurement of Mobile Antenna Systems*, Artech House, Norwood, 2001.

[2] Ammann, M. J., *Design of Rectangular Micro strip Patch Antennas for the 2.4 GHz Band, Applied Microwave and wireless ,9*, (6), pp 24-34, 1997.

[3] Balanis, C. A., *Antenna theory, Analysis and Design*, John Wiley & Sons, New York, 1997.

[4] Bhartia P, Bahl I.J., *Microstrip antennas,* Artech House, pp 1-22

[5] Bhartia P, Tomar R.S., Rau K.U.S, *Milimeter-wave Microstrip and printed circuit antennas,* Artech House, pp 41-86

[6] Cardama, A., *Antenas*, Ediciones UPC, Barcelona 1998.

[7] Clemens M. and Weiland T., 'Discrete Electromagnetism with the Finite Integration Technique', *Progress In Electromagnetics Research,* PIER 32, 65–87, 2001

[8] Chen W-S, "A novel broadband design of a printed rectangular slot antenna for wireless applications", *Microwave Journal*, pp 122-130, January 2006

[9] Chuang H.R., Kan Y.C., "A printed UWB triangular monopole antenna" *Microwave journal*, pp 108-120, January 2006

[10] Edward J. and Rees D., "A broadband printed dipole with integrated balun," *Microwave J.*, pp. 339–344, May 1987.

[11] Electromagnetic waves series 28, *Handbook of microstrip antennas Vol1,* JR James and PS Hall, Vol1 pp 275-281

[12] Electromagnetic waves series 28, *Handbook of microstrip antennas Vol2,* JR James and PS Hall, Vol1 pp 815-843

[13] Faton, T. and Craig, A.G., 'Design of Broad-Band and Dual-Band Antennas Comprised of Series-Fed Printed-strip Dipole Pairs', *IEEE Transactions on antennas and propagation,* 48,no 6, Jun 2000

[14] Friis, H., 'A Note on Simple Transmission Formula' *Proc.* IRE, 34, pp 34-39, 1946.

[15] Fujimoto K. and James J.R., *Mobile Antenna Systems Handbook*, Artech House, Norwood, 2001.

[16] Hallen E., , "Theoretical investigations into the transmitting and receiving qualities of antennae", *Nova Acta Regiae Soc. Sci. Upsaliensis*, Sec. IV, 11, No. 4, pp. 1-44. 1938.

[17] Herscovici N. I., Pozar D. M.; "Full-wave solution for an aperture-coupled patch fed by perpendicular coplanar strips", *IEEE Trans. Antennas Propagat.*, vol. 42, pp. 544-547, April 1994.

[18] Hilton G.S., Railton C.J., Ball G. J., Hume A. L., and Dean M., "Finite difference time-domain analysis of a printed dipole antenna" *9th Int.IEEE Antennas and Propagation Conf.*, pp. 72–75,vol. 1, 1995.

[19] Hsu P., Chen S., "A modified quasi-yagi antenna fed by a microstrip lines" *Proceedings of 2003 Asia-Pacific Microwave Conference (APMC 2003)*, pp. 1741-1743, Seoul, Korea, Nov. 2003.

[20] Huey-Ru C., Liang-Chen K., Chi-Chang L. and Wen-Tzu C., 'A 2.4 GHz Polarization-diversity Planar Printed Dipole Antenna for WLAN and Wireless Communication Applications', *Microwave Journal*, pp. 895-900, Sep 2002.

[21] Hsu P., Chen S., "A modified quasi-yagi antenna fed by a microstrip lines" *Proceedings of 2003 Asia-Pacific Microwave Conference (APMC 2003)*, pp. 1741-1743, Seoul, Korea, Nov. 2003.

[22] Jasik H, Johnson R.C., *Antenna Engineering Handbook,,* MacGraw-Hill, 2nd edition, pp 4.1-4.13 and 17.1-17-13

[23] Jokanovic B, Marincic A, "Analysis of the parasitic effects in double-Y baluns", *IEE Proc. Microw. Antennas propagation*, Vol. 148, No.4, pp. 239-245, August 2001

[24] Kaneda N., "A broadband microstrip-to-waveguide transition using quasi-Yagi antenna", *IEEE Transactions on microwave theory and techniques*, Vol. 47, No. 12, pp. 2562-2567, December 1999

[25] Kian S. A., Roberston I. A., "Analysis and design of impedance-transforming planar marchand baluns", *IEEE Transactions on microwave theory and techniques*, vol 49, No 2, pp. 402-406, February 2001.

[26] Kim J.I., Lee B.M. and Yoon Y.J., "Wideband printed dipole antenna for multiple wireless services". *Radio and Wireless Conference 2001*, Waltham, MA, pp.153-156, 2001

[27] Kim J.I., Yoon Y.J and Choi J.I., "Wideband printed fat dipole with folded balun". *JINA (International Symposium on Antennas)2002*, vol. 1 pp 259-262, Nice, France, 2002

[28] King R. W. P, "The linear antenna, eighty years of progress", *Proceedings of the IEEE*, Vol. 55, No 1, pp. 2-16 January, 1967

[29] Kraus,J., *Antennas,* MacGraw-Hill, pp. 239-251 , 318-328 and 426-441, London 1950

[30] Lee H F, Chein W, *Advances in microstrip and printed antennas,* Wiley-Interscience, 1997

[31] Lee H., Lim Y., "A design of double T-type microstrip antennas for broadband and control of resonance", *Microwave Journal*, pp. 132-140, January 2006

[32] Mahmoud B, Prasad S. N, "Wideband, planar, log-periodic balun", IEEE,1998

[33] Michishita N., Arai H., Nakano M., Satoh T. and Matsuoka T., "FDTD analysis for printed dipole antenna with balun," in *Asia–Pacific Microwave Conf.*, pp. 739–742, 2000.

[34] Milligan T., Meys R., "Measuring the impedance of balanced antennas by an S-Parameter Method", IEEE *Antennas and propagation magazine*, Vol. 40, No. 6, pp. 62-65, Decenber 1998

[35] Nesic A, Jovanovic S, Radnovic I; "Wideband printed antenna with circular polarization", *1997 IEEE Int. Antennas Propagat. Symp.* Dig. vol. 35, pp. 1882 - 1885, June 1997.

[36] Pitman, *Antenna theory design*, Williams P., Vol. 2, pp. 118-127, London 1966

[37] Pozar D.M., *Microwave Engineering*, Second Edition, John Wiley & Sons, Inc., pp. 183-190 and 288-292, 1998.

[38] Pozar D M, Jackson Jr. R W.; An aperture coupled microstrip antenna with a proximity feed on a perpendicular substrate, IEEE Trans. Antennas Propagat., vol. 35, pp. 728 -731, June 1987.

[39] Puglia K. V., "Electromagnetic simulation of some common balun structures", *IEEE Microwave magazine*, pp. 56-61, September 2002

[40] Shih-Yuan Chen and Powen Hsu, "A modified quasi-yagi antenna fed by a microstrip line", *Proceedings of 2003 Asia-Pacific Microwave Conference (APMC 2003)*, pp. 1741-1743, Seoul, Korea, Nov. 2003

[41] Shu L, Elshabini-Riad A, "Characterization and modelling of a wideband microstrip balun", IEEE, pp.220-221, 1990

[42] Simons R. N., Dib N. I., "Coplanar stripline to microstrip transition", *Electronic letters*, Vol. 31, No 20, pp. 1725-1726

[43] Smolders A.B., Arts M. J., "Wideband antenna element with integrated balun", *IEEE APS int. Symposium Atlanta*, USA 1998

[44] Sun J. S., Chen G. Y., "A novel design of the planar coupled-line balun", 3rd *International conference on microwave and millimetre wave technology proceedings*, pp. 1117-1120. 2002

[45] Trifunovic V., Jokanovic B., "Review of printed marchand and double Y baluns: Characteristics and Application", IEEE Transactions on microwave theory and techniques, vol 42, No. 8, pp 1454-1462, August 1994

[46] Weem J.P., Notaros B.M., "Broadband element array considerations for SKA", A.B. Smolders and M.P. Haarlem (eds.), *Perspectives on Radio Astronomy – Techonologies for Large Antenna Arrays*, Netherlands Foundation for Research in Astronomy, 1999

[47] Win M., Scholtz R.A. and Barnes M. A., "Ultra-Wide Bandwidth Signal Propagation for Indoor Wireless Communications," in *IEEE Int. Conf. Communications*, pp. 56–60, June 1997.

PUBLICATIONS

F. Leon-Lerma, M. John, G, Ruvio, M. J. Ammann and N. Herscovici
Wideband Directional Base-Station Antenna with Dual-linear and Circular-Polarization Capabilities
IEE Irish Signals & Systems Conf, 253-256, 2006.

Leon Lerma, F, Ruvio G., Ammann M. J
A Microstrip-fed Printed Crossed Dipole for Wireless Applications
Microwave and Optical Technology Letters, 2006, (4), 751-753

N. Herscovici, Leon Lerma, F, Ammann M. J,
A New Architecture for a Multi Polarized, Perpendicularly-Fed, Radiating Element
IEEE International Antennas & Propagat. Symp., Dig. 2005, (3), 487-490

Evans J. A, Leon Lerma, F and Ammann M. J,
Printed Antenna with Electromagnetically-coupled Slotted Element
9th IEEE HFPGS Colloq. Digest, 2004, IEEE Catalog No: 04TH8740, 81-86.

APPENDIX A1

Equipment

37369A Vector Network Analyzer Anritsu

The network analyser 37369A Anritsu is used to measure the Scattering Parameters of the antennas. Mainly it has been used to measure the return loss, S11.

Vector Network Analyzers (VNA) are designed to measure S-Parameters of RF and Microwave devices and circuits. S-Parameters are by definition ratios and as such the actual test power utilized is not critical. When amplifier S-Parameters are measured it becomes important to know approximate input and output power levels so that the user can insure that the amplifier is operating in its proper range and that the instrument's power handling capability is not exceeded. The frequency range is 40MHz-40GHz.

Fig. A1.1: Network analyser Anritsu 37369A

8753B Network Analyzer Hewlett Packard

The Hewlett Packard 8753-B Network analyser is used for Gain and Radiation Pattern measurements on all antennas.

The network analyser is essentially a Superheterodyne Receiver. Superheterodyne means to mix two frequencies together to produce a different frequency output. Here the audio signal is down converted and demodulated from the higher carrier frequency. In a similar way the high frequency input RF signal to the Network Analyser is frequency shifted down to a lower frequency that can be sampled by the analogue to digital converter. The frequency range is 300kHz-6GHz.

Fig. A1.2: Network analyser Hewlett Packard 8753B

E5070B vector Network Analyser Agilent Technologies

This Network Analyser was used to carry out the measurements on the crossed dipole antenna with improved feed system.

The Agilent ENA dramatically improves measurement accuracy and responds to current and future test needs. Because it performs up to 125 dB wide dynamic range at 10 Hz IFBW, the sweep speed can be faster at the required dynamic range. The trace noise is lowered to 0.001 dB rms at 3 kHz IFBW. It delivers accurate pass band ripple measurement of a filter. The ENA's excellent measurement performance improves test quality and repeatability as well as test throughput, which affect production yield and the overall cost of test. The frequency range is 300 kHz to 3 GHz and the number of ports is 4.

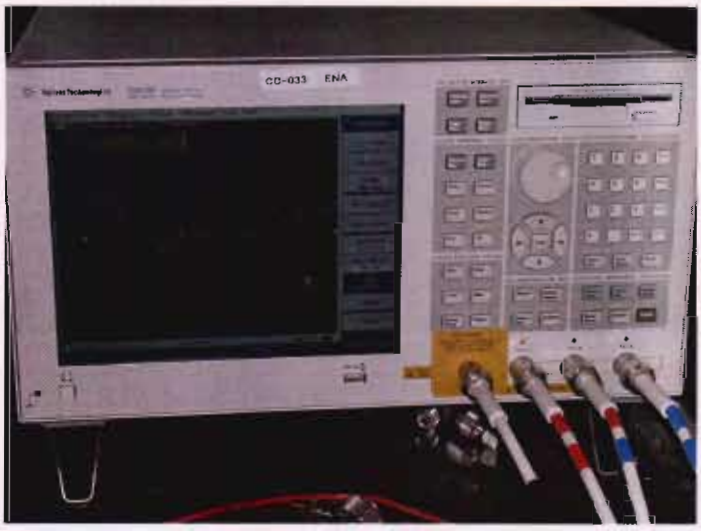

Fig. A1.3: Network analyser Agilent Technologies E5070B

ZVA24 vector Network analyser Rohde & Schwarz

This Network Analyser was used to carry out the measurements on the crossed dipole antenna with improved feed system.

The R&S ZVA24 is the new high-end model of the vector network analyzer family from Rohde & Schwarz. The new model comes with two or four test ports and is designed to operate in the frequency range from 10 MHz to 24 GHz. With a dynamic range of more than typ. 145 dB, an IF bandwidth of up to 1 MHz and a measurement speed of 3.5 µs per test point, the R&S ZVA24 offers features unparalleled in the field of network analysis. Its excellent characteristics make the analyzer an ideal choice for applications where the most exacting demands for accuracy, dynamic range, sensitivity and flexibility have to be fulfilled

Fig. A1.4: Network analyser ZVA24 Rohde&Schwarz

APPENDIX A2

Antenna fabricated

Single Patch

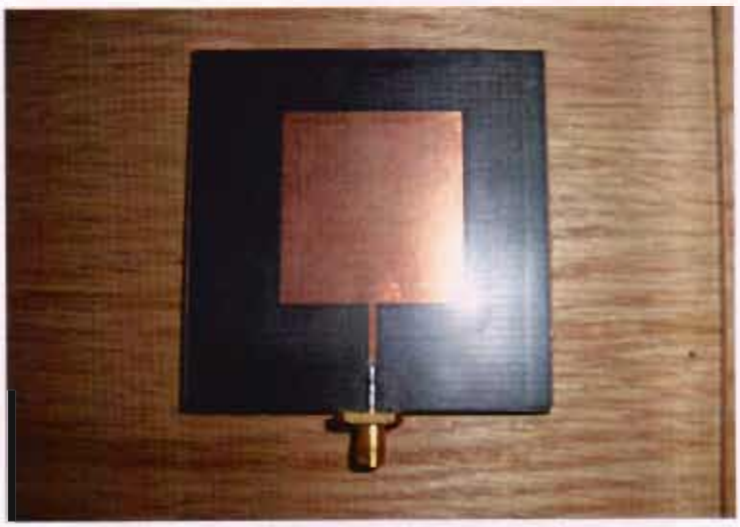

Fig. A2. 1.: Microstrip single patch

Array

Fig. A2. 2: Microstrip Array

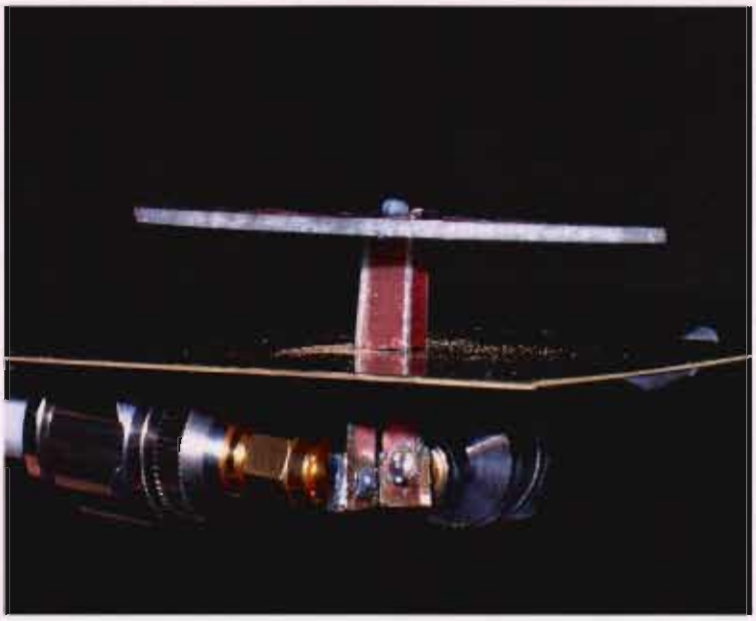

Fig. A2. 5: Crossed dipole antenna with improved feed system, left view

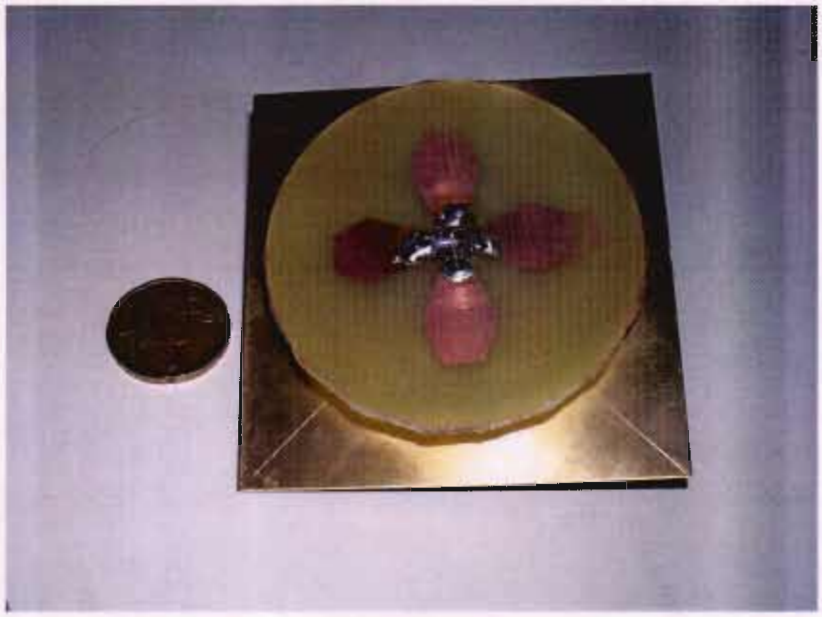

Fig. A2. 6: Crossed dipole antenna with improved feed system, front view

APPENDIX A3

3D Simulated Radiation Patterns

In the next figures we can see the 3D radiation pattern plots of the four different antennas that have been designed. Several antenna parameters can also be seen in the figures.

Single Patch

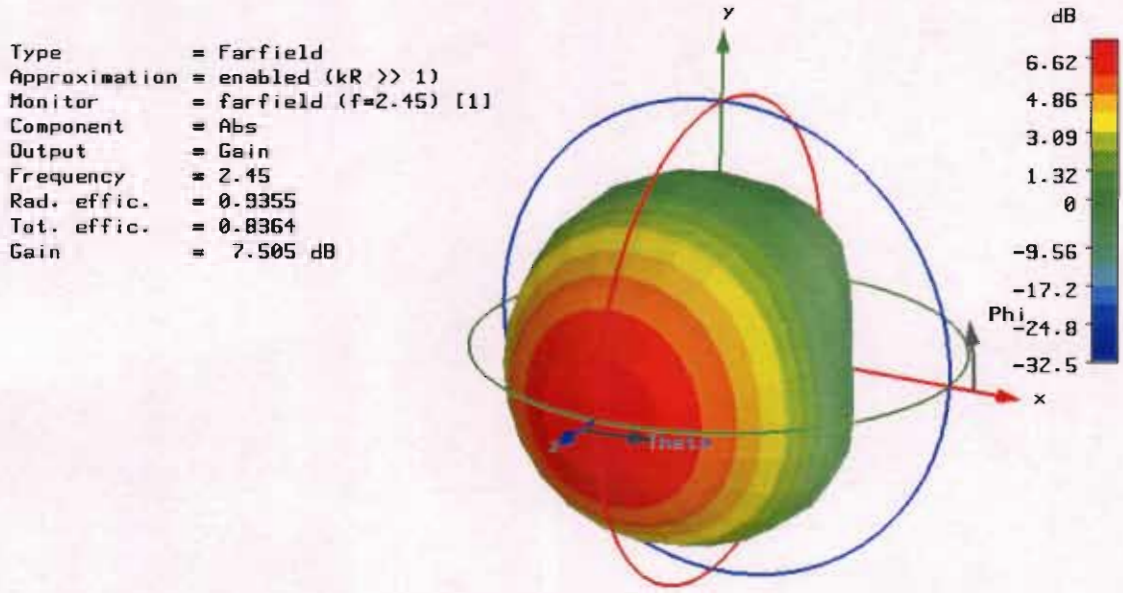

Fig. A 3.1: 3D Radiation pattern for microstrip single antenna

Array

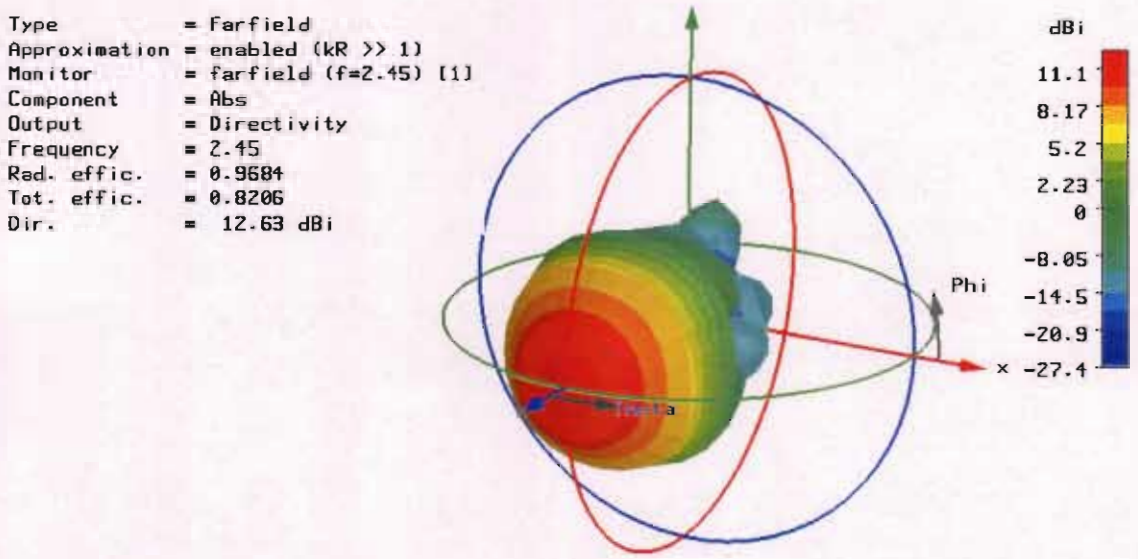

Fig. A3.2: 3D Radiation pattern for microstrip array antenna

Crossed dipole antenna

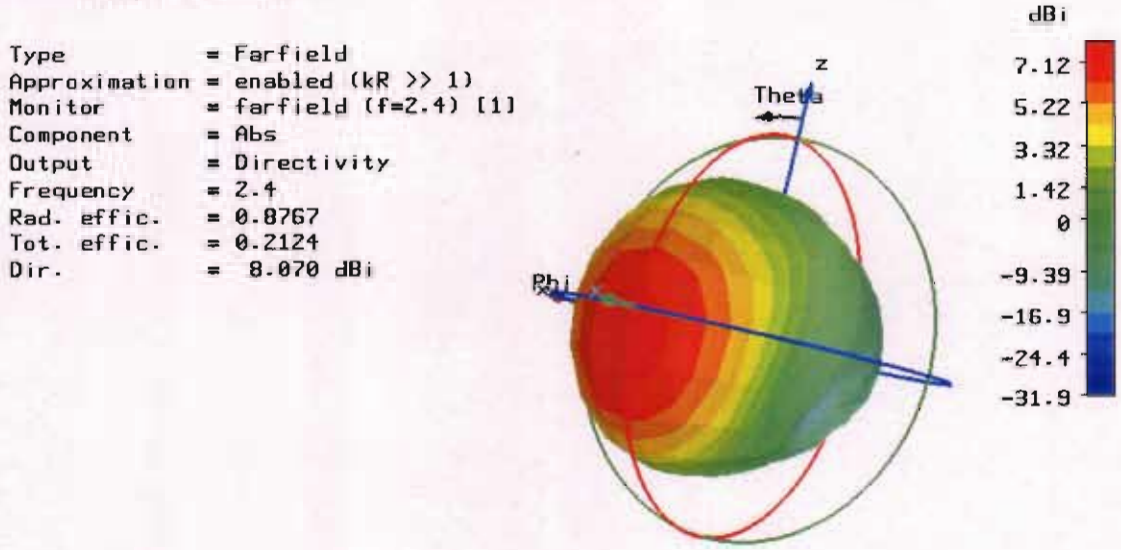

Fig. A3.3: 3D Radiation pattern for the dual polarized antenna

Crossed dipole antenna with improved feed system

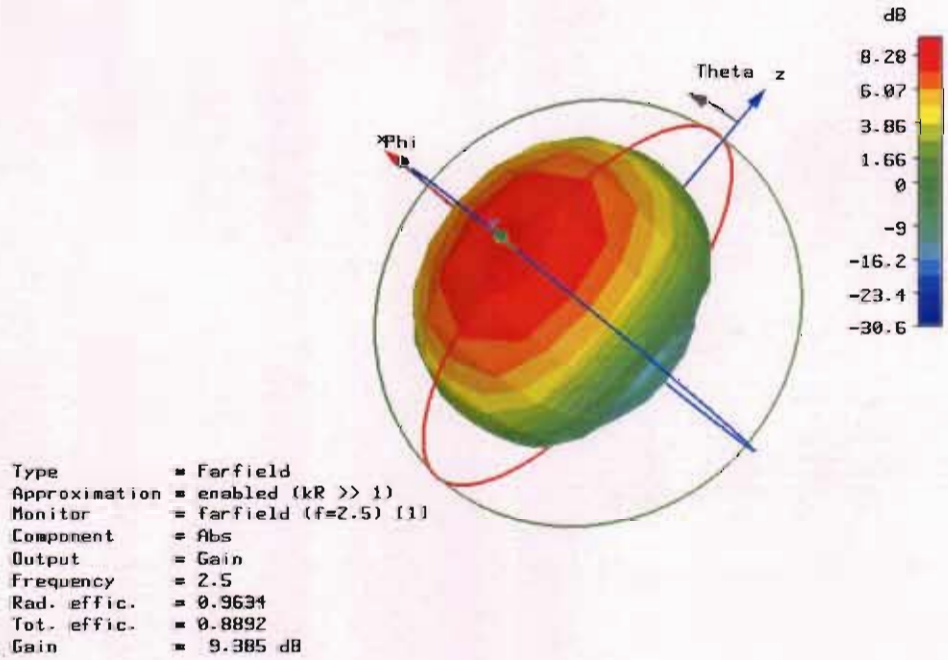

Fig. A3.4: 3D Radiation pattern for the dual polarized antenna with improved feed system

APPENDIX A4

Measured Radiation Patterns

In the next figures we can see the measured radiation pattern plots and the gain of the crossed dipole antenna for each linear polarization with improved feed system. Several antenna parameters can also be seen in the figures.

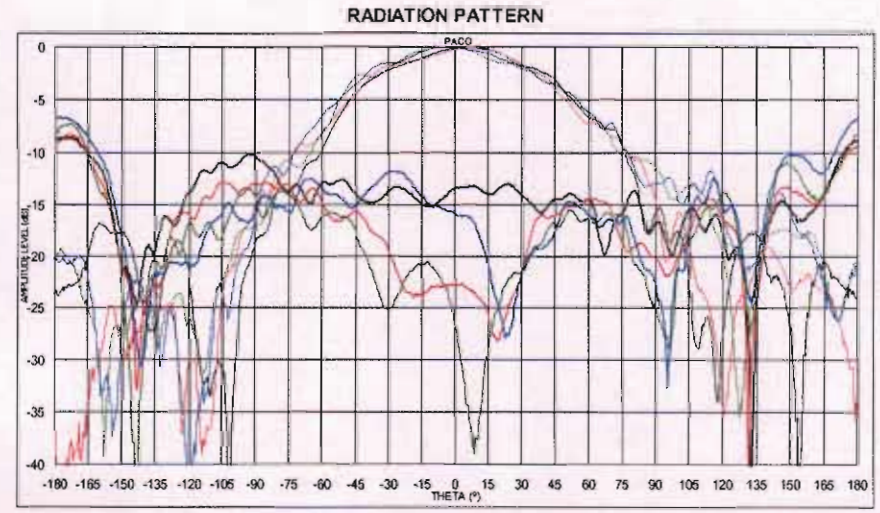

	CP-45 2300Mhz			
-3dB Beamwidth	81.7°	77.5°	87.6°	80.2°
-10dB Beamwidth	136.6°	149.5°	142.9°	149.7°
-3 dB Bw. Beam-Tilt	3.4°	-0.1°	-0.8°	-1.8°
Horizont Vs Beam Max (dB at °)	-0.11 dB at 6.53°	-0.21 dB at 5.67°	-0.04 dB at -1.83°	-0.06 dB at -5.31°

Front to Back

F/B Rel (CP+XP) at +-30 dB	-8.6 dB at -176.1°	-8.3 dB at -174.1°	-7.1 dB at -173.7°	-6.6 dB at -178.2°
F/B CP at +-30 dB	-16.8 dB at -159.3°	-21.6 dB at 156.2°	-17.4 dB at 157.7°	-15.9 dB at 150.7°

Crosspolar values

Radiation axis Xpolar	-13.3 dB at 2.9°	-22.7 dB at -0.7°	-25.6 dB at -1.2°	-15.5 dB at -2.7°
-3dB Bw range XPD	-11.3 dB at -27.7°	-13.1 dB at 37.6°	-14.0 dB at 44.8°	-10.3 dB at -29.7°
-3dB range max level	-13.0 dB at 23.8°	-16.1 dB at 37.6°	-7.1 dB at 44.8°	-11.8 dB at -29.7°
-10dB Bw range XPD	-3.1 dB at -60.1°	-4.2 dB at -73.1°	-5.9 dB at 72.8°	-4.0 dB at -66.7°
-10dB range max level	-12.6 dB at -51.1°	-13.4 dB at -64.7°	-15.5 dB at 50.8°	-11.8 dB at -29.7°
+-30° range XPD	-11.3 dB at -27.7°	-17.6 dB at -33.2°	-19.6 dB at 29.5°	-10.3 dB at -29.7°
+-30° range max level	-13.0 dB at 23.8°	-19.6 dB at -30.2°	-20.5 dB at -12.7°	-11.8 dB at -29.7°
+-60° range XPD	-3.1 dB at -60.1°	-8.8 dB at -60.2°	-8.1 dB at -60.2°	-7.1 dB at -60.2°
+-60° range max level	-12.6 dB at -51.1°	-14.4 dB at 59.9°	-15.5 dB at 50.8°	-11.8 dB at -29.7°

	Copolar File	Normaliz. Value	Date	Xpolar File	Normaliz. Value	Date
Trace 1	[illegible]	[illegible]	[illegible]	[illegible]	-55.01	[illegible]
Trace 2	[illegible]	[illegible]	[illegible]	[illegible]	[illegible]	[illegible]
Trace 3	[illegible]	[illegible]	[illegible]	[illegible]	[illegible]	[illegible]
Trace 4	[illegible]	[illegible]	[illegible]	[illegible]	[illegible]	[illegible]

Fig. A4.1: Measured radiation pattern for -45 degrees plane

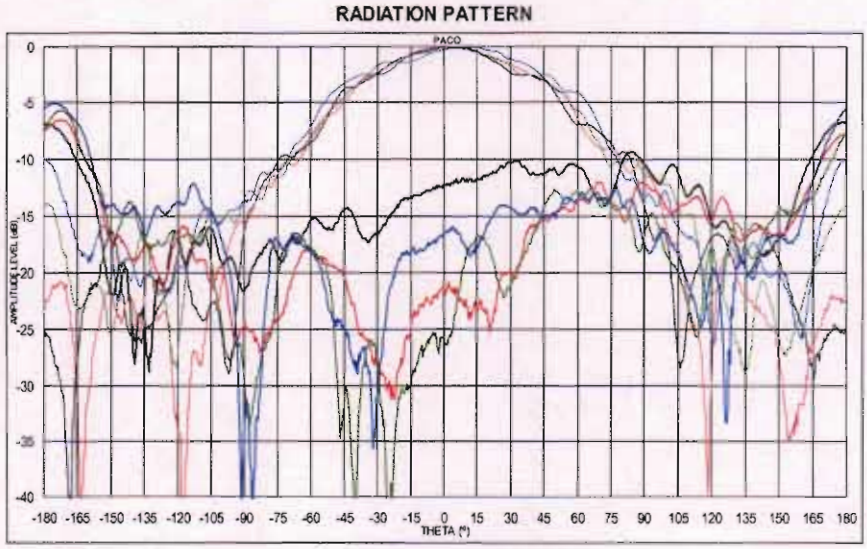

MEDIDA 1

	POL +45 2300Mhz.			
-3dB Beamwidth	80.2°	79.4°	86.1°	87.5°
-10dB Beamwidth	158.2°	144.7°	141.3°	148.1°
-3 dB Bw. Beam-Tilt	2.5°	4.1°	3.8°	3.6°
Horizont Vs Beam Max. (dB at °)	-0.07 dB at 2.62°	-0.05 dB at 2.86°	-0.25 dB at 7.20°	-0.28 dB at 14.74°

Front to Back

F/B Rel (CP+XP) at +-30 dB	-6.9 dB at 179.4°	-6.4 dB at -172.7°	-5.4 dB at -173.7°	-4.1 dB at -177.7°
F/B CP at +-30 dB	-16.5 dB at -150.4°	-20.7 dB at -172.9°	-13.9 dB at -178.8°	-9.9 dB at -179.8°

Crosspolar values

Radiation axis Xpolar	-12.1 dB at 1.8°	-21.6 dB at 3.3°	-25.4 dB at 3.3°	-16.1 dB at 2.7°
-3dB Bw range XPD	-7.5 dB at 31.9°	-12.6 dB at 42.3°	-10.0 dB at 46.7°	-12.1 dB at 44.8°
-3dB range max. level	-10.1 dB at 31.9°	-15.5 dB at 42.3°	-13.0 dB at 46.7°	-14.1 dB at 26.3°
-10dB Bw range XPD	0.8 dB at 83.9°	-3.0 dB at 69.8°	-4.0 dB at 71.8°	-2.5 dB at 77.3°
-10dB range max. level	-9.4 dB at 83.9°	-12.0 dB at 69.4°	-12.7 dB at 65.8°	-12.2 dB at 76.2°
+-30° range XPD	-8.0 dB at 29.9°	-18.3 dB at 29.9°	-16.1 dB at 15.8°	-13.1 dB at 29.3°
+-30° range max. level	-10.3 dB at 28.9°	-19.9 dB at 29.9°	-16.7 dB at 14.8°	-14.1 dB at 26.3°
+-60° range XPD	-3.7 dB at 59.4°	-7.2 dB at 59.7°	-7.2 dB at 59.3°	-9.3 dB at 54.8°
+-60° range max. level	-10.1 dB at 31.9°	-13.7 dB at 59.7°	-12.7 dB at 49.3°	-13.4 dB at 54.8°

	Copolar File	Normaliz. Value	Date	Xpolar File	Normaliz Value	Date
Trace 1	[illegible]	-47.51	29-07-05	[illegible]	-54.26	29-07-05
Trace 2	[illegible]	[illegible]	[illegible]	[illegible]	[illegible]	[illegible]
Trace 3	[illegible]	[illegible]	[illegible]	[illegible]	[illegible]	[illegible]
Trace 4	[illegible]	[illegible]	[illegible]	[illegible]	[illegible]	[illegible]

Fig. A4.2: Measured radiation pattern for +45 degrees plane

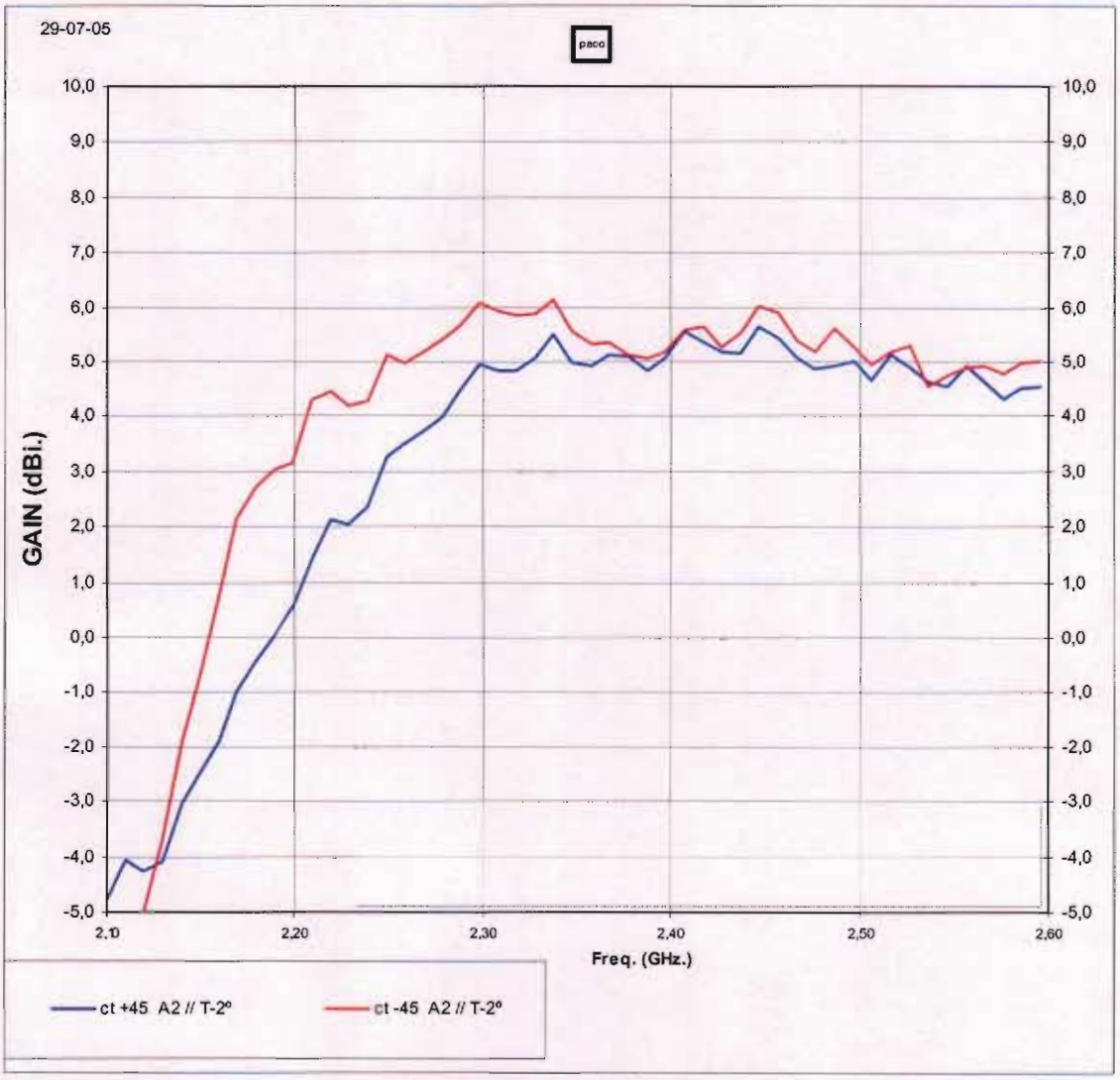

Fig. A4.3: Measured gain

APPENDIX A5

Gain and radiation patterns measurements

The network analyser 8753B Hewlett Packard (see appendix A1), a turntable and a computer have being used to measure the radiation pattern of all the antennas, as shown in the figure A5.1. The network analyser is controlled by a PC over a general purpose instrumentation bus GPIB. The turntable and the network analyser are synchronised. To get the radiation patterns, the antenna under test is rotated through 360° with respect to a fixed antenna of known gain. The data consists of 201 magnitude values of the S_{21} expressed in dB which are stored in the device on completion of measurement. The data is then read into a file in the PC over the GPIB bus. The data is normalised and converted to polar format to be plotted.

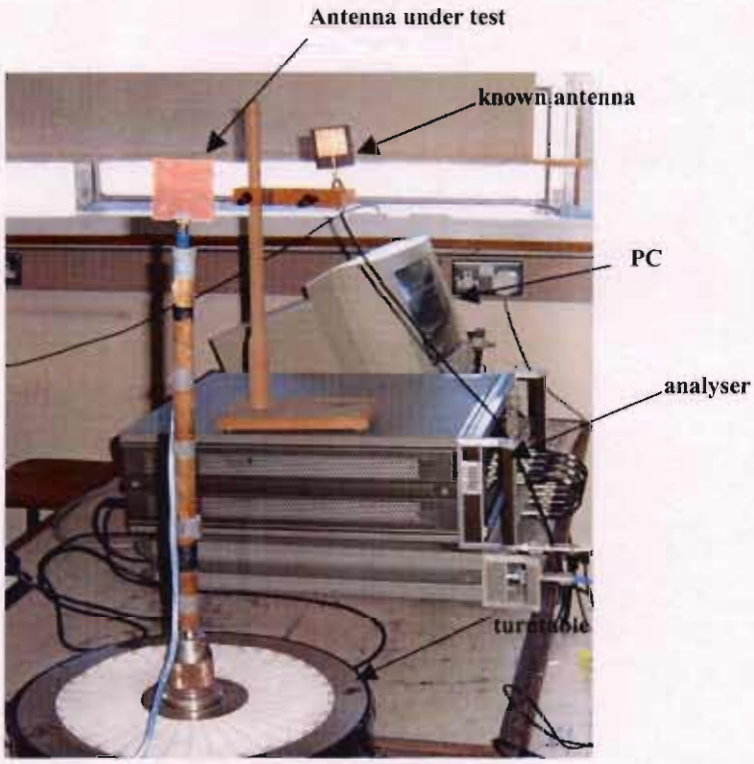

Fig. A5.1: Antenna pattern measurement set-up

The network analyser is also used to measure the gain and the S-parameters.

The dual polarized with improved feed system antenna was measured in a free space elevated range. Figure A5.2 shows the picture of the range. The dimensions of the range are: 19m of height and 43m between the two towers. Its frequency range goes from 500MHz to 6GHz. Some of the main features of the range are the interferences suppression and the very low levels of reflected signals. MI Technologies equipments are placed in both sides of the range. The antenna under test was placed on a tower (white pole in the Figure) that consists of a lower azimuth axis, elevation axis, higher azimuth axis and polarization axis. The standard calibrated pyramidal horn antenna was placed in the other tower that consists of an up/down carriage, polarization axis and elevation axis. Gain was also measured in the free space range using the comparison method.

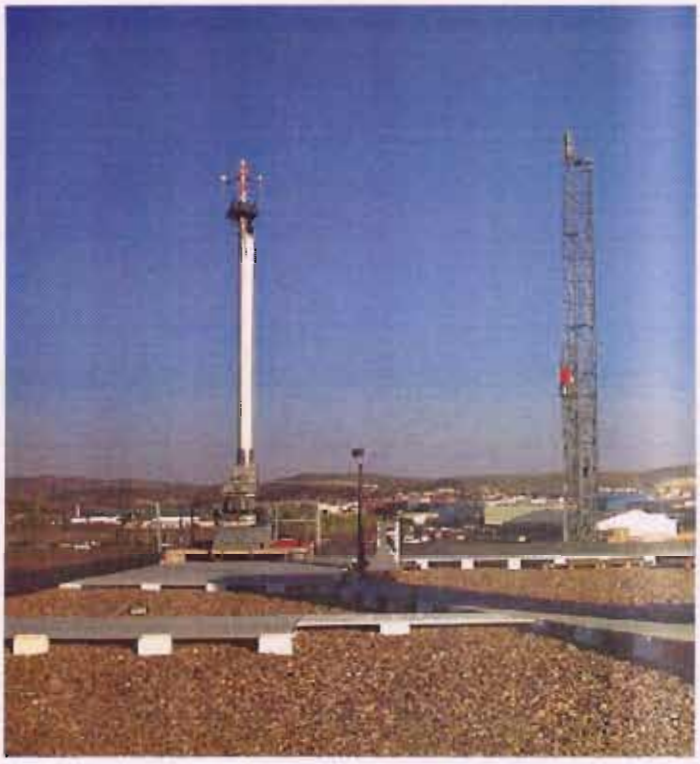

Fig. A5.2: Free space elevated antenna range

APPENDIX A6

Impedance and wavelength calculations

CST provides a tool to calculate the impedance of different types of material. As can be seen in the figure A6.1 parameters such as the height, h, width, w, and epsilon, ϵ, have to be set to calculate the impedance Z.

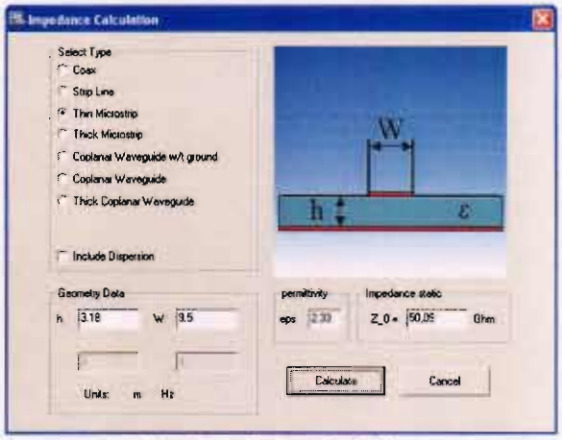

Fig. A6.1: Impedance calculation

Figure A6.2 shows a plot of the tool to calculate the wavelength. The frequency of operation, ϵ_r and μ_r have to be introduced.

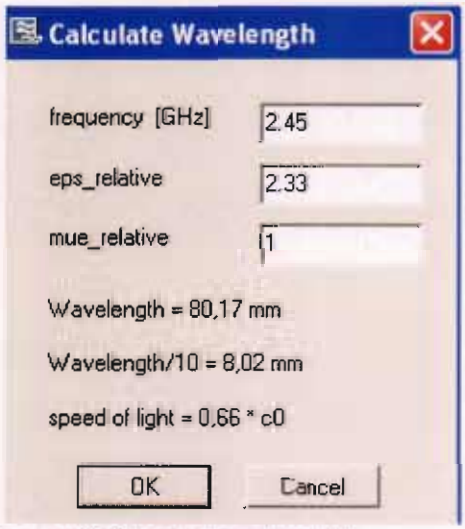

Fig. A6.2: Wavelength calculation

APPENDIX A7

Meshing and coordinate systems in CST Microwave Studio

Mesh Generation Overview

For the spatial discretization the Finite Integration Method (FI-Method) in conjunction with the Perfect Boundary Approximation™ (PBA) is used. The simulated structure and the electromagnetic fields are mapped to hexagonal mesh. The mesh is generated by the automatic mesh generator. This generator, an expert system in connection with optional adaptive mesh refinement features, ensures a good compromise between the need of an accurate structure and field discretization and a short simulation time. The following topics will try to explain how the mesh influences the simulation and what requirements should be fulfilled to obtain a good mesh. The way a structure is discretized strongly influences the accuracy of the results. In theory, the results converge against the "continuous world" results when the mesh size gets smaller and smaller until the discrete lengths vanish or, being more exact, become differentials. So, generally speaking the structure and the fields are simulated best with a very fine mesh.

Mesh and Simulation Time: As far as the results are concerned, the finer the mesh, the better. However, a very fine mesh has a great number of mesh cells and with this a great number of unknowns to be solved. Every increase of unknowns extends the need of memory and simulation time. For the increase of simulation time, there are two different mechanisms. One is quite obvious, the more unknowns there are, the more operations have to be computed. The other mechanism is caused by the properties of the solver used. The frequency domain and the eigenvalue solver converge slower with smaller mesh step sizes than with greater ones. Also, for smaller mesh step sizes the time domain solver needs smaller time steps to remain stable

Mesh view: In the mesh view the so far generated mesh is visualized and all actions concerning the further mesh creation can be done. The automatic mesh generator can be controlled and the resulting mesh is displayed. This view should

always be checked before a simulation is started, because the mesh has a strong influence on the achievable accuracy of the results.

Coordinate Systems

Two kinds of coordinate systems are available: global and local coordinates. At any time, only one particular coordinate system is active.

When the global coordinate system is active, all structure definitions will be performed in x/y/z coordinates. You cannot change the orientation of these coordinate axes. In order to define a structure which is not aligned with the axes of the global coordinate system, (e.g. a brick) you can create the shape in global coordinates first and then apply a transformation. However, a more flexible way is to define a local coordinate system before starting the shape creation and then to create the shape in this local coordinate system. Such local coordinates are also referred to as working coordinate systems (WCS). In general, a local coordinate system (or WCS) is defined by the orientation of its u, v and w axes and the position of its origin. Since the coordinate axes still need to be orthogonal to each other, it is sufficient to define the orientation of the w and u axes.

APPENDIX A8

Substrate effects

In this appendix the influence of the relative permittivity of the dielectric substrate on the dipole resonant frequency, for different thicknesses is presented.

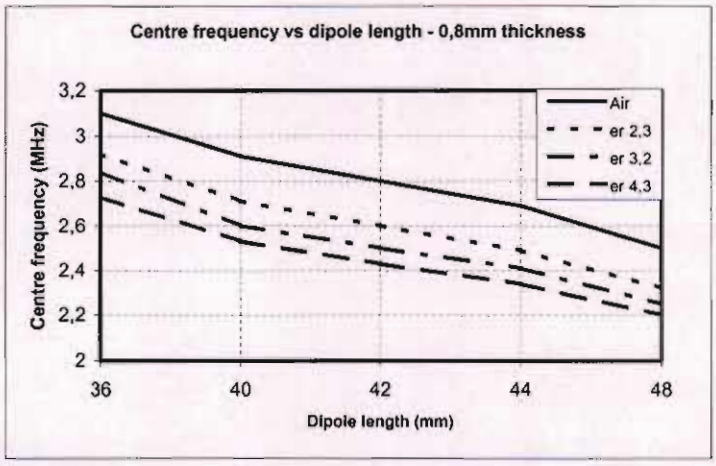

Fig. A8.1: Centre frequency versus dipole length for different substrate permitivity. 0.8mm thickness

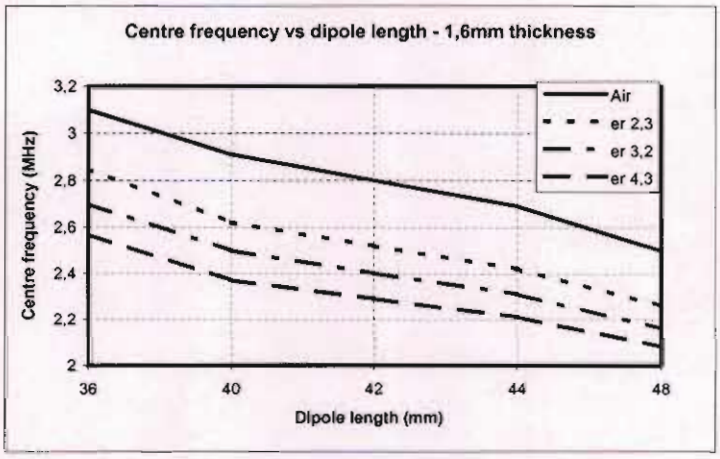

Fig. A8.2: Centre frequency versus dipole length for different substrate permitivity. 1.6mm thickness

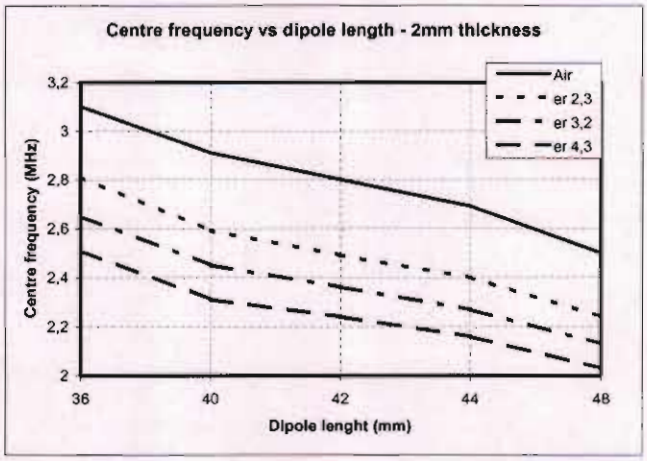

Fig. A8.3: Centre frequency versus dipole length for different substrate permitivity. 2mm thickness

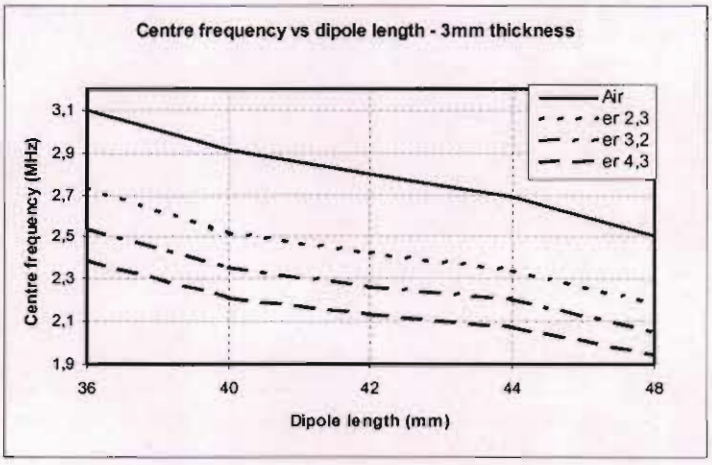

Fig. A8.4: Centre frequency versus dipole length for different substrate permitivity. 3mm thickness

APPENDIX A9

Regulations

CONTENTS

1 INTRODUCTION .....

2 TABLE 1 - Description of Short Range Devices permitted for use in Ireland (from ERC/REC/ 70-03 .....

3 TABLE 2 - Description of Short Range Devices permitted for use in Ireland (National SRDs) .....

4 GLOSSARY OF TERMS .....

ANNEX 1 .....

1 INTRODUCTION

The term "Short Range Device" (SRD) is intended to cover the radio transmitters which provide either uni-directional or bi-directional communication and which have low capability of causing interference to other radio equipment. SRDs use either integral, dedicated or external antennas and all modes of modulation can be permitted subject to meeting the reference standard or equivalent.

ERC Recommendation 70-03 (ERC/REC/70-03) sets out the general position on common spectrum allocations for SRDs for countries within CEPT. It is intended as a reference document for member states and represents the most widely accepted position within CEPT. Appendix 3 of the document lists the National restrictions where member states indicate where their National regulations deviate from the CEPT position. The Recommendation describes the spectrum management requirements for SRDs relating to specific frequency bands, maximum power levels, channel spacing and duty cycle.

Table 1 of this document outlines the types of device, with associated parameters, detailed in ERC/REC/70-03 which may be used in Ireland without the requirement of an individual user licence under the Wireless Telegraphy Act 1926 except for those which are restricted and accordingly listed in 'Appendix 3 – National Restrictions' of the Recommendation. Those devices restricted in Ireland by Appendix 3 of the Recommendation have not been included in Table 1. The full text of ERC/REC/70-03 is available from the ERO web-site (www.ero.dk).

In addition to the types of devices described in ERC/REC/70-03 several other devices may be used in Ireland as SRDs. Table 2 of this document describes the types of device, beyond the scope of ERC/REC/70-03, permitted for use as Short Range Devices in Ireland without the requirement of an individual user licence under the Wireless Telegraphy Act 1926.

This exemption shall not absolve an operator from any requirement in law to obtain additional consents, permissions, authorisations or licences as may be necessary (e.g. for the provision of services to the public). All devices intended to be placed on the market in Ireland must meet the requirements of the R&TTE Directive, details of which are available from the ODTR web-site (Ref. Document No: 00/61).

Short Range Devices operate on a non-interference and non-protected basis i.e. they are not permitted to cause harmful interference to other users of the band and cannot claim protection from interference received. Due to the growing interest in the use of SRDs throughout Europe for a wide range of applications, it is necessary to harmonise frequencies and regulations for these devices and to distinguish between different applications.

2 TABLE 1 – Description of Short Range Devices permitted for use in Ireland (from ERC/REC/70-03)

Frequency Bands K=kHz M=MHz G=GHz	Application	Max Radiated Power or Field Strength Limits & Channel spacing*	Reference ETSI Standard	Additional Information
9 – 59.75 K	Inductive Applications	72 dBμA/m @ 10 m	300 330	ERC/REC/70-03 ERC/DEC/(01)13
59.75 – 60.25 K	Inductive Applications	42 dBμA/m @ 10 m	300 330	ERC/REC/70-03 ERC/DEC/(01)13
60.25 – 70 K	Inductive Applications	72 dBμA/m @ 10 m	300 330	ERC/REC/70-03 ERC/DEC/(01)13
70 – 119 K	Inductive Applications	42 dBμA/m @ 10 m	300 330	ERC/REC/70-03 ERC/DEC/(01)13
119 – 135 K	Inductive Applications	72 dBμA/m @ 10 m	300 330	ERC/REC/70-03 ERC/DEC/(01)13
6765 – 6795 K	Inductive Applications	42 dBμA/m @ 10 m	300 330	ERC/REC/70-03 ERC/DEC/(01)14
6765 – 6795 K	Non-specific SRD	42 dBμA/m @ 10 m	300 330	ERC/REC/70-03 ERC/DEC/(01)01
7400 – 8800 K	Inductive Applications	9 dBμA/m @ 10 m	300 330	ERC/REC/70-03 ERC/DEC/(01)15
13.553 – 13.567 M	Inductive Applications	42 dBμA/m @ 10 m	300 330	ERC/REC/70-03 ERC/DEC/(01)14
13.553 – 13.567 M	Non-specific SRD	42 dBμA/m @ 10 m	300 330	ERC/REC/70-03 ERC/DEC/(01)01
26.957 – 27.283 M	Inductive Applications	42 dBμA/m @ 10 m	300 330	ERC/REC/70-03 ERC/DEC/(01)16
26.957 – 27.283 M	Non-specific SRD	10 mW erp	300 220	ERC/REC/70-03 ERC/DEC/(01)02
26.99 – 27.20 M	Surface Model Control	100 mW erp : 10 kHz	300 220	ERC/REC/70-03 ERC/DEC/(01)10
34.995 – 35.225 M	Aircraft Model Control	100 mW erp : 10 kHz	300 220	ERC/REC/70-03 ERC/DEC/(01)11
40.66 – 40.7 M	Surface Model Control	100 mW erp : 10 kHz	300 220	ERC/REC/70-03 ERC/DEC/(01)12
40.66 – 40.7 M	Non-specific SRD	10 mW erp	300 220	ERC/REC/70-03 ERC/DEC/(01)03
173.965 – 174.015 M	Wireless Microphones	2 mW erp : 50 kHz	300 422	ERC/REC/70-03
402 – 405 M	Medical Implants	25 μW erp : 25 kHz	300 220	ERC/REC/70-03 ERC/DEC/(01)17
433.05 – 434.79 M	Non-specific SRD	10 mW erp	300 220	ERC/REC/70-03 Duty Cycle <10%
433.05 – 434.79 M	Non-specific SRD	1 mW erp	300 220	ERC/REC/70-03 Duty Cycle ≤ 100%
434.04 – 434.79 M	Non-specific SRD	10 mW erp : 25 kHz	300 220	ERC/REC/70-03 Duty Cycle ≤ 100%
863 – 865 M	Wireless Audio Systems	10 mW erp	301 357	ERC/REC/70-03 ERC/DEC/(01)18
863 – 865 M	Wireless Microphones	10 mW erp : 200 kHz	301 357	ERC/REC/70-03
864.8 – 865 M	Wireless Audio Systems	10 mW erp : 50 kHz	300 220	ERC/REC/70-03
868 – 868.6 M	Non-specific SRD	25 mW erp	300 220	ERC/REC/70-03 ERC/DEC/(01)04
868.6 – 868.7 M	Alarms	10 mW erp : 25 kHz	300 220	ERC/REC/70-03 ERC/DEC/(01)09

Frequency Bands K=kHz M=MHz G=GHz	Application	Max Radiated Power or Field Strength Limits & Channel spacing*	Reference ETSI Standard	Additional Information
868.7 – 869.2 M	Non-specific SRD	25 mW erp	300 220	ERC/REC/70-03 ERC/DEC/(01)04
869.2 – 869.25 M	Social Alarms	10 mW erp : 25 kHz	300 220	ERC/REC/70-03 ERC/DEC/(97)06
869.25 – 869.3 M	Alarms	10 mW erp : 25 kHz	300 220	ERC/REC/70-03 ERC/DEC/(01)09
869.4 – 869.65 M	Non-specific SRD	500 mW erp : 25 kHz	300 220	ERC/REC/70-03 ERC/DEC/(01)04
869.65 – 869.7 M	Alarms	25 mW erp : 25 kHz	300 220	ERC/REC/70-03 ERC/DEC/(01)09
869.7 – 870.0 M	Non-specific SRD	5 mW erp	300 220	ERC/REC/70-03 ERC/DEC/(01)04
1785.7 – 1799.4 M	Wireless Microphones	10 mW eirp : 200kHz	301 840	ERC/REC/70-03
2400 – 2483.5 M	Non-specific SRD	10 mW eirp	300 440	ERC/REC/70-03 ERC/DEC/(01)05
2400 – 2483.5 M **	Wideband Data Transmission Systems	100 mW eirp	300 328	ERC/REC/70-03 ERC/DEC/(01)07
2400 – 2483.5 M	FDDA	25 mW eirp	300 440	ERC/REC/70-03 ERC/DEC/(01)08
2446 – 2454 M	AVI for railways	500 mW eirp	300 761	ERC/REC/70-03
2446 – 2454 M	RFID	500 mW eirp 4 W eirp (indoor use)	300 440	ERC/REC/70-03
5150 – 5350 M **	HIPERLAN: indoor use only (Nomadic)	200 mW eirp	301 893	ERC/REC/70-03 ERC/DEC/(99)23
5470 – 5725 M **	HIPERLAN: indoor/outdoor use (Nomadic)	1 W eirp	301 893	ERC/REC/70-03 ERC/DEC/(99)23
5725 – 5875 M	Non-specific SRD	25 mW eirp	300 440	ERC/REC/70-03 ERC/DEC/(01)06
5795 – 5805 M	RTTT	2 W eirp	300 674 201 674	ERC/REC/70-03 ECC/DEC/(02)01
5805 – 5815 M	RTTT (Expansion Spectrum)	2 W eirp	300 674 201 674	ERC/REC/70-03 ECC/DEC/(02)01
9200 – 9500 M	FDDA	25 mW eirp	300 440	ERC/REC/70-03
9500 – 9975 M	FDDA	25 mW eirp	300 440	ERC/REC/70-03
10.5 – 10.6 G	FDDA	25 mW eirp	300 440	ERC/REC/70-03
13.4 – 14 G	FDDA	25 mW eirp	300 440	ERC/REC/70-03
17.1 – 17.3 G	HIPERLAN	100 mW eirp		ERC/REC/70-03
24.00 – 24.25 G	Non-specific SRD	100 mW eirp	300 440	ERC/REC/70-03
24.05 – 24.25 G	FDDA	100 mW eirp	300 440	ERC/REC/70-03
76 – 77 G	RTTT	55 dBm peak eirp	301 091	ERC/REC/70-03

* Maximum Permitted Channel Spacing

** Provision of services to the public is permitted. Public service provider is required to hold an appropriate Telecommunications Licence (ref. ODTR 98/44R)

NOTE: ***When selecting parameters for new SRDs, which may have inherent safety of human life implications, manufacturers and users should pay particular attention to the potential for interference from other systems operating in the same or adjacent bands. Manufacturers should advice users on the risks of potential interference and its consequences***

3 TABLE 2 – Description of Short Range Devices permitted for use in Ireland (National SRDs)

Frequency Bands K=kHz M=MHz G=GHz	Application	Max Radiated Power or Field Strength Limits & Channel spacing*	Reference ETSI Standard	Additional Information
285 – 400 K	Inductive Applications	38 dBµA/m @ 10 m	300 330	
1650 – 1950 K	Inductive Applications	8 dBµA/m @ 10 m	300 330	
1800 – 2200 K	Inductive Applications	-8 dBµA/m @ 10 m	300 330	
2540 – 3560 K	Inductive Applications	-8 dBµA/m @ 10 m	300 330	
31.025 – 31.325 M	Analogue cordless phones	10 mW erp	-	Radio info in National Std TTE 9
39.925 – 40.225 M	Analogue cordless phones	10 mW erp	-	Radio info in National Std TTE 9
49.82 – 49.98[1] M	Baby Monitors	10 mW erp	300 220	
49.82 – 49.98 M	Low Power Radio Transmitters	10 mW erp	300 220	
173.2125 – 173.2375 M	Non-specific SRD - telecommand only	10 mW erp : 25 kHz	300 220	
173.2375 – 173.275 M	Non-specific SRD	100 mW erp : 25 kHz	300 220	
173.7 – 175.1 M	Wireless Microphones	10 mW erp	300 422	
864.1 – 868.1 M	CT2 cordless phones	10 mW erp	300 131	Subject to review
1880 – 1900 M	DECT cordless phones	250 mW erp (peak)		DIR 91/287/EEC, S.I 168. 1994
5150 – 5250 M **	Wideband Data Transmission Systems : Indoor use only (Nomadic)	30 mW (no TPC)	301 893	See Annex 1
5150 – 5250 M **	Wideband Data Transmission Systems : Indoor use only (Nomadic)	60 mW (with TPC)	301 893	See Annex 1
5150 – 5350 M **	Wideband Data Transmission Systems : Indoor use only (Nomadic)	60 mW (no TPC)	301 893	See Annex 1
5150 – 5350 M **	Wideband Data Transmission Systems : Indoor use only (Nomadic)	120 mW (with TPC)	301 893	See Annex 1
5725 – 5875 M **	Wideband Data Transmission (Fixed)	100mW/MHz up to a maximum of 2W eirp	TBA	Registration of base-stations required

* Maximum Permitted Channel Spacing

** Provision of services to the public is permitted. Public service provider is required to hold an appropriate Telecommunications Licence (ref. ODTR 98/44R)

NOTE: ***When selecting parameters for new SRDs, which may have inherent safety of human life implications, manufacturers and users should pay particular attention to the potential for interference from other systems operating in the same or adjacent bands. Manufacturers should advice users on the risks of potential interference and its consequences***

[1] When operating short range devices on these frequencies in close proximity to domestic television receivers care must be taken as the domestic television receivers may suffer interference

4 GLOSSARY OF TERMS

"Inductive Applications" means systems which operate by producing a controlled magnetic field within which a predetermined recognisable signal is formed;

"Non-specific SRD" means Non-specific Short Range Device which is an apparatus for wireless telegraphy including telemetry, telecommand, alarms and data;

"Model Control" means apparatus for wireless telegraphy used to control the movement of a model in the air, on land or over/under the surface of water;

"Baby Monitors" means apparatus for wireless telegraphy which transmit sound to a remote receiver and is commonly used to monitor infants;

"Low Power Radio Transmitter" means apparatus for wireless telegraphy for short range two-way voice communications;

"Wireless Microphones" means apparatus for wireless telegraphy which transmit audio or voice over short distances to a remote receiver;

"Duty Cycle" means the ratio, expressed as a percentage, of the maximum transmitter 'on' time on one carrier frequency, relative to a one hour period;

"Medical Implant" means apparatus for wireless telegraphy for programming and occasional communications with a medical device implanted in the body;

"Wireless Audio Systems" means apparatus for wireless telegraphy which transmit audio or voice over short distances to a remote receiver;

"CT2 Cordless Phones" means apparatus for wireless telegraphy which meets the European CT2 standard;

"Alarms" means apparatus for wireless telegraphy used exclusively for alarm systems including social alarms and alarms for security and safety;

"DECT Cordless Phones" means apparatus for wireless telegraphy which meets the European DECT standard;

"Wideband Data Transmission Systems" means a wireless local, metropolitan or personal area network utilising apparatus for wireless telegraphy;

"FDDA" means Field Disturbance and Doppler Apparatus which is apparatus for wireless telegraphy which operates by creating a radiated field and responding to disturbances/changes within that field;

"AVI for Railways" means Automatic Vehicle Identification for Railways which is apparatus for wireless telegraphy used to track and identify railway vehicles;

"RFID" means Radio Frequency Identification which is apparatus for wireless telegraphy used to identify tagged articles;

"HIPERLAN" means apparatus for wireless telegraphy which meets the ETSI harmonised standard EN 301 893;

"RTTT" means Road Transport and Traffic Telematics which are apparatus for wireless telegraphy for applications relating to road traffic and transport management including automatic road toll collection, route guidance systems, traffic information and advance incident warning;

"erp" means Effective Radiated Power and **"eirp"** means Effective Isotropic Radiated Power as defined in the Radio Regulations;

"Radio Regulations" means the Radio Regulations annexed to the Constitution of the International Telecommunications Union;

"Nomadic" means a communications network/topology which permits limited mobility of one or more devices within the network;

"Fixed" means a communications network/topology in which all devices are in a fixed geographical location within the network;

"TPC" means Transmitter Power Control which is a feature of an apparatus for wireless telegraphy which ensures a reduction in radiated power of 50% when the transmitting device is in close proximity to the intended receiver.

ANNEX 1

Current regulations in Ireland regarding the operation of Wireless Local Area Networks in the 5GHz band require equipment to comply with the technical conditions detailed in ERC/DEC/(99)23 and the draft harmonised standard for HIPERLAN Type 2 (EN 301 893).

The ODTR is aware that there are some technical difficulties at present in obtaining equipment that will operate Dynamic Frequency Selection (DFS), as mandated by ERC/DEC/(99)23, and that the specification for this facility has not yet been completed. Therefore in the interim period, prior to the completion of the specification of the DFS performance characteristics, it has been decided to permit the operation of suitable equipment without the DFS feature in accordance with the technical requirements detailed below (e.g. IEEE 802.11a). This interim solution shall be withdrawn on the completion of the DFS performance characteristics and the publication of the harmonised standard in the Official Journal of the European Communities.

Technical Requirements:

1. Equipment shall meet the draft harmonised standard EN 301 893 except for the requirement of DFS.
2. Equipment may only be used INDOORS.
3. The frequency band of operation may be either 5150 – 5250MHz or 5150 – 5350MHz. The maximum permitted radiated power shall vary depending on the selection of frequency band (see Table 3 below).
4. A random channel selection mechanism shall be implemented across the entire band selected, to ensure a uniform channel loading over the entire band.
5. Transmitter Power Control (TPC), where implemented, shall provide at least 3dB mitigation.

Table 3: Maximum Permitted Radiated Powers for Interim Solution

Frequency Band (MHz)	Maximum Permitted Radiated Power (EIRP)	
	TPC	No TPC
5150 – 5250	60 mW	30 mW
5150 – 5350	120 mW	60 mW